Universidade de Aveiro
2015
Departamento de Eletrónica, Telecomunicações e Informática

Hélder Alexandre Machado Cardoso

Amplificadores de Baixo Ruído para Aplicações em Radioastronomia

Universidade de Aveiro
2015
Departamento de Eletrónica, Telecomunicações e Informática

Hélder Alexandre Machado Cardoso

Amplificadores de Baixo Ruído para Aplicações em Radioastronomia

Dissertação apresentada à Universidade de Aveiro para cumprimento dos requisitos necessários à obtenção do grau de Mestre em Engenharia Eletrónica e Telecomunicações, realizada sob a orientação científica do Professor Doutor Luis Filipe Mesquita Nero Moreira Alves, Professor Auxiliar do Departamento de Eletrónica, Telecomunicações e Informática da Universidade de Aveiro.

Aos meus pais,

O Júri

Presidente

Prof. Dr. José Carlos Esteves Duarte Pedro
Professor Catedrático do Departamento de Eletrónica, Telecomunicações e Informática da Universidade de Aveiro

Arguente

Dr. Luis Manuel Santos Rocha Cupido
Diretor Executivo da LC Technologies

Prof. Dr. Luis Filipe Mesquita Nero Moreira Alves
Professor Auxiliar do Departamento de Eletrónica, Telecomunicações e Informática da Universidade de Aveiro

Agradecimentos

Agradeço aos meus pais, avó, irmã e irmão pela educação, pelas condições que me proporcionaram durante estes anos de formação e pelo apoio e confiança demonstrados em todas as etapas da minha vida. Ao Frederik e à Rosário pelo apoio, confiança e ajuda em tornarem o impossível em realidade. À Mateja pela sua presença, confiança e apoio incondicional. Aos meus amigos mais próximos pela sua amizade e por todos os momentos partilhados.

Agradeço ao meu orientador, o Professor Doutor Luis Nero, pela oportunidade proporcionada, pelo apoio e preocupação demonstrados ao longo do trabalho. Agradeço, em especial, ao Mestre Miguel Bergano pelo auxílio essencial em todas as etapas do desenvolvimento deste trabalho, pelas críticas construtivas efetuadas ao longo do mesmo, pela motivação transmitida e pelo companheirismo. Agradeço ao Paulo Gonçalves do corpo técnico do Instituto de Telecomunicações pela disponibilidade e auxílio na implementação dos circuitos. Agradeço também ao Instituto de Telecomunicações pelas condições proporcionadas durante a realização deste trabalho.

Palavras-chave

Amplificador de Baixo Ruído, Ruído Térmico, Temperatura de Ruído, Figura de Ruído, Radioastronomia, Banda X, Simulação, Desenho, Eletrónica de RF/Microondas

Resumo

Atualmente, a investigação do Universo representa um desafio enorme para a Humanidade e qualquer descoberta ou inovação é sempre significativa. A radioastronomia tem sido responsável por alguns destes avanços tais como a descoberta de pulsares e da radiação cósmica de fundo em microondas. O nosso conhecimento acerca do Universo é ainda limitado e esta busca pelo desconhecido continua. A prova disso mesmo está no início da construção do Square Kilometre Array que é rotulado como o maior e mais sensível radiotelescópio do mundo. Este projeto vai abrir novos horizontes na descoberta científica e terá como objectivo responder a algumas questões fundamentais da astronomia.

Este trabalho enquadra-se precisamente na área da radioastronomia. Inovação nesta área de investigação exige o desenvolvimento e o teste de novas tecnologias de recetores de radioastronomia. A necessidade de elevada resolução exige recetores contribuindo com pouco ruído relativamente à medição a efetuar e uma largura de banda muito maior do que um sistema de telecomunicações normal. O componente crítico no desempenho do recetor em termos de ruído é o amplificador de baixo ruído.

Este trabalho de Mestrado consiste no desenho e implementação de um amplificador de baixo ruído funcional na banda X para ser selecionado como candidato para uma experiência em radioastronomia. Os resultados da simulação do amplificador e do respetivo desempenho em laboratório também estão documentados.

Keywords

Low-Noise Amplifier, Thermal Noise, Noise Temperature, Noise Figure, Radio Astronomy, X Band, Simulation, Design, RF/Microwave Electronics.

Abstract

Nowadays, understanding the Universe still represents a great challenge for the mankind and what may look like a small step forward becomes a huge leap all from a sudden. Radio astronomy has been responsible for some of these huge scientific leaps with many discoveries made in radio frequencies such as the discovery of pulsars and the cosmic microwave background. Our knowledge about the Universe is still limited and this search for the unknown continues. Evidence of this is the beginning of the construction of the Square Kilometre Array that is labeled as the world's largest and most sensitive radio telescope. This project will lead the way in scientific discovery and will aim to solve some of the biggest questions in the field of astronomy.

This work precisely falls within the radio astronomy scientific field. Advances in radio astronomy research require the development and evaluation of new technologies of radio astronomy receivers. The demanding of higher resolution requires receivers with front-ends adding low noise relatively to the weak signal to measure and a wider bandwidth than an average telecommunication system. The critical component of a receiver in terms of noise performance is the low-noise amplifier.

This Master's thesis consists in the design and implementation of a low-noise amplifier operating within the X band to be selected as a candidate for a radio astronomy experience. The simulation results of the amplifier and the respective performance in a laboratory environment are also presented.

Contents

List of Figures

List of Tables

List of Acronyms

ADS	Advanced Design System
DC	Direct Current
DUT	Device Under Test
EM	Electromagnetic
EMI	Electromagnetic Interference
EMR	Electromagnetic Radiation
ENR	Excess Noise Ratio
ESL	Equivalent Series Inductance (L is inductance)
ESR	Equivalent Series Resistance
GPS	Global Positioning System
IF	Intermediate Frequency
IIP3	Third Order Input Intercept Point
LNA	Low-Noise Amplifier
MAG	Maximum Available Gain
MIM	Metal-Insulator-Metal
MSG	Maximum Stable Gain
PCB	Printed-Circuit-Board
PRF	Parallel Resonant Frequency
PSD	Power Spectral Density
RF	Radio Frequency
RL	Return Loss
RMS	Root Mean Square
SKA	Square Kilometre Array
SMA	SubMiniature version A
SMD	Surface Mount Device
SNR	Signal-To-Noise (Power) Ratio
SOLT	Short-Open-Load-Through
SRF	Series Resonant Frequency

Chapter I

1 Introduction

The performance of communication systems is limited by noise, which can be coupled into a receiver or generated within the system itself. In either case, the noise level of the system establishes the threshold for the minimum signal detected by a receiver in the presence of noise. Noise is a random signal and generally may be defined as any unwanted form of energy yet unavoidable which tends to interfere with the proper reception and reproduction of a desired signal. However, the desired signal in some cases, such as radiometers or radio astronomy systems, is actually noise power collected by an antenna [60].

Noise, regarding its source, can be put into two categories: external noise and internal noise. External noise, i.e. noise whose sources are external, may be inserted into a system either by a receiving antenna or via electromagnetic interference (EMI).

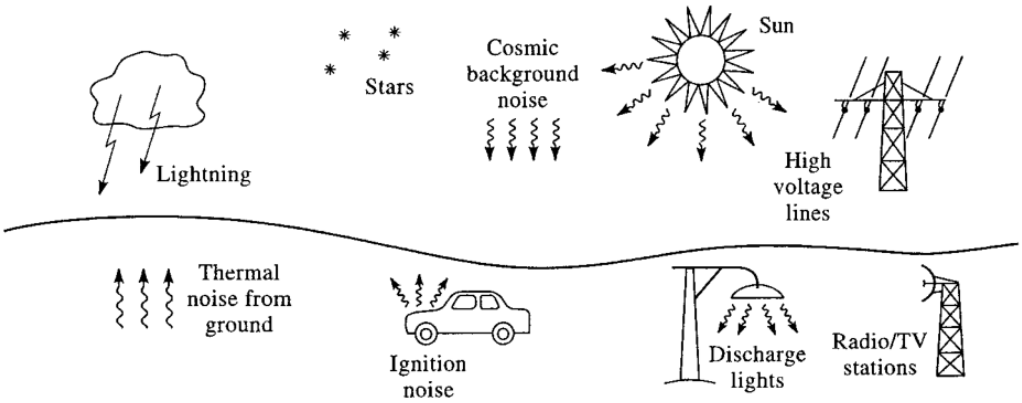

Figure 1: Sources of external noise [60].

External noise has neither a specific frequency nor direction, and consequently, some external noise will always be present in a system regardless the receiver's tuning frequency or the antenna's pointing direction. External noise can be classified as terrestrial or extra-terrestrial. The former, as its name suggests, is connected to warm objects and phenomena on the Earth (Figure 1). It can be due to natural causes (atmospheric and ground noise) or generated by humans (man-made/industrial noise). There are also very warm objects in outer space – sources of extra-terrestrial noise. Hereupon, due to the proximity of those sources to Earth, extra-terrestrial noise can be put into two subgroups: the noise produced by distant celestial bodies, such as stars and planets, can be classified as cosmic noise while the noise emanating from the Sun can be classified simply as solar noise.

Internal noise, however, consists in noise generated within a receiver, communication system or electrical device including resistors and semiconductors. All those objects are noisy by some degree, and therefore a general receiver not only amplifies the desired signal along with the external noise coupled into the system but also adds noise that it internally generates. Thus, it is generally desired to minimize the residual noise level of a system to achieve the best performance. The first stage of a receiver front-end has the dominant effect on the noise performance of the system, and therefore a preamplifier contributing with low noise to the system but presenting enough gain to boost the power of the input signal above the receiver noise floor is required. The device providing such a performance is a low-noise amplifier (LNA) and plays an important role as a building block of any communication system. The LNA is an amplifier used to capture and amplify very weak signals and the random noise presented at its input within the bandwidth of interest. Low-noise amplifiers are used in many applications that involve the detection of very weak signals. Several wireless communication applications demand low-noise amplifiers with distinct specifications and some examples are in mobile phones, global positioning system (GPS) receivers, satellite communication systems or radio astronomy receivers.

1.1 Motivation

This work falls within the radio astronomy scientific field. Radio astronomy is the study of celestial bodies at radio wavelengths and seeks to detect and measure the extremely weak electromagnetic radiation (EM radiation or EMR) from distant

celestial sources [8, 52]. Microwave radiometry, which plays a significant role in remote sensing, is of interest in radio astronomy. Radiometry, in general, is a passive method of detecting the radiation of matter. Its techniques extract information about a target from the intensity and spectral distribution of its emitted electromagnetic radiation, either detected directly or through reflection from surrounding bodies, allowing the thermal characterization of the radiant body as well as its environment, all independently of distance [60]. This EMR power, i.e. noise, is measured by a specially designed sensitive receiver called radiometer [60, 65].

The observations conducted in microwave radiometry employ antenna receiver systems called radio telescopes in radio astronomy. A radio telescope can be described, in its simplest form, by a directional antenna, pointing towards the sky, connected to a low-noise receiver [19].

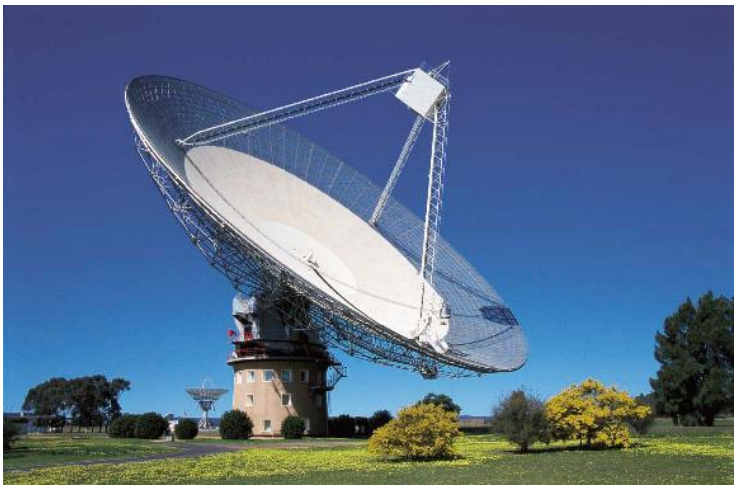

Figure 2: A typical radio telescope [53].

Nowadays, radio telescopes commonly employ dish-shaped antennas (Figure 2) that can be pointed toward any part of the sky in order to gather up the radiation and reflect it to a central focus where the weak electric current, induced by the radio waves, can then be amplified by a receiver making use of the lowest noise preamplifiers that can be produced these days, in order to boost a weak signal to a measurable level [19]. The low-noise receiver is merely a microwave radiometer whose goal, in practice, is to measure the power radiated by astronomical objects [54]. This signal power level is commonly quite low, and so a radiometer for passive microwave radiometry demands high sensitivity to be able to detect extremely small signal powers.

New advances in radio astronomy demand high-performance receivers, and therefore low-noise amplifiers with better performance are essential. Current technology development and radio astronomy research have already enabled the planning and the beginning of the construction of the next-generation radio telescope that will far exceed the capabilities of any existing radio telescope: the Square Kilometre Array (SKA) [68]. The SKA is an international radio astronomy effort to build the world's largest and most sensitive radio telescope consisting of thousands of antennas linked together by high bandwidth optical fiber, and so has attracted the attention of the radio astronomers around the globe [7, 67]. The SKA is a long term project with a phased approach built over two sites: an infrastructure will take place in Western Australia and another will be deployed in southern Africa [67, 68, 69]. The SKA project implies deploying thousands of radio telescopes in three unique configurations in a manner that they will work together as one gigantic virtual instrument allowing international scientists to make ground-breaking observations and discoveries about the Universe [67, 68]. Thus, the SKA will perfectly augment, complement and lead the way in scientific discovery [58].

1.2 Purpose

A low-noise amplifier was required for an X-band receiver application. The device proposed required the following performance:

Table 1: LNA required performance.

Parameter	Performance	Unit
Center Frequency	10	GHz
Bandwidth	≥ 500	MHz
Gain	≥ 15	dB
Noise Figure	≤ 0.4	dB
Input Impedance	50	Ω
Output Impedance	50	Ω

No requirements were imposed in terms of linearity, such as the third order input intercept point (IIP3), or in terms of supply voltage or current. Additionally, in terms of input and output impedances, there will always be a mismatch to the required $50\,\Omega$ that can be measured in terms of return loss (RL), and therefore the values to obtain should be the best possible. In order to fulfil the design goals, a two-stage transistor amplifier approach was chosen.

1.3 Structure of the Document

Besides this opening chapter, this document contains four additionally chapters. Chapter II outlines the fundamental concepts concerned with a LNA. It starts by characterizing and quantifying noise at device level and extending the concepts to a system level where the basics of noise measurement are briefly presented. Furthermore, two-port networks are described in terms of representation and characteristic parameters in order to introduce the design considerations and techniques common to LNA design.

Chapter III covers the design steps of the LNA, the expected results obtained via simulation and the implementation of the device.

Chapter IV deals with the measurements carried out in a laboratory environment by taking in account cautions and corrections in order to improve accuracy. The procedure adopted is explained in detail and the results are presented.

Chapter V ends this document with an overview of the work and an analysis of the results, evaluating limitations and considering further improvements to apply while designing a LNA as well as additional ideas to accomplish in future works.

Chapter II

2 Fundamental Concepts

The internally generated noise is a key performance parameter in a LNA, and therefore this chapter starts with a brief description of noise characteristics, how it can be quantified in a device and the extension of the concept to a system. Thereafter, the fundamental features of noise measurement are discussed. The chapter also covers the behavior of two-port networks and how their performance can be characterized. Finally, the last section focuses on the analysis and techniques employed for the design of a LNA.

2.1 Noise Characteristics

The noise internally generated in a device or component is usually caused by the random motion of charge carriers, which in turn constitutes a fluctuating alternating current that can be detected as random noise [34]. Such motions may be due to several mechanisms, leading to various types of noise in electrical circuits.

Thermal noise, also known as Johnson or Nyquist noise, occurs due to vibrations of conduction electrons and holes due to their finite temperature [31]. Shot noise arises from the quantized and random nature of current flow and normally occurs when there is a potential barrier [31]. The power spectrum of both thermal and shot noises is essentially uniform across the entire radio and microwave ranges. Thus, thermal and shot noises are examples of white noise over those regions. Flicker noise, also known as pink noise, is basically any noise whose power spectrum varies inversely with frequency, and so is often called 1/f noise [60]. Thus, it is dominant only at low frequencies.

Noise characterization usually refers to the combined effect from all the causes in a component [61], as shown in the following figure.

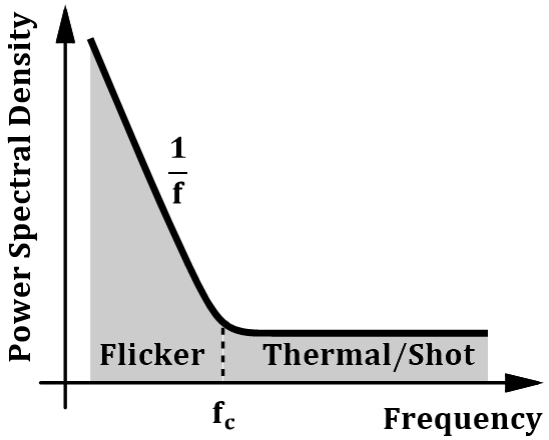

Figure 3: Power spectrum of noise in a device [61].

At microwave frequencies, the combined effect is often referred to as if it all were caused by thermal noise [31].

2.1.1 Noise Voltage

The random motion of charge carriers is caused by heating, which in turn is connected to resistive loads when dissipating energy. Thus, thermal noise is always linked with resistance values, and therefore a resistor can serve as a noise generator. All random motion stops at absolute zero [34], i.e. 0 Kelvin, and so any object whose temperature is above the absolute zero is said to be warm, and therefore generates noise [55]. Thus, a resistor at a physical temperature above 0 Kelvin generates noise. The free electrons in this resistor are in random motion with a kinetic energy proportional to the temperature, which in turn creates a small electric field within the device, and therefore produces a small, random voltage, $u_n(t)$, across the resistor [60], as it can be seen in the following figure.

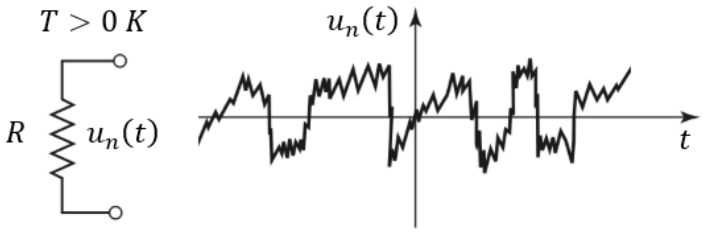

Figure 4: Random voltage generated by a resistor [60].

The instantaneous value of noise cannot be predicted since noise is a random signal, and therefore it cannot be characterized deterministically. However, it can be described statistically, i.e. in terms of average values [61]. Although the random voltage has a zero average value, $\langle u_n(t) \rangle$, it can still be characterized statistically by either noise variance, $\langle u_n^2(t) \rangle$, or root mean square (RMS) value, $\sqrt{\langle u_n^2(t) \rangle}$.

The RMS value of the random noise voltage is given, in Volt, by

$$U_n = \sqrt{\frac{4hfRB}{e^{hf/kT} - 1}} \tag{1}$$

where T is the physical temperature of the resistor in Kelvin, R is the resistance in Ohm, f stands for the center frequency, in Hertz, of the finite system bandwidth B, also in Hertz while $k = 1.380 \times 10^{-23}\, J/K$ and $h = 6.626 \times 10^{-34} Js$ are the Boltzmann and Planck constants, respectively.

However, the above result can be reduced to Johnson's formula [30] for open circuit noise voltage when the Rayleigh-Jeans limit applies, i.e. whenever the condition $hf \ll kT$ is satisfied [51, 60].

$$U_n = \sqrt{4kTRB} \tag{2}$$

This last result is commonly used in microwave circuit design.

2.1.2 Noise Power

The noise generated by a thermal noise source, such as a resistor, can be transferred to the remaining circuit. A general result can be obtained by connecting

a source impedance, at a temperature above absolute zero, to a load impedance where both of them have real part, i.e. a resistance value. Every microwave circuit has a finite bandwidth that will limit the amount of noise power that is transferred. Due to this fact, let us consider an ideal bandpass filter perfectly matched connected between the source and the load impedances as shown in the figure below.

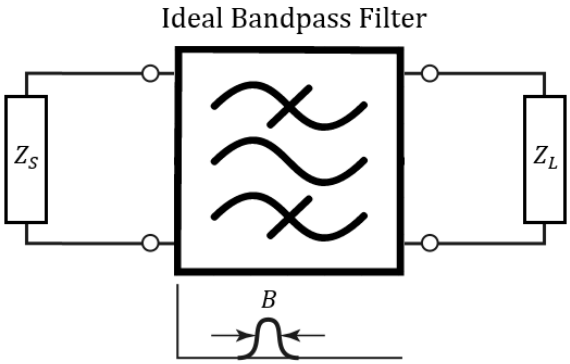

Figure 5: Equivalent circuit of a noise transfer situation.

Each resistance generates random currents, and in thermal equilibrium the power generated by each one of them is equal to the power absorbed, i.e. the noise power transferred in one direction is equal to the one transferred in opposite direction [57]. The average noise power, in Watt, transferred to the load is equal to

$$P_n = \frac{U_n^2}{(Re\{Z_S + Z_L\})^2 + (Im\{Z_S + Z_L\})^2} Re\{Z_L\} \tag{3}$$

where U_n is the noise voltage, as given by Equation 2, produced by the source resistance. This quantity reaches a maximum when impedance matching is verified, i.e. $Z_S = Z_L^*$, and therefore maximum noise power transfer is obtained. So, the thermal noise power delivered by a resistor into an impedance matched load is

$$P_n = kTB \tag{4}$$

This result gives the maximum available noise power from a noisy resistor at a physical temperature T, and due to this fact is also called the available noise power. At any temperature above absolute zero, the thermal noise power generated in a conductor is proportional to its physical temperature on the absolute scale but is

independent on the source impedance, and therefore the thermal noise produced by a resistor does not depend on its ohmic value but only on its temperature. However, it is evident that its resistance cannot be zero or infinity, i.e. it must be able to absorb power.

Every circuit component, from near-perfect conductors to near-perfect insulators, generates thermal noise. However, the impedance of most individual components is grossly mismatched to typical detection systems, and thus only a tiny fraction of the available noise power is normally detected [34]. The noise power detected by a receiver is proportional to the bandwidth in which the noise is measured. Hence, systems with smaller bandwidths collect less noise power. The bandwidth is usually limited by the passband of the system.

Another quantity widely used is the thermal noise power spectral density (PSD), which can be defined through the Nyquist formula [51], in Watt per Hertz, as

$$N = kT \tag{5}$$

Also called the noise spectral density, this quantity is simply the noise power per unit bandwidth. In this case, the spectrum considered is one-sided, i.e. the PSD is constructed for positive frequencies only [61].

2.1.3 Noise Temperature

In addition to the external noise coupled into a receiver, each component within itself generates its own internal noise. Let us consider the following figure where a device under test (DUT) is placed ahead of a noise source, which is represented by a resistor at the temperature T_{in}, and followed by a noise-free receiver.

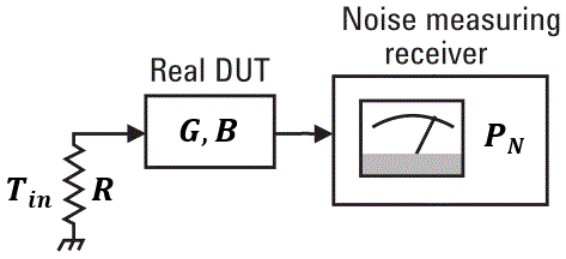

Figure 6: Noise power measurement of an excited noisy network [34].

Let us also assume that the DUT is matched to the noise source and to the input of the noise-free receiver. Equation 4 establishes a power-temperature relation, i.e. noise power can also be quantified in terms of its equivalent noise temperature. Hence, the input signal consists only of thermal noise with an equivalent noise temperature T_{in} and at the output is likewise noise but with an equivalent noise temperature T_{out}. Equation 4 also establishes the measured power as

$$P_n^{out} = kT_{out}B \tag{6}$$

Firstly, let us consider the DUT as an active two-port network. A noisy active device, such as an amplifier, has a gain G and an operational bandwidth B. The device amplifies the magnitude of the thermal noise at the input by a factor of G as it would do to any signal. Additionally, the amplifier outputs its own noise, generated in the device itself, along with the amplified input noise, and therefore the noise at the output of the amplifier consists of two components. Both sources of noise are independent, and so the noise power at the output is simply the sum of each of the two components

$$P_n^{out} = (GkT_{in} + N_{add})B \tag{7}$$

where N_{add} is the PSD of the internally generated noise at the output of the device. The noise measuring receiver cannot distinguish these two components of noise.

The internal noise is generated by every resistor and semiconductor throughout the amplifier, and so the value N_{add} specifies the total value of the noise internally generated exiting the device.

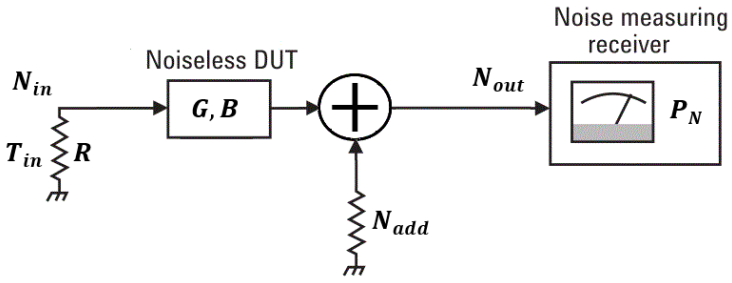

Figure 7: Modelling of a noisy device with an output noise source.

As a result, an active two-port network can be modelled as a noiseless device followed by an output noise source producing thermal noise, as represented in Figure 7.

However, the model that is typically used when considering the internal noise of an amplifier refers this added noise to the input of the device, and therefore the real DUT can be alternatively modelled assuming this internally generated noise occurring at the input [72], as it can be seen in Figure 8.

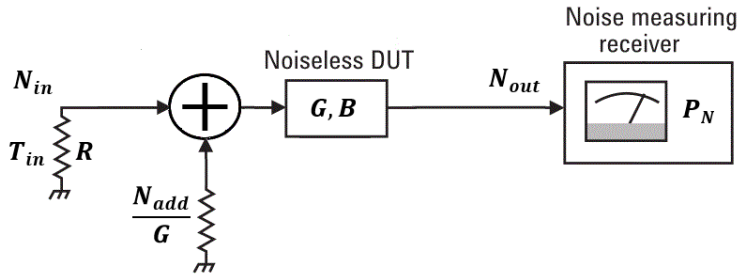

Figure 8: Modelling of a noisy device with an input noise source.

So, all this noise is amplified by a factor of G. Thus, the real DUT is modelled as a noise-free equivalent device from which all internal noise sources have been removed combined with an additional thermal noise source at the input. This situation is equivalent to a noise-free DUT driven by an input resistor heated to some higher temperature $T_{in} + T_e$ where

$$T_e = \frac{N_{add}}{kG} \tag{8}$$

The equivalent noise temperature T_e is defined as the effective input noise temperature of the DUT. Generally, the word effective (or equivalent) is taken as understood, and the normal term is simply noise temperature [34].

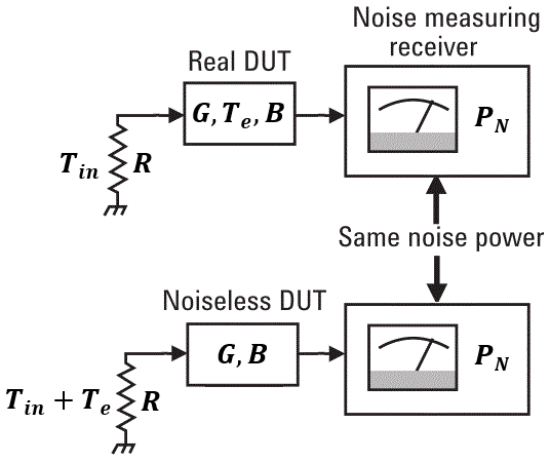

Figure 9: Effective input noise temperature concept [34].

Thus, the effective input noise temperature for an active device is simply the equivalent noise temperature of a noise source into a noise-free device that would produce the same added noise as a noisy device would (Figure 9). The noise power of this system is constrained to the finite bandwidth B, and therefore Equation 8 becomes

$$T_e = \frac{P_n^{add}}{kGB} \tag{9}$$

The effective input noise temperature is a two-port device parameter just like the gain, and it shows how noisy an amplifier is. The previous equation states that $P_n^{add} \propto T_e$, and consequently the lower the value of T_e, the lower is the added noise by the amplifier. An ideal amplifier, i.e. noiseless, has $T_e = 0$.

Specifying the internal amplifier noise in this fashion allows us to relate the input and the output noise temperatures in a very straightforward manner.

$$T_{out} = G(T_{in} + T_e) \tag{10}$$

Thus, the noise power at the output of the DUT, in the case considered, is given by Equations 6 and 10 as follows

$$P_n^{out} = Gk(T_{in} + T_e)B \tag{11}$$

The concept of effective input noise temperature also applies to passive devices. Hereupon, let us consider the DUT on the previous analysis as a two-port network consisting of a passive, lossy component, such as an attenuator or transmission line, instead of an active device. Thus, let us assume the DUT as a matched attenuator at the same temperature as the source resistor, T_{in}. The gain, G, of a lossy network is less than the unity, and so the loss factor, L, can be defined as

$$L = \frac{1}{G} \tag{12}$$

In this case, let us suppose the entire system is in thermal equilibrium at the temperature T, thus $T_{in} = T_{out} = T$ holds. Considering this last condition, Equations 6 and 7 for the output noise power from the active device analysis, which are also valid for a passive device, and the definition of PSD we obtain the noise generated by the attenuator itself as

$$P_n^{add} = (1 - G)kTB \tag{13}$$

By considering Equation 12, this result turns to

$$P_n^{add} = \left(1 - \frac{1}{L}\right)kTB \tag{14}$$

By expressing P_n^{add} in terms of equivalent noise temperature using Equation 9 shows that the attenuator has an effective input noise temperature given by

$$T_e = (L - 1)T \tag{15}$$

2.1.4 Signal-to-Noise Power Ratio

The input of a noisy network, in addition to noise, will also include the desired signal. Thus, the input power comprises both the input signal power, P_s^{in}, and the input noise power, P_n^{in}. The output of the network will likewise include both a signal with power P_s^{out} and noise with power P_n^{out}. This is illustrated in the following figure.

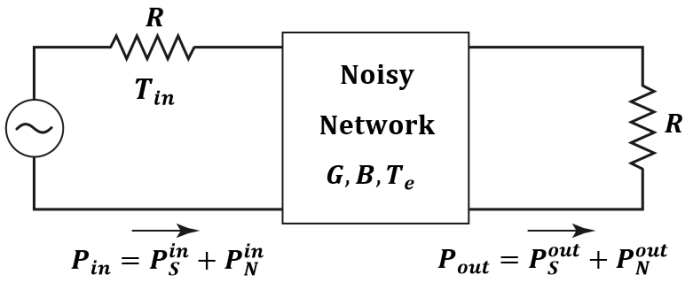

Figure 10: Power considerations of a noisy network [60].

Evidently, the output signal power relates to the input signal power linearly through the gain factor as

$$P_s^{out} = GP_s^{in} \tag{16}$$

while the output noise power is expressed (recall Equation 7) as

$$P_n^{out} = GP_n^{in} + P_n^{add} \tag{17}$$

Both input and output can be characterized in terms of quality of signal by the signal-to-noise power ratio (SNR), which is the ratio of the desired signal power to the undesired noise power.

$$SNR = \frac{P_s}{P_n} \tag{18}$$

A noiseless network would amplify or attenuate the noise applied at its input along with the desired signal by the same factor, so that the SNR remains the same at its input and output. A noisy network, however, also adds some internally generated noise from its own components and at the output the noise power is increased more than the signal, so that the SNR is reduced at the output. Hence, let us take the ratio of the input SNR to the output SNR

$$\frac{SNR_{in}}{SNR_{out}} = 1 + \frac{P_n^{add}}{GP_n^{in}} \tag{19}$$

The input noise power defined across the bandwidth of the network is simply expressed by the power-temperature relation of Equation 4, while the noise power generated internally is given by Equation 9. Thus,

$$\frac{SNR_{in}}{SNR_{out}} = 1 + \frac{T_e}{T_{in}} \tag{20}$$

All real devices add a finite amount of noise to the signal, i.e. $T_e > 1$, and so the ratio between the SNR at the input and its counterpart at the output is always greater than unity. As a result, the SNR will always be degraded as the signal travels through each component. Thus, the SNR ratio essentially quantifies the degradation of SNR by a network. Equation 20 states that the degradation of the SNR in a network is exclusively dependent on its effective input noise temperature and on the temperature of the source that excites the network. While the former is a device parameter, the latter is independent of the device itself.

2.1.5 Noise Factor

The SNR ratio is a widely used parameter for specifying the noise performance of a two-port device. This alternative characterization to the noise temperature, called noise factor, was introduced by Harold Friis [31]. The noise factor of a network is defined as the ratio of the SNR at the input of the network to the SNR at the output, for a specific input noise temperature. Friis suggested a reference source temperature, denoted by T_0, of 290 K [34], which is equivalent to 16.8 °C and 62.3 °F.

$$F = \left[\frac{SNR_{in}}{SNR_{out}}\right]_{T_{in}=T_0} = 1 + \frac{T_e}{T_0} \tag{21}$$

Thus, the noise factor of a network represents the degradation in the SNR as the signal travels through the network for the specific reference source temperature T_0, and for that specific condition only [72].

As shown previously, the noise factor of a given device is dependent on its effective input noise temperature. Hereupon, a bridge between the former and the latter can be made, since the noise factor can be calculated from the effective input noise temperature (Equation 21) and vice versa by

$$T_e = (F - 1)T_0 \tag{22}$$

Thus, the noise power at the output of a DUT can be obtained in function of the noise factor by using Equation 22 into Equation 11

$$P_n^{out} = Gk(T_{in} + (F - 1)T_0)B \tag{23}$$

Similarly to the effective input noise temperature analysis, the passive devices are also a special case in terms of noise factor. It was determined earlier that the noise factor of a two-port device is related to its effective input noise temperature according with Equation 21. Recalling Equation 15, the noise factor of a passive device is

$$F = 1 + (L - 1)\frac{T}{T_0} \tag{24}$$

If the passive network is at physical temperature T_0, then

$$F = L \tag{25}$$

Thus, for a passive device, the noise factor is equal to its attenuation. This result is important since the condition $T = T_0$ verifies in most cases as T_0 is taken as the standard room temperature [60].

2.1.6 Noise Figure

The noise factor F in Equation 21 has historically been called noise figure, however that name is now more commonly reserved for the quantity F expressed in decibel units [3, 34].

$$NF = 10\log_{10}(F) \tag{26}$$

The contemporary convention refers to the ratio F as noise factor or sometimes noise figure in linear terms (since it is a dimensionless value), and uses

noise figure to refer only to the decibel quantity NF [31]. Noise figure is widely used to represent the noise performance of a device rather than the noise factor. Both concepts will be used in the remainder of the document and it is up to the reader to acknowledge if either a ratio or a decibel quantity is mentioned.

2.1.7 Multistage Systems

The concepts of effective input noise temperature and noise factor covered in the previous sections, which can describe the noise performance of individual components such as a single transistor amplifier, can also be applied to a complete multistage system such as a receiver. In a typical receiver the input signal travels through a cascade of many different components, each of which may degrade the SNR to some degree. If the gain and the internal noise, either in terms of noise temperature or noise factor, of the individual stages are known, the overall noise performance of the cascade connection of stages can also be determined.

Let us consider two cascaded stages, each with a different gain, effective input noise temperature and noise factor as presented in Figure 11 (a).

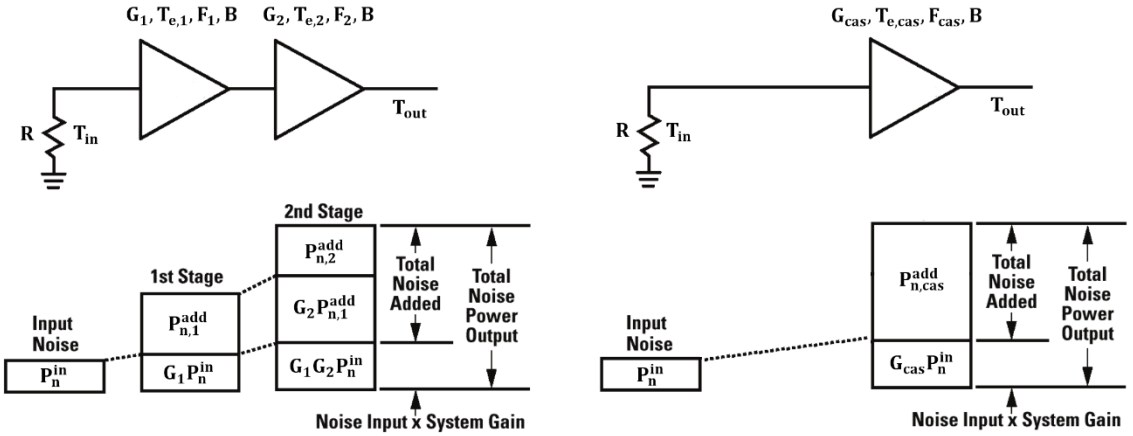

(a) Two cascaded networks (b) Equivalent network

Figure 11: How noise builds up in a multistage system [31, 34].

The two cascaded networks can also be thought of as a unique device with the following overall parameters: gain, effective input noise temperature and noise factor as shown by Figure 11 (b).

First of all, let us assume that B is the operational bandwidth of the system, which means that all the noise powers are constrained to this finite frequency range. Thereafter, the input noise power of the system, which is determined by Equation 4, is

$$P_n^{in} = kT_{in}B \tag{27}$$

Now, let us consider the case of the two cascaded networks (Figure 11 (a)). The noise powers at the output of the first and second stages, which are determined by Equation 17, are given by

$$P_{n,1}^{out} = G_1 P_n^{in} + P_{n,1}^{add} \tag{28}$$

and

$$P_n^{out} = G_2 P_{n,1}^{out} + P_{n,2}^{add} \tag{29}$$

respectively.

The internally generated noise by the first stage, $P_{n,1}^{add}$, and by the second stage, $P_{n,2}^{add}$, can be represented in terms of its equivalent noise temperature by means of Equation 9, and therefore

$$P_{n,1}^{add} = G_1 kT_{e,1}B \tag{30}$$

stands for the first stage, while

$$P_{n,2}^{add} = G_2 kT_{e,2}B \tag{31}$$

stands for the second stage. So, by using Equations 27 and 30 into Equation 28, and the latter along with Equation 31 into Equation 29, the output noise power of the two cascaded networks reduces to

$$P_n^{out} = G_1 G_2 k \left(T_{in} + T_{e,1} + \frac{T_{e,2}}{G_1}\right) B \tag{32}$$

Now, let us consider the equivalent network (Figure 11 (b)). The total system gain is given by

$$G_{cas} = G_1 G_2 \tag{33}$$

Let us recall Equation 10 to establish a relation between the equivalent input noise temperature, the system's noise temperature and the equivalent noise temperature at the output. On these terms, the output noise power, which is determined by Equation 11, is

$$P_n^{out} = G_1 G_2 k\left(T_{in} + T_{e,cas}\right)B \tag{34}$$

The noise power at the output of both the two-stage system and the equivalent network must be equal, and therefore an equality between Equations 32 and 34 must be verified. Thus, the effective input noise temperature of a two-stage system, in function of the noise temperature of each individual stages within, is

$$T_{e,cas} = T_{e,1} + \frac{T_{e,2}}{G_1} \tag{35}$$

Equivalent results can be obtained by expressing noise temperature in terms of noise factor by Equation 22. Thus, from Equation 35, the noise factor of a two-stage system, also known as the cascade noise equation, is

$$F_{cas} = F_1 + \frac{(F_2 - 1)}{G_1} \tag{36}$$

The second term in either Equation 35 or 36, $T_{e,2}/G_1$ or $(F_2 - 1)/G_1$, respectively, is due to the second stage contribution [31, 34]. The noise performance in a multistage system is dominated by the characteristics of the first stage if its gain, G_1, is high enough that the second stage contribution is reduced, and the overall effective input noise temperature and overall noise factor will be mostly determined by the first stage contribution alone, i.e. by $T_{e,1}$ and F_1, respectively. Thus, for the best overall system noise performance, the first stage has the most critical impact, and therefore it should have a low noise figure and at least moderate gain. This is why the ideal first device for a low-noise receiver is a low-noise amplifier.

The system's noise temperature and noise factor can be generalized to an arbitrary number of stages, n, in a cascade of networks, as

$$T_{e,cas} = T_{e,1} + \frac{T_{e,2}}{G_1} + \frac{T_{e,3}}{G_1 G_2} + \cdots + \frac{T_{e,n}}{G_1 G_2 G_3 \ldots G_{n-1}} \tag{37}$$

and

$$F_{cas} = F_1 + \frac{(F_2 - 1)}{G_1} + \frac{(F_3 - 1)}{G_1 G_2} + \cdots + \frac{(F_n - 1)}{G_1 G_2 G_3 \ldots G_{n-1}} \tag{38}$$

For the sake of completeness, the output noise power can also be expressed as function of the overall noise factor as

$$P_n^{out} = G_1 G_2 k(T_{in} + (F_{cas} - 1)T_0)B \tag{39}$$

Additionally, a case of interest appears when the input noise temperature corresponds to the reference source temperature T_0 and the previous equation simply reduces to

$$P_n^{out} = G_1 G_2 k T_0 F_{cas} B \tag{40}$$

2.2 Noise Measurement

The equations of overall noise factor or overall noise temperature constrained to two stages are the basis for most noise figure measurement instruments. The following figure illustrates the noise figure measurement setup where the DUT is always labelled as Stage 1 and the instrumentation that follows is labelled as Stage 2.

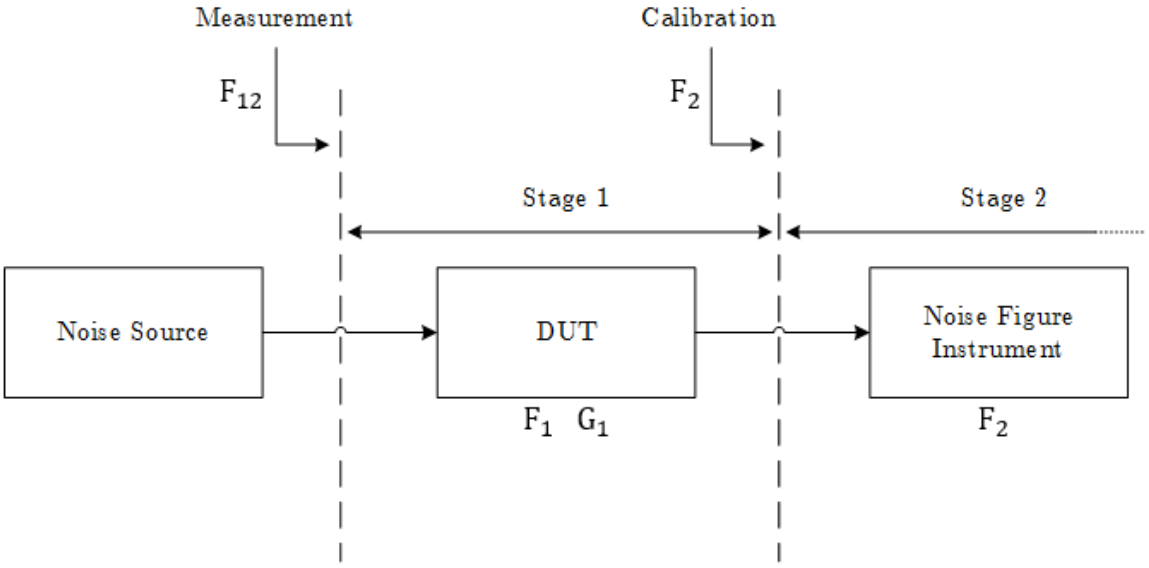

Figure 12: Noise figure measurement setup.

2.2.1 Noise Power Linearity

In principle, the noise added by a DUT is the measured output noise power when a noiseless matched load is connected at its input [60]. However, in practice, a noiseless source cannot be obtained, so a different method must be used. A linear two-port device is characterized by an output noise power linearly dependent on the input noise power, which in turn is proportional to the temperature of the noise source, as it can be seen in the following figure.

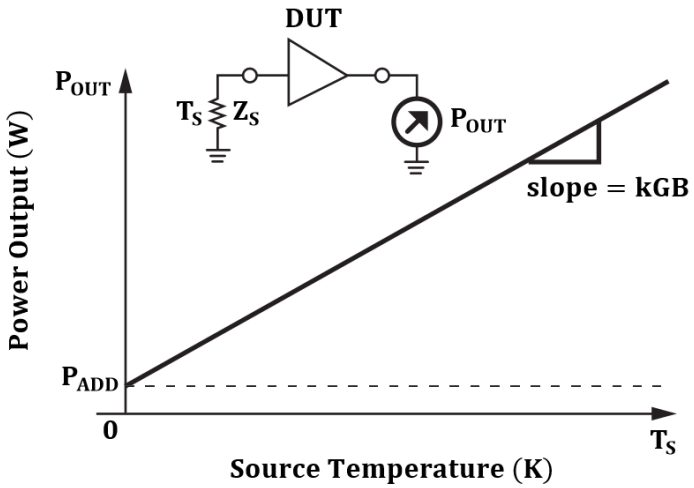

Figure 13: Linear two-port network noise power characteristic [31].

The value of the internally generated noise of the DUT can be found if both the slope of the noise power characteristic and a reference point are known. This is the basis of the Y-factor method, which can be applied if two matched loads at significantly different temperatures are available [31]. The Y-factor technique is the most common method of measuring the quantities required by the cascaded noise formulas in order to calculate the noise factor F_1 of the DUT [31, 34, 37].

2.2.2 Noise Source

A passive noise source may simply consist of a resistor held at a constant temperature while an active noise source may use a diode or transistor to provide a calibrated noise power output [60]. Figure 14 consists in the schematic of an active noise source.

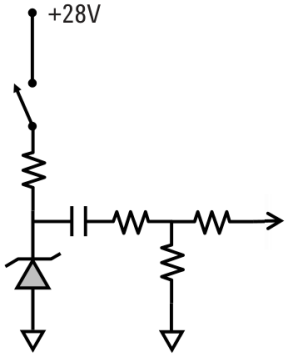

Figure 14: Schematic of an active noise source [3].

A calibrated noise source is a device that provides two different levels of noise (hot and cold) and has a pre-calibrated Excess Noise Ratio (ENR) [3, 37], defined as

$$ENR = \frac{T_S^{ON} - T_S^{OFF}}{T_0} \tag{41}$$

where T_S^{ON} and T_S^{OFF} are the noise temperatures of the noise source in its on (hot) and off (cold) states, and T_0 is the reference temperature of 290 K. The calibrated ENR of a noise source is commonly expressed in decibel units [37].

2.2.3 Y-Factor Method

The Y-factor technique requires that the DUT is connected to one of two matched loads at different temperatures [37]. The noise slope can be determined by applying these two different levels of input noise and measure the output power change.

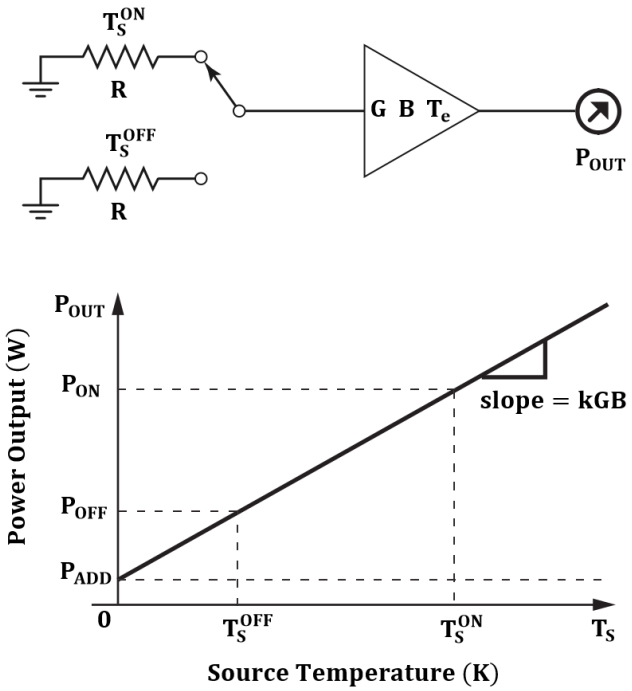

Figure 15: Representation of the Y-factor Method [31, 60].

In practice, the noise measurement instrument drives the noise source on and off to generate two temperature points, T_S^{ON} and T_S^{OFF}, on the straight line kGB, and measures the two power outputs of the DUT, P_{ON} and P_{OFF}, for these two temperatures [31]. The output noise power consists of noise power generated by the DUT as well as noise power from the noise source.

$$P_{ON} = GkT_S^{ON}B + GkT_eB \tag{42}$$

$$P_{OFF} = GkT_S^{OFF}B + GkT_eB \tag{43}$$

The Y-factor is the ratio of these two noise power levels and is measured by repeatedly pulsing the noise source on and off, so that an average value can be computed [34].

$$Y = \frac{P_{ON}}{P_{OFF}} \tag{44}$$

Extrapolating the straight line to the $T_S = 0$ point gives the noise added by the DUT, P_{ADD}. Hereupon, noise factor and effective input noise temperature may be obtained.

Additionally, from Equations 42, 43 and 44, the effective input noise temperature can be written in function of the source temperatures and the Y-factor as

$$T_e = \frac{T_S^{ON} - YT_S^{OFF}}{Y - 1} \tag{45}$$

The complete Y-factor measurement of a DUT noise factor and gain requires both calibration and measurement steps as already shown in Figure 12 to calculate all necessary quantities.

In this context, a noise measuring receiver of interest for this work is the radiometer due to its role in radio astronomy. This receiver and some additional radiometry concepts are covered in Appendix A.

2.3 Characteristics of a Two-Port Network

The behavior of a two-port network can be characterized by a set of scattering parameters, which are defined in terms of incident and reflected signals, and by a set of noise parameters characteristic of the device. The scattering parameters along with the impedance terminations of a two-port network may characterize a device

in terms of gain and mismatch while the noise parameters allow the evaluation of the noise performance of the device.

2.3.1 Scattering Parameters

Figure 16 considers a two-port network where a generator with a source impedance Z_1 is placed at the input port and a load impedance Z_2 is connected to the output port.

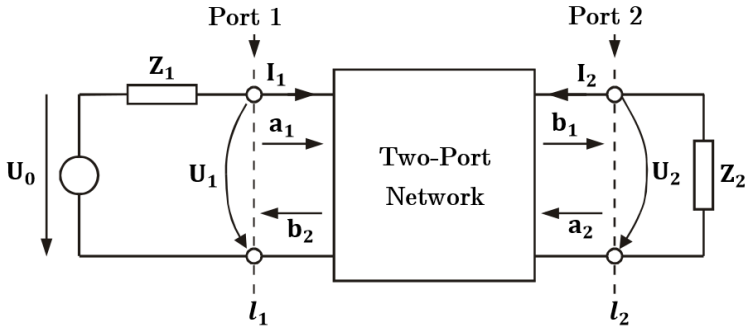

Figure 16: General two-port network [40].

Dealing with wave propagation phenomena implies defining reference planes as l_1 and l_2 at the input and output ports, respectively. The quantities U_i and I_i stand for the total values of voltage and current, respectively, at the port $i = \{1, 2\}$. In general, the normalized power waves are defined by

$$a_i = \frac{U_i + Z_i I_i}{2\sqrt{|Re(Z_i)|}} \tag{46}$$

as the incident power wave and

$$b_i = \frac{U_i - Z_i^* I_i}{2\sqrt{|Re(Z_i)|}} \tag{47}$$

as the reflected power wave. The dimension of these normalized equations is the square-root of power.

In general, both source and load impedances may be complex. However, the reference impedance Z_i is usually chosen to be real and equal to the characteristic impedance of the transmission line, Z_{0i}, connected to the respective port i [40]. A general two-port network taking into account the characteristic impedance of the transmission lines connected to the input and output port is represented in the following figure.

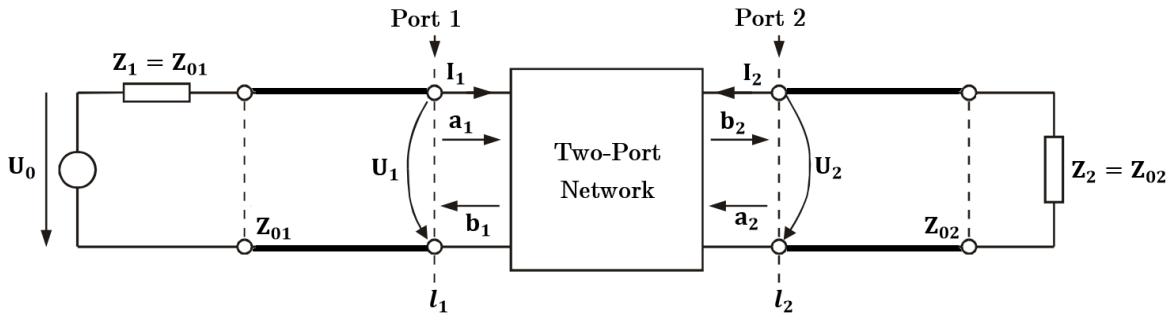

Figure 17: Practical case of a general two-port network.

The reflected power wave b_i at any port i will be composed by two components: the first results from the reflection of the incoming power wave a_i at the same port i, while the second results from the transmission through the network of the incoming power wave a_j $(j \neq i)$ at the other port. Thus, for a two-port network, it follows

$$b_1 = S_{11}a_1 + S_{12}a_2 \tag{48}$$

$$b_2 = S_{21}a_1 + S_{22}a_2 \tag{49}$$

The parameters S_{ji} are found by driving the port i with an incident power wave a_i and measuring the reflected power wave b_j coming out of port j, while the incident power wave a_j on port j is terminated in matched load to avoid reflections. Thus, S_{ii} is the reflection coefficient seen looking into port i when port j is terminated in matched load,

$$S_{ii} = \left.\frac{b_i}{a_i}\right|_{a_j=0}, j \neq i \tag{50}$$

and S_{ji} is the transmission coefficient from port i to port j when port j is terminated in matched load.

$$S_{ji} = \left.\frac{b_j}{a_i}\right|_{a_j=0}, j \neq i \tag{51}$$

The frequency dependent parameters S_{11}, S_{12}, S_{21} and S_{22}, which represent reflection and transmission coefficients, are called the scattering parameters (or simply S parameters) of a two-port network, measured at specific locations at port 1 and 2 [23], and normalized to a specific reference impedance at each port.

Equations 48 and 49 can also assume a matrix form as $[b] = [S][a]$, and consequently this set of parameters can be represented as the scattering matrix

$$[S] = \begin{bmatrix} S_{11} & S_{12} \\ S_{21} & S_{22} \end{bmatrix} \tag{52}$$

The scattering parameters imply a direct proportionality of outgoing and incoming power waves, which is a property of linear networks [40]. In the case of active networks, such as amplifiers, device characterization by scattering parameters depends on bias conditions and applies only for the small-signal regime [23].

2.3.2 Power Transport and Gain

Several power gain equations can be defined when an arbitrary two-port network, characterized by its scattering matrix, is terminated by arbitrary source and arbitrary load impedances. The power transport from the source into the load through the two-port network arises different concepts of power, which are described by the scattering parameters of the general two-port network and the reflection coefficients at its ports, as shown in the following figure.

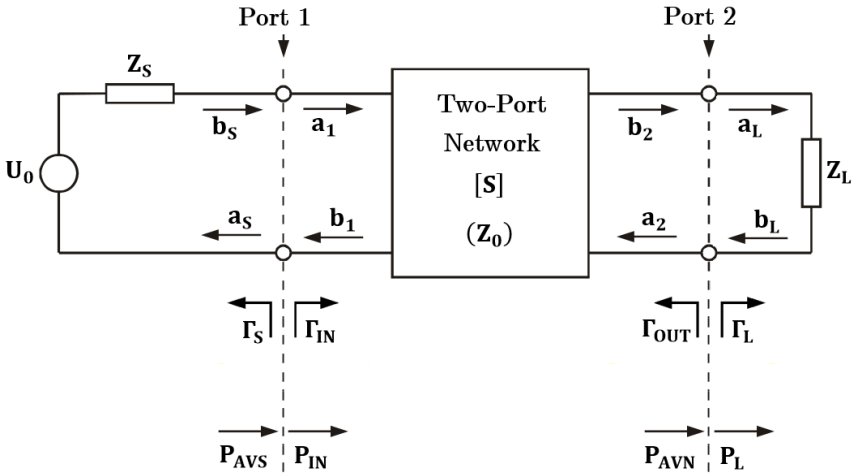

Figure 18: General two-port network with arbitrary source and load impedances.

The reflection coefficient seen looking toward the load is

$$\Gamma_L = \frac{Z_L - Z_0}{Z_L + Z_0} \tag{53}$$

while the reflection coefficient seen looking toward the source is

$$\Gamma_S = \frac{Z_S - Z_0}{Z_S + Z_0} \tag{54}$$

where Z_0 is the characteristic impedance of the system.

The input impedance seen looking into port 1 of the two-port network when port 2 is terminated by Z_L, is mismatched with a reflection coefficient given by

$$\Gamma_{IN} = S_{11} + \frac{S_{12}S_{21}\Gamma_L}{1 - S_{22}\Gamma_L} \tag{55}$$

while, similarly, the reflection coefficient seen looking into port 2 of the two-port network when port 1 is terminated by Z_S is

$$\Gamma_{OUT} = S_{22} + \frac{S_{12}S_{21}\Gamma_S}{1 - S_{11}\Gamma_S} \tag{56}$$

The power dissipated by the load is given by the difference between the incident and reflected power,

$$P_L = \frac{1}{2}|b_2|^2 - \frac{1}{2}|a_2|^2 \tag{57}$$

Similarly, the power delivered to the input of the two-port network is

$$P_{IN} = \frac{1}{2}|a_1|^2 - \frac{1}{2}|b_1|^2 \tag{58}$$

The power available from a source is defined as the power delivered by the source to a conjugate matched load. Thus, the power available from the source is given by

$$P_{AVS} = P_{IN}(\Gamma_{IN} = \Gamma_S^*) \tag{59}$$

The power available from the two-port network is the power delivered by the network to a conjugate matched load, that is

$$P_{AVN} = P_L(\Gamma_L = \Gamma_{OUT}^*) \tag{60}$$

Hereupon, the power gain definitions, which differ primarily in the way the source and the load are matched to the two-port device, can be defined. The operating power gain (or simply called power gain) is the ratio of the power dissipated in the load P_L to the power delivered to the input of the two-port network P_{IN}, and is independent of the source impedance Z_S [23, 60].

$$G_P = \frac{1}{1 - |\Gamma_{IN}|^2}|S_{21}|^2 \frac{1 - |\Gamma_L|^2}{|1 - S_{22}\Gamma_L|^2} \tag{61}$$

The available power gain is the ratio of the power available from the two-port network P_{AVN} to the power available from the source P_{AVS}, and depends on Z_S, but not Z_L [23, 60].

$$G_A = \frac{1 - |\Gamma_S|^2}{|1 - S_{11}\Gamma_S|^2} |S_{21}|^2 \frac{1}{1 - |\Gamma_{OUT}|^2} \tag{62}$$

The transducer power gain is the ratio of the power delivered to the load P_L to the power available from the source P_{AVS} [23, 60]. It depends on both Z_L and Z_S, and therefore it usually appears as function of either the input reflection coefficient (Equation 55),

$$G_T = \frac{1 - |\Gamma_S|^2}{|1 - \Gamma_S\Gamma_{IN}|^2} |S_{21}|^2 \frac{1 - |\Gamma_L|^2}{|1 - S_{22}\Gamma_L|^2} \tag{63}$$

or the output reflection coefficient (Equation 56),

$$G_T = \frac{1 - |\Gamma_S|^2}{|1 - S_{11}\Gamma_S|^2} |S_{21}|^2 \frac{1 - |\Gamma_L|^2}{|1 - \Gamma_L\Gamma_{OUT}|^2} \tag{64}$$

The transducer power gain equation can also be defined in a different fashion without the numeric dependence of either input or output reflection coefficients [59], which consists in

$$G_T = \frac{(1 - |\Gamma_S|^2)|S_{21}|^2(1 - |\Gamma_L|^2)}{|(1 - S_{11}\Gamma_S)(1 - S_{22}\Gamma_L) - S_{21}S_{12}\Gamma_S\Gamma_L|^2} \tag{65}$$

Whenever conjugate matching is verified at both the input and output with respect to the two-port network, then the gain is maximized and $G_P = G_A = G_T$ holds. In contrast to conjugate matching, a special case occurs when both the input and output are matched for no reflection ($\Gamma_S = \Gamma_L = 0$ holds), and therefore the transducer power gain reduces to $G_T = |S_{21}|^2$. Another special case arises when S_{12} is negligibly small, which is true for several devices, and therefore the transducer power gain is defined as unilateral.

Hereupon, it is of interest to mention the definition of gain employed in the cascaded noise equations of section 2.1 was the available power gain.

2.3.3 Noise Parameters

In terms of noise, an active two-port network, such as a transistor amplifier, is characterized by an equivalent noise resistance, R_N, and the minimum noise factor possible for the device, F_{min}, that is only achieved when a particular reflection coefficient, Γ_{opt}, is presented to the input of the two-port network. The quantities R_N, F_{min} and Γ_{opt} are characteristics of a particular transistor and are called the noise parameters of the device [23]. The noise parameters fully characterize the noise performance of a device for a specific set of conditions such as frequency, bias and temperature [59].

Thus, the noise factor of a noisy two-port network can be expressed as

$$F = F_{min} + \frac{4r_N\left|\Gamma_S - \Gamma_{opt}\right|^2}{(1 - |\Gamma_S|^2)\left|1 + \Gamma_{opt}\right|^2} \tag{66}$$

where r_N is the equivalent normalized noise resistance of the transistor (i.e. $r_N = R_N/Z_0$) and Γ_S is simply the source reflection coefficient. The following figure consists of a two-port network described by its noise parameters.

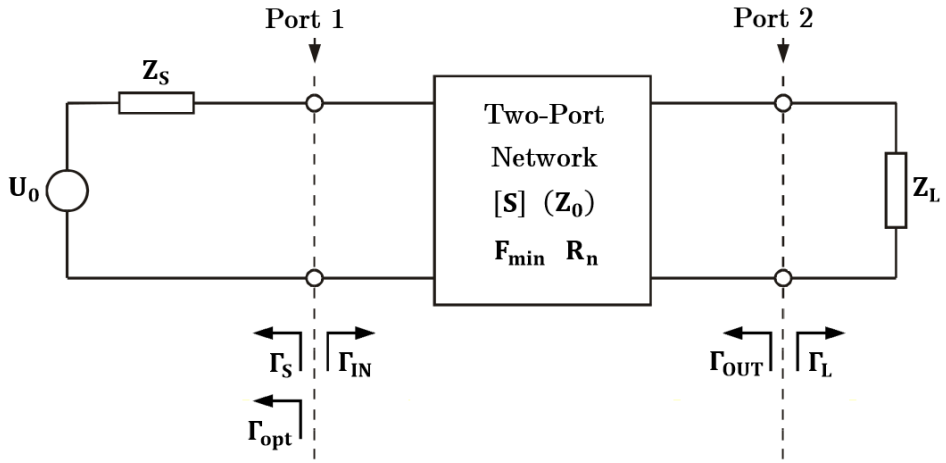

Figure 19: Noisy two-port network described by its noise parameters.

Equation 66 describes the noise performance of a transistor, which is independent of the load termination and is determined solely by its source termination and noise parameters of the device.

The noise parameters of a device may be given by its manufacturer or measured and derived experimentally by varying the source reflection coefficient [59]. The minimum noise factor F_{min} occurs when $\Gamma_S = \Gamma_{opt}$ and the rate at which the noise factor increases depends on the equivalent normalized noise resistance, r_N, which can be obtained by the noise factor value when the input is terminated by the characteristic impedance Z_0, as follows

$$r_N = \left(F_{\Gamma_S=0} - F_{min}\right)\frac{\left|1+\Gamma_{opt}\right|^2}{4\left|\Gamma_{opt}\right|^2} \tag{67}$$

2.4 Low-Noise Amplifier Design

In the design of any microwave transistor amplifier there are three distinct approaches according with the desired performance: high gain, low noise figure and high output power [16]. Appropriate matching networks set the specific performance of the transistor by establishing the required load and source impedances at the device ports. The stability of a transistor, or its resistance to oscillate, is also an important consideration in the design, and depends on the scattering parameters of the device, the matching networks and the respective terminations. The general circuit diagram used in the design of a microwave amplifier is represented in the figure below.

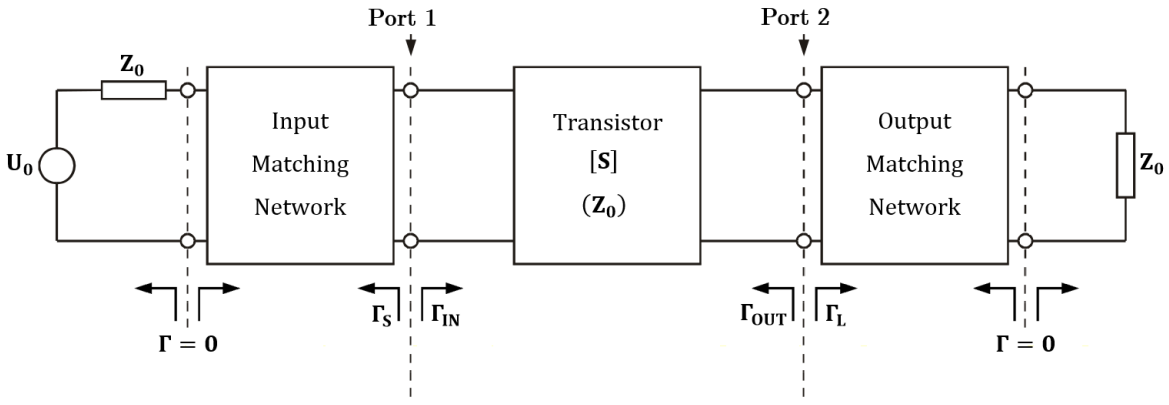

Figure 20: The general transistor amplifier circuit [40].

A LNA typically requires a compromise between gain and noise figure [22]. As long as the input signal power is low enough so that the device can be assumed to operate as a linear device, it is considered a small-signal amplifier. In the following sections stability is discussed along with the matching methods for maximum gain and low noise figure.

2.4.1 Stability Considerations

Oscillations are possible if either the input or output port impedances of a two-port network present a negative resistance, which occur when $|\Gamma_{IN}| > 1$ or $|\Gamma_{OUT}| > 1$, respectively. Stability contemplates two cases: unconditional and conditional stability. The first applies if $|\Gamma_{IN}| < 1$ and $|\Gamma_{OUT}| < 1$ are satisfied for all passive load and source impedances, i.e. $|\Gamma_L| < 1$ and $|\Gamma_S| < 1$. Thus, all passive terminations provide a stable behavior for an unconditionally stable two-port network. The second applies if $|\Gamma_{IN}| < 1$ and $|\Gamma_{OUT}| < 1$ are satisfied only for a certain range of passive load and source impedances. Thus, certain passive terminations may cause unstable behavior in a conditionally stable two-port network producing oscillations, and therefore this case is also referred to as potentially unstable.

The stability condition of an active two-port network is frequency dependent since the input and output matching networks generally depend on frequency as well as the scattering parameters of the device, which also depend on the bias conditions, and so a transistor is possible to be stable at its design frequency but unstable at other frequencies. An unconditional stable approach should require an unconditionally stable two-port network at all frequencies in order to guard against unexpected oscillations [59]. A conditional stable approach, however, requires extreme care to guarantee that a source or load termination that causes an oscillation is never presented to the device. This applies to all frequencies in-band and out-of-band.

Two-port stability is analyzed using either a graphical or numerical method [59]. The inequalities $|\Gamma_{IN}| < 1$ and $|\Gamma_{OUT}| < 1$ define a range of values for Γ_L and Γ_S where the device will be stable. This range is established by stability circles plotted on a Smith chart that define the boundaries between stable and potentially unstable

regions of Γ_L and Γ_S. The locus in the Γ_L plane for which $|\Gamma_{IN}| = 1$ is defined as the output stability circle with center

$$C_L = \frac{(S_{22} - \Delta S_{11}^*)^*}{|S_{22}|^2 - |\Delta|^2} \tag{68}$$

and radius

$$r_L = \left|\frac{S_{12}S_{21}}{|S_{22}|^2 - |\Delta|^2}\right| \tag{69}$$

while the locus in the Γ_S plane for which $|\Gamma_{OUT}| = 1$ is defined as the input stability circle with center

$$C_S = \frac{(S_{11} - \Delta S_{22}^*)^*}{|S_{11}|^2 - |\Delta|^2} \tag{70}$$

and radius

$$r_S = \left|\frac{S_{12}S_{21}}{|S_{11}|^2 - |\Delta|^2}\right| \tag{71}$$

where $\Delta = S_{11}S_{22} - S_{12}S_{21}$ is defined as the determinant of the scattering matrix.

The stable region of the Smith chart is identified by checking if its center is a stable operating point, which means that all of the Smith chart that is exterior to the stability circle defines the stable region. On one hand, if $|S_{11}| < 1$ ($|S_{22}| < 1$) when $Z_L = Z_0$ ($Z_S = Z_0$) then $|\Gamma_{IN}| < 1$ ($|\Gamma_{OUT}| < 1$) when $\Gamma_L = 0$ ($\Gamma_S = 0$) and the center of the Smith chart represents a stable operating point. On the other hand, if $|S_{11}| > 1$ ($|S_{22}| > 1$) when $Z_L = Z_0$ ($Z_S = Z_0$) then $|\Gamma_{IN}| > 1$ ($|\Gamma_{OUT}| > 1$) when $\Gamma_L = 0$ ($\Gamma_S = 0$) and the center of the Smith chart represents an unstable operating point. Stability is illustrated in the following two consecutive figures.

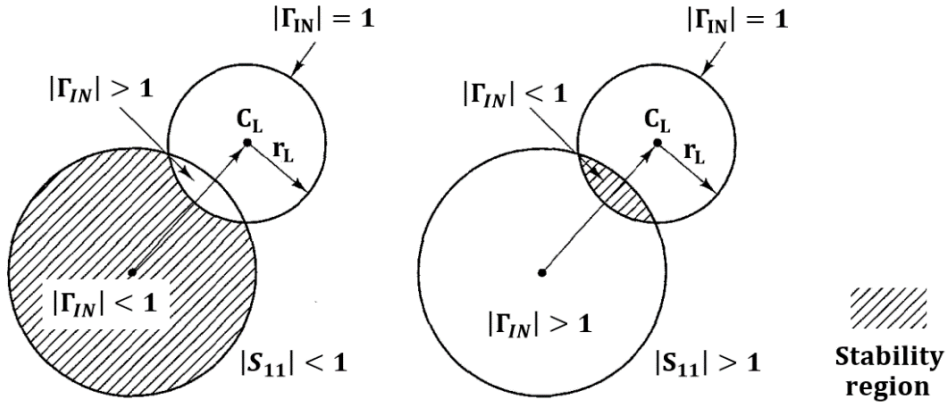

Figure 21: Stable and unstable regions in the Γ_L plane [23].

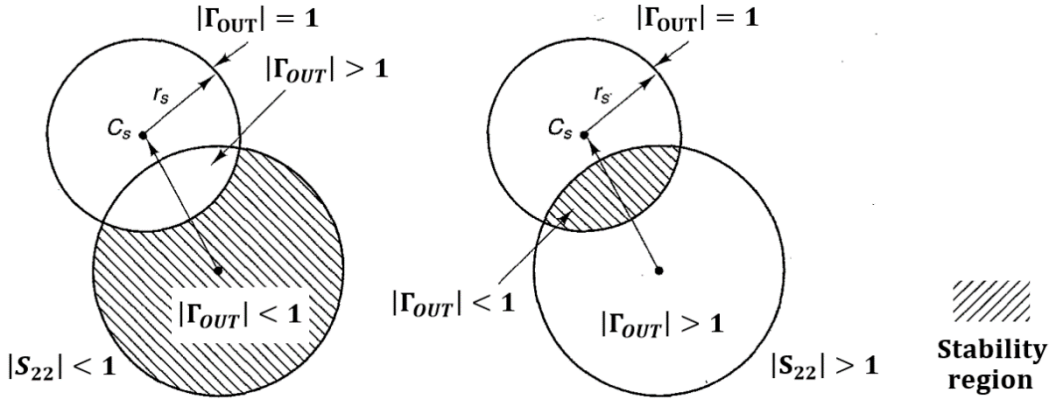

Figure 22: Stable and unstable regions in the Γ_S plane [23].

Unconditional stability imposes the stability circles to fall completely outside (or totally enclose) the Smith chart for $|S_{11}| < 1$ (output stability circle) and $|S_{22}| < 1$ (input stability circle). Under these circumstances, the conditions for unconditional stability for all passive source and load impedances are expressed as $\big||C_L| - r_L\big| > 1$ and $\big||C_S| - r_S\big| > 1$ [23].

The scattering parameters of a device also allow a numerical analysis in order to conclude about its unconditional stability. A set of stability equations, in function of the two-port S parameters, may be defined as follows

$$K = \frac{1 - |S_{11}|^2 - |S_{22}|^2 + |\Delta|^2}{2|S_{12}S_{21}|} \tag{72}$$

$$|\Delta| = |S_{11}S_{22} - S_{12}S_{21}| \tag{73}$$

$$B_1 = 1 + |S_{11}|^2 - |S_{22}|^2 - |\Delta|^2 \tag{74}$$

$$B_2 = 1 + |S_{22}|^2 - |S_{11}|^2 - |\Delta|^2 \tag{75}$$

The two-port network, in order to achieve unconditional stability, must satisfy the Rollet's condition $K \geq 1$ and either inequality $|\Delta| < 1$, $B_1 > 0$ or $B_2 > 0$. If either $|\Delta| < 1$, $B_1 > 0$ or $B_2 > 0$ is satisfied, all three conditions are, by definition, satisfied. Therefore, when one of these inequalities is also met along with the Rollet's condition, two necessary and sufficient conditions for unconditional stability are obtained [59]. This test involves constraints on two separate parameters.

Alternatively, a test involving only a single condition consists in calculating one of the following equations.

$$\mu_{source} = \frac{1 - |S_{11}|^2}{|S_{22} - \Delta S_{11}^*| + |S_{12}S_{21}|} \tag{76}$$

$$\mu_{load} = \frac{1 - |S_{22}|^2}{|S_{11} - \Delta S_{22}^*| + |S_{12}S_{21}|} \tag{77}$$

Hereupon, the necessary and sufficient condition for unconditional stability consists in either $\mu_{source} \geq 1$ or $\mu_{load} \geq 1$. If $\mu_{source} \geq 1$ then, by definition, $\mu_{load} \geq 1$ and vice versa [59].

If the device scattering parameters do not satisfy any of these tests, the device is not unconditionally stable, and stability circles must be used to determine the stable regions for Γ_S and Γ_L.

2.4.2 Gain Match

Maximum power gain is accomplished when the matching networks provide a simultaneous conjugate match between the transistor and the source and load impedances of the amplifier. Thus, maximum power gain transfer from the input matching network to the transistor will occur when $\Gamma_{IN} = \Gamma_S^*$ and from the transistor

to the output matching network will occur when $\Gamma_L^* = \Gamma_{OUT}$. With the assumption of lossless matching networks along with the matching of the input and output ports of the amplifier to the characteristic impedance of the system, the overall transducer power gain is maximized.

The general case of gain match implies a bilateral device, so the input and output matching networks must be matched simultaneously [23]. The required values of Γ_S and Γ_L for a simultaneous conjugate match are

$$\Gamma_{MS} = \frac{B_1 \pm \sqrt{B_1^2 - 4|C_1|^2}}{2C_1} \tag{78}$$

and

$$\Gamma_{ML} = \frac{B_2 \pm \sqrt{B_2^2 - 4|C_2|^2}}{2C_2} \tag{79}$$

where the coefficients B_1 and B_2 are given by Equations 74 and 75, respectively. The remaining coefficients are defined as $C_1 = S_{11} - \Delta S_{22}^*$ and $C_2 = S_{22} - \Delta S_{11}^*$. Thus, in the design of an amplifier for maximum gain, the purpose is to transform the input and output terminations with Γ_1 and Γ_2 to the conjugately matched counterparts of the device Γ_{MS} and Γ_{ML}.

The condition that a device can be simultaneously matched with $|\Gamma_{MS}| < 1$ and $|\Gamma_{ML}| < 1$ is $K > 1$. If the device is unconditional stable, the maximum transducer gain can be simply rewritten as follows

$$G_{T,max} = \left|\frac{S_{21}}{S_{12}}\right| \left(K - \sqrt{K^2 - 1}\right) \tag{80}$$

and is also called the maximum available gain (MAG) since under simultaneously conjugate match $G_T = G_P = G_A$ holds.

If the device is potentially unstable $G_{T,max}$ does not exist, however a minimum value of the transducer power gain can be defined when $K > 1$ and $|\Delta| > 1$ as

$$G_{T,min} = \left|\frac{S_{21}}{S_{12}}\right| \left(K + \sqrt{K^2 - 1}\right) \tag{81}$$

In the same context of conditional stability, a maximum value of transducer power gain with $K = 1$ can be defined as

$$G_{MSG} = \left|\frac{S_{21}}{S_{12}}\right| \tag{82}$$

and is called the maximum stable gain (MSG).

Usually, the maximum power gain procedure obtains a narrowband result and in order to improve bandwidth or because a specific value of transducer power gain below the maximum possible is required, mismatches are purposely introduced to reduce the overall gain [23]. Thus, a family of circles that provide a specific amount of mismatch at the device input (available power gain circles) and a family of circles that provide a specific amount of mismatch at the device output (operating power gain circles) are constructed and plotted on the Smith chart.

The method of the operating power gain circles is similar to that of the available power gain circles, and therefore only one of them is presented in this section. For low-noise amplifier design, the available power gain design approach is typically performed [31]. If the output of a device is conjugately matched, which mathematically yields $\Gamma_L = \Gamma_{OUT}^*$, for a given source termination the transducer power gain as given by Equation 64 reduces to the available power gain as given by Equation 61. The latter along with Equation 56 to express the output of the device in terms of the source reflection coefficient yields

$$G_A = \frac{(1 - |\Gamma_S|^2)|S_{21}|^2}{|1 - S_{11}\Gamma_S|^2 \left(1 - \left|\frac{S_{22} - \Delta\Gamma_S}{1 - S_{11}\Gamma_S}\right|^2\right)} \tag{83}$$

An available power gain circle with a particular constant value of gain may be constructed with a center given by

$$C_A = \frac{g_A C_1^*}{1 + g_A(|S_{11}|^2 - |\Delta|^2)} \tag{84}$$

and a radius that consists in

$$r_A = \frac{(1 - 2K|S_{12}S_{21}|g_A + |S_{12}S_{21}|^2 g_A^2)^{\frac{1}{2}}}{1 + g_A(|S_{11}|^2 - |\Delta|^2)} \tag{85}$$

where $C_1 = S_{11} - \Delta S_{22}^*$ and $g_A = G_A/|S_{21}|^2$.

2.4.3 Noise Match

The minimum noise factor is solely obtained when the input matching network that terminates the transistor provides the optimum reflection coefficient for the best achievable noise match, i.e. $\Gamma_S = \Gamma_{opt}$. As the source termination departs from Γ_{opt} the noise factor degrades. Thus, a family of constant noise circles can be plotted in the Γ_S plane, where each contour yields a specific noise performance for a particular source termination. The constant noise factor circles are plotted by first locating the center of a particular circle using

$$C_{F_i} = \frac{\Gamma_{opt}}{1 + N_i} \tag{86}$$

and the radius of each noise circle using

$$r_{F_i} = \frac{1}{1 + N_i}\sqrt{N_i^2 + N_i(1 - |\Gamma_{OUT}|^2)} \tag{87}$$

where the noise parameter, N_i, is calculated for various noise factors, F_i, as

$$N_i = \frac{F_i - F_{min}}{4r_N}\left|1 + \Gamma_{opt}\right|^2 \tag{88}$$

which is a constant for a given noise factor and set of noise parameters.

Maximum gain and minimum noise figure seldom occur at the same impedance state [20]. On one hand, enhanced noise performance is achieved with a source termination closer to the optimum noise termination Γ_{opt} at the expense of gain while on the other hand improved gain results occur when the source

termination is closer to the required value of Γ_S for a simultaneous conjugate match, i.e. Γ_{MS}. Thus, plotting available gain circles along with noise contours allows to establish a trade-off between gain and noise figure by inserting purposely a mismatch at the input providing neither optimum noise nor maximum gain whereas the output is perfectly matched for the best achievable gain associated with a specific source termination.

At this point, the fundamental concepts of LNA design have been exposed and explained. The knowledge within this chapter allowed the design of the building blocks of the LNA proposed, which in turn will be presented in the following chapter.

Chapter III

3 Design and Simulation

The design of the LNA was carried out in a phased approach. A step-by-step procedure was followed starting by the selection of components. Thereafter, the design and simulation of the amplifier's building blocks – direct current (DC) block, transistor (bias networks included) and matching sections – took place.

The design of the amplifier and respective simulations were developed within a computer aided circuit design software for radio-frequency (RF) and microwave applications called Advanced Design System (ADS) from Keysight Technologies (former Agilent Technologies).

3.1 Two-Stage Low-Noise Amplifier Design Method

The design of a two-stage LNA implies the optimization of the overall noise figure. When compared to a single-stage LNA, the challenge in a two-stage design arises due to the interstage matching, which plays an important role in the bandwidth as well as the gain of the amplifier. Thus, two methods were used for interstage matching (as seen in [15]): in a first approach, both the output impedance of the first stage and the input impedance of the second stage were matched to the characteristic impedance of the system, i.e. two separated single-stages cascaded through a DC block; in a second approach, the output impedance of the first stage and the input impedance of second stage were conjugated into each other through a DC block at the input of the second stage.

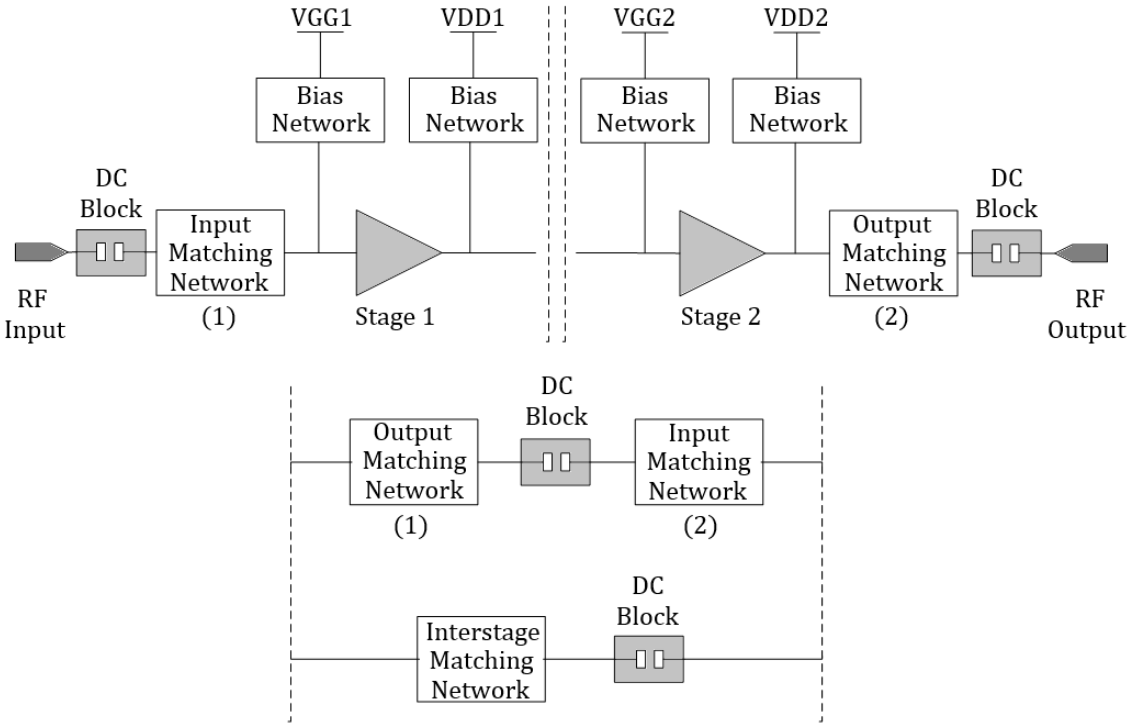

Figure 23: Two-stage amplifier design: interstage matching techniques.

Another aspect of designing an amplifier is connected to the design of the matching networks. At high frequencies, the parasitic elements in lumped components usually cannot be controlled, and additionally the device response may not be characterized at such frequencies. Thus, distributed components are more reliable than discrete components in the design of matching networks at higher frequencies. The microstrip technology was chosen for this microwave circuit.

3.2 Components Selection

3.2.1 Printed-Circuit-Board

Printed-Circuit-Board (PCB) materials play a major role in the design of an amplifier. Gain, stability and output power can be improved by selecting an optimum substrate material for an amplifier [18].

RT/Duroid 5880 high frequency laminates from Rogers Corporation (see [62]), which are polytetrafluoroethylene composites reinforced with glass microfibers,

were available for this work. The substrate material has a low permittivity with a relative dielectric constant (ε_r) of 2.20 and a tolerance of ± 0.02 providing an excellent isolation for low-frequency signals, particularly when dense circuits with closely spaced conductive lines are employed. The RT/Duroid 5880 has a low dissipation factor ($\tan\delta$) of 0.0009 measured at 10 GHz. The low dielectric loss make this laminate well suited for the design of an X-band LNA since losses need to be minimized.

The RT/Duroid 5880 offers different standard thicknesses of copper cladding (T) on the surface of the dielectric material, which in turn has also available different standard thicknesses (H).

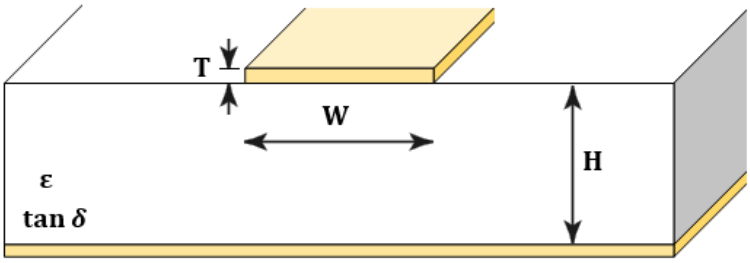

Figure 24: Substrate Parameters.

The available sample had a standard thickness of 0.508 mm and a copper cladding thickness of 35 µm. The copper conductors, which have an electrical conductivity of 5.88×10^7 S/m, could have a minimum width and length of 0.2540 mm, a minimum separation of 0.2032 mm and a maximum resolution of 0.01 mm in all dimensions (width, length and separation) due to the available technology offered by the selected circuit manufacturer for this work (see [17]).

3.2.2 Active Device Selection

The selection of the transistor is the crucial step in LNA design and will depend on the specifications we are attempting to meet [20]. The selected device should have specifications that should yield a design with the desired performance. The most important features in selecting a low-noise transistor are the operating frequency, minimum intrinsic noise figure and resultant maximum associated gain,

maximum available gain, and linearity. The choice of the transistor determines the ultimate performance of an amplifier since after adding the biasing and matching sections, neither we can achieve more gain than the specified maximum available, nor less noise figure than the specified minimum.

An aspect of high importance during the active device selection procedure is whether or not a small-signal model including noise performance and a large-signal model exist for the chosen low-noise transistor. The small-signal model consists in the measured scattering and noise parameters for a specific bias condition, characteristic impedance, substrate and device placement with well-defined measurement reference planes. The large-signal model, also known as nonideal model, tries to model the real device and represents its operation.

Several manufacturers produce high performance transistors that are suitable for this particular design. Some transistors were selected as candidates for the LNA design by inspection of corresponding data sheets as given by the manufacturer. Many devices were quickly eliminated since neither measured data was available from the particular manufacturer in electronic form nor a nonlinear model compatible with ADS. Thus, the MGF4937AM from Mistubishi Electric (see [46]), which is an indium gallium arsenide (InGaAs) transistor, was chosen. Both small-signal and large-signal models were available for the selected device. A two-stage LNA may be built by either using the same transistor for both stages or using two different devices. Therefore, a very similar device to the MGF4937AM in terms of performance was additionally selected: the MGF4941AL (see [47]).

The MGF4937AM was the first choice for this work due to its superior performance and is the one that will play the main role on the design. Thus, the procedures for the design of the amplifier involving the MGF4937AM will be exposed in the following sections. Since both the selected transistors are very similar, the procedure for the MGF4937AM is taken as understood for the MGF4941AL.

3.2.3 Passive Devices

Like in any amplifier, there are roles to be played by passive devices, such as capacitors and resistors, even when the goal of the design is to use distributed elements for both the matching and bias networks. Inductors were not an option since the commercially available discrete inductors were not characterized for the required frequency range covered by this work.

Generally, passive devices are used in both the signal and bias paths of an amplifier. On the former case, they may provide DC blocking or stabilization while on the latter case, they belong to the bias networks providing low-frequency bypassing and additionally preventing instabilities from occurring. In terms of stability, such components are not selected before knowing the behavior of the selected transistor.

Due to the component assembly procedure, only surface mount devices (SMD) were considered and all selected passive devices were constrained to the code sizes 0603 or 0805 (imperial nomenclature).

3.3 DC Block Design

A DC blocking application implies placing a component in series with a transmission line to prevent the DC voltage from one circuit from affecting another [10]. A component for this purpose is best selected so that its impedance is as low as possible at the frequency of interest, i.e. at the amplifier passband. In simple terms, an ideal DC block should provide an open circuit at DC and a short circuit at the operating frequency. This goal can be achieved either by the use of discrete passive devices, such as capacitors, or by the simple use of the selected substrate by implementing microstrip components, such as parallel coupled-line filters, interdigital capacitors, metal-insulator-metal (MIM) capacitors or gap capacitors. For this work, a capacitor was selected and a parallel coupled-line filter was implemented.

An extremely careful selection of a DC blocking component must be taken when designing a LNA since the first DC block will be the nearest component to the input, and thus it will have a dominant effect on the overall noise figure of the amplifier.

3.3.1 Capacitor

Ideally, the impedance magnitude of a series capacitor will vary from infinite (open circuit) at DC to zero (short circuit) at infinite frequency. However, the existence of parasitic elements results in a nonideal response. A capacitor, as a practical device, contains parasitic elements that are important at microwave

frequencies, and thus exhibits not only capacitance but also resistance and inductance [10, 26]. The equivalent model of a microwave capacitor is shown below.

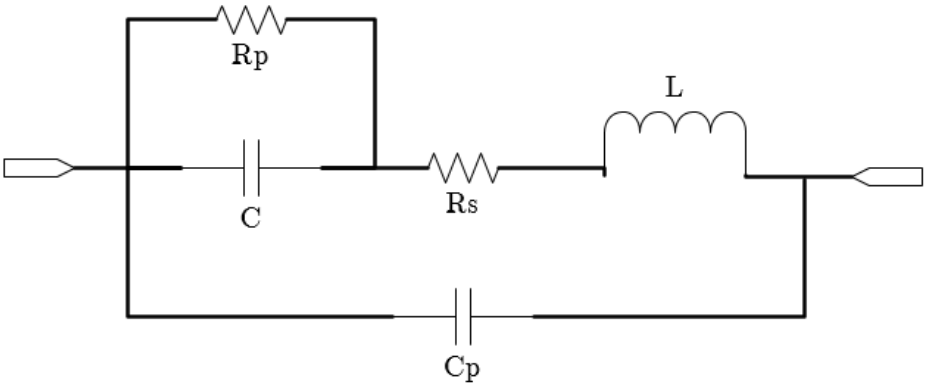

Figure 25: Equivalent circuit of a microwave capacitor.

The desired capacitance C, corresponds to the nominal value of the component and is typically determined by a measurement at a test frequency where the effects of the parasitic elements become negligible. This primary capacitance is shunted by a very high value resistance R_p, which is of concern only at DC and low frequencies, that represents the insulation resistance or leakage. The leads and plates of the capacitor present an equivalent series resistance (ESR) and an equivalent series inductance (ESL) modeled by the resistance R_s and the parasitic inductance L, respectively. The parasitic parallel capacitance C_p, which has a very small value, only affects the response of the component at really high frequencies.

There is a frequency known as the series resonant frequency (SRF) that occurs when the reactance of the parasitic inductance equals that of the capacitor and the device appears as a small resistor with the lowest insertion loss possible for the device [22]. Well beyond the SRF, there is a frequency much higher than the SRF called the parallel resonant frequency (PRF) that occurs when the reactance of the parasitic inductance equals that of the parallel capacitor and the device appears as a large resistor with a high insertion loss [6, 29].

A capacitor for a DC blocking application should have an SRF falling within the operating passband since the best performance in terms of low insertion loss is obtained near the SRF. The selected capacitor was a thin-film chip capacitor with the ACCU-P technology from AVX Corporation (see [11]). The selection was carried out by considering different parameters as the SRF and the required case size by

inspection of datasheets. Thereafter, a simulation was done, with the nonideal model from the manufacturer, in order to check the behavior of the device and its impedance near the SRF. The following figures show that performance.

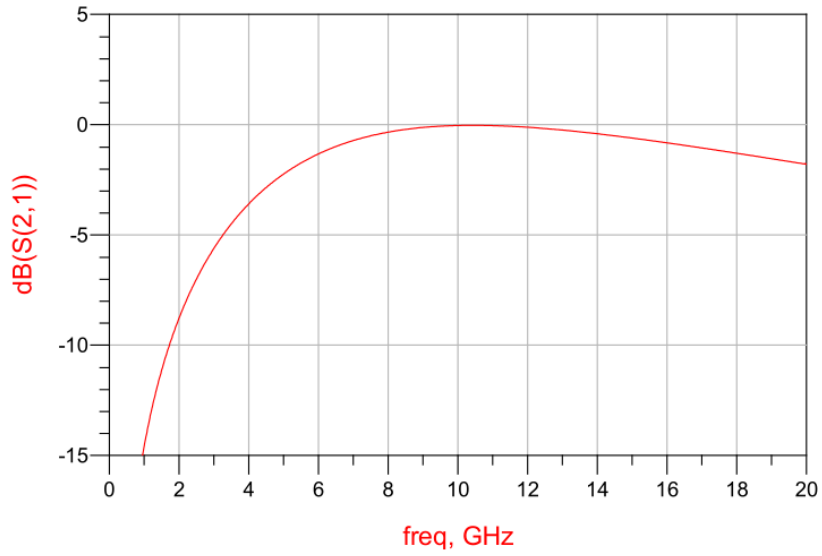

Figure 26: Insertion loss of the selected capacitor.

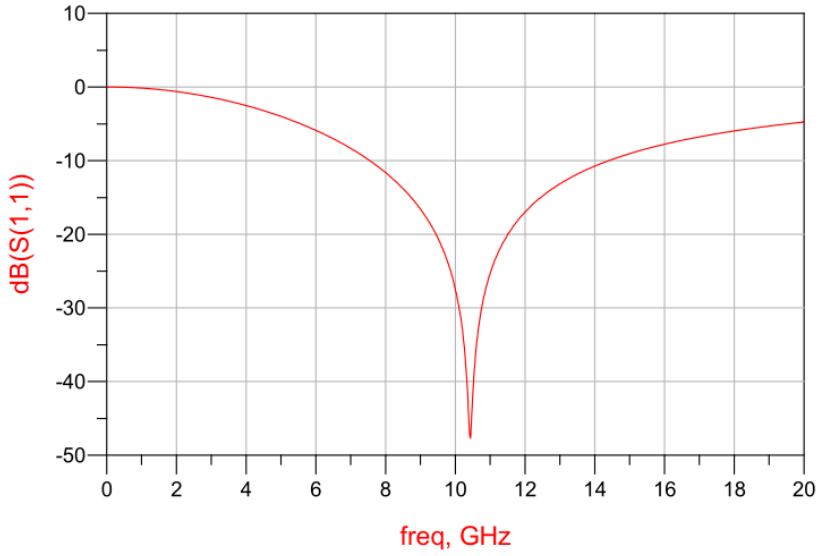

Figure 27: Return loss of the selected capacitor.

Figure 28: Magnitude of impedance of the selected capacitor.

3.3.2 Parallel Coupled-Line Filter

A parallel coupled-line filter was also implemented by making use of the concept of a low insertion loss bandpass filter [50]. To obtain a simple and symmetric design, three degrees of freedom were available: parallel coupled-lines length and width, and gap between them. In order to satisfy the low insertion loss requirement, a small width value was selected, and therefore the impedance of each of the parallel coupled-lines was higher than the system characteristic impedance. Thus, impedance steps were needed and discontinuities would arise. A discontinuity in microstrip is caused by an abrupt change in geometry of the strip conductor, and causes a modification of the electric and magnetic field distributions. To reduce this effect, tapers were implemented in order to smooth the impedance step. The implemented coupled-line filter is shown below.

Figure 29: Parallel coupled-line filter.

Additionally, an electromagnetic simulation was carried out and the respective model was obtained and used in the remainder of the amplifier design and simulation.

The following figure compares the performance obtained via simulation of the schematic with the performance obtained via EM simulation.

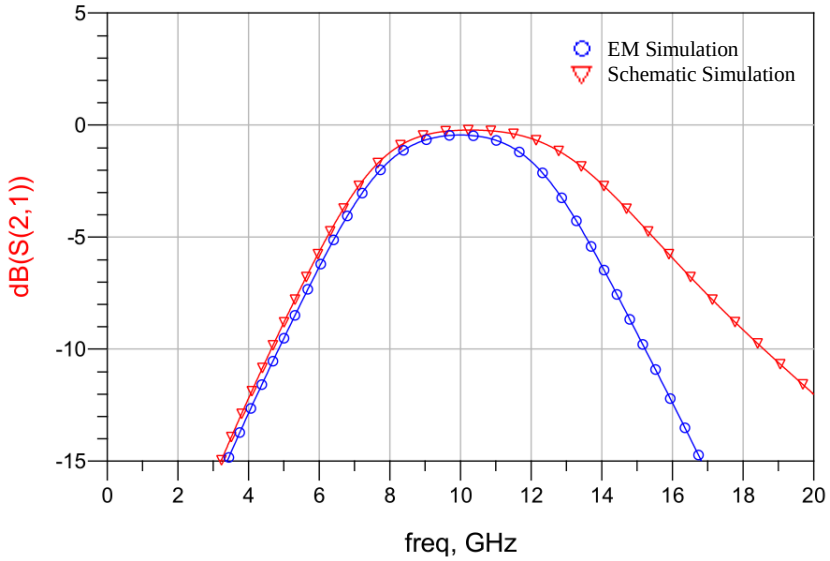

Figure 30: Insertion loss of the parallel coupled-line filter.

3.4 Transistor Analysis

3.4.1 Model Validation

The design of a LNA can be accomplished by making use of either the large-signal model or the small-signal model. The ideal case is when the large-signal model is used to represent the device. Unfortunately, the nonideal model sometimes produce neither accurate scattering parameters nor noise data. However, it is useful for DC simulations. The most accurate case is when the small-signal model, obtained via measurement at specific conditions, is used to represent the device. This model is created by loading the measured scattering parameters and the noise data as given by the manufacturer into the ADS. Since it has fixed biasing, no DC simulations will be possible with this model, but it will characterize the scattering parameters and noise data accurately.

Since both small-signal and large-signal models for the selected transistors (MGF4937AM and MGF4941AL) were available, a quick validation within the ADS was possible and recommended. Thus, the fixed bias of the small-signal models should be applied as external bias to the nonideal models. The selected bias scheme was an ideal bias network composed by a DC feed inductor in series with the bias path followed by a RF bypass capacitor in shunt with the bias path. The validation was carried out by comparing the scattering parameters (Figure 31) and the noise parameters (Figure 32) of both models.

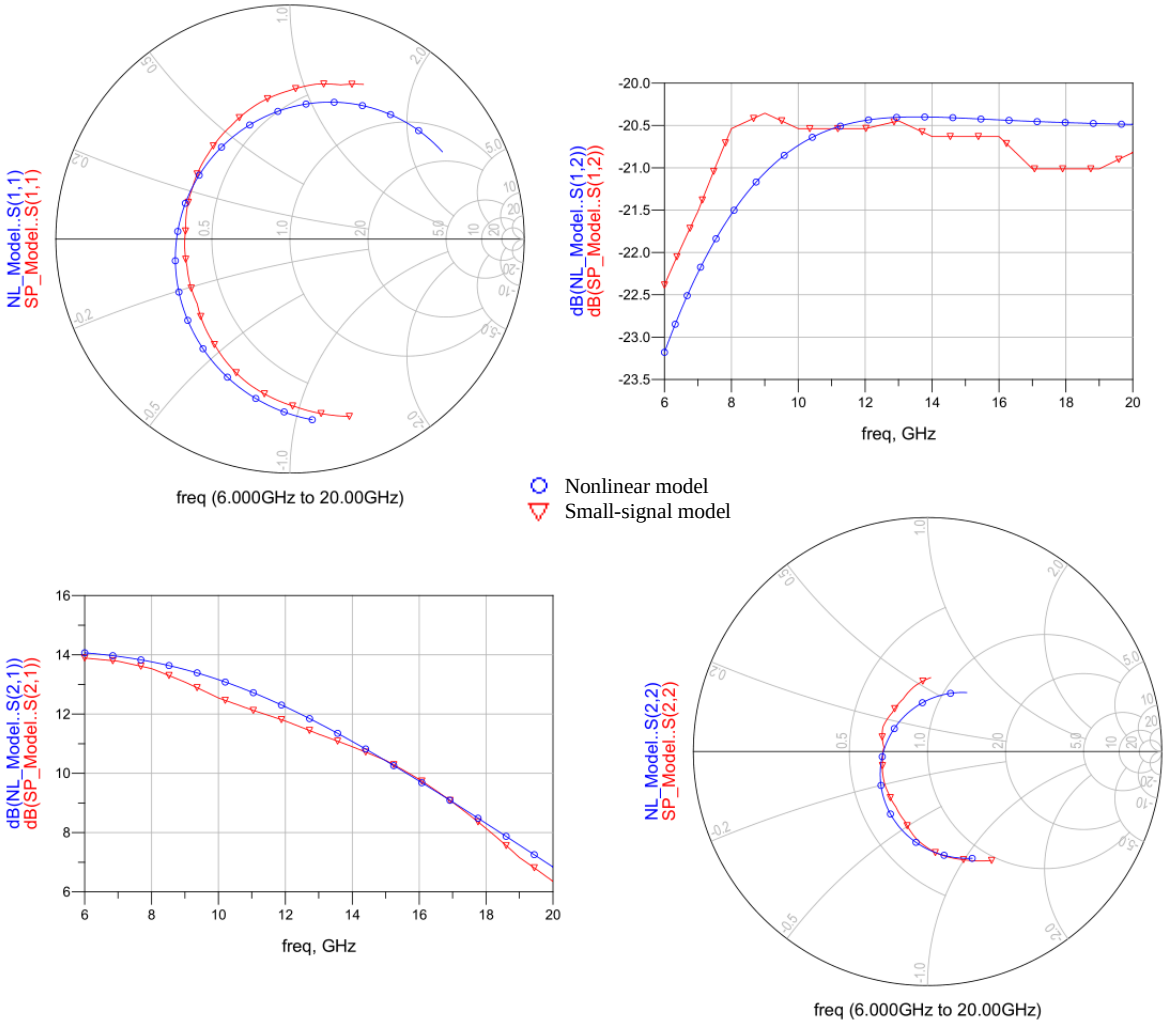

Figure 31: Scattering parameters validation for the MGF4937AM.

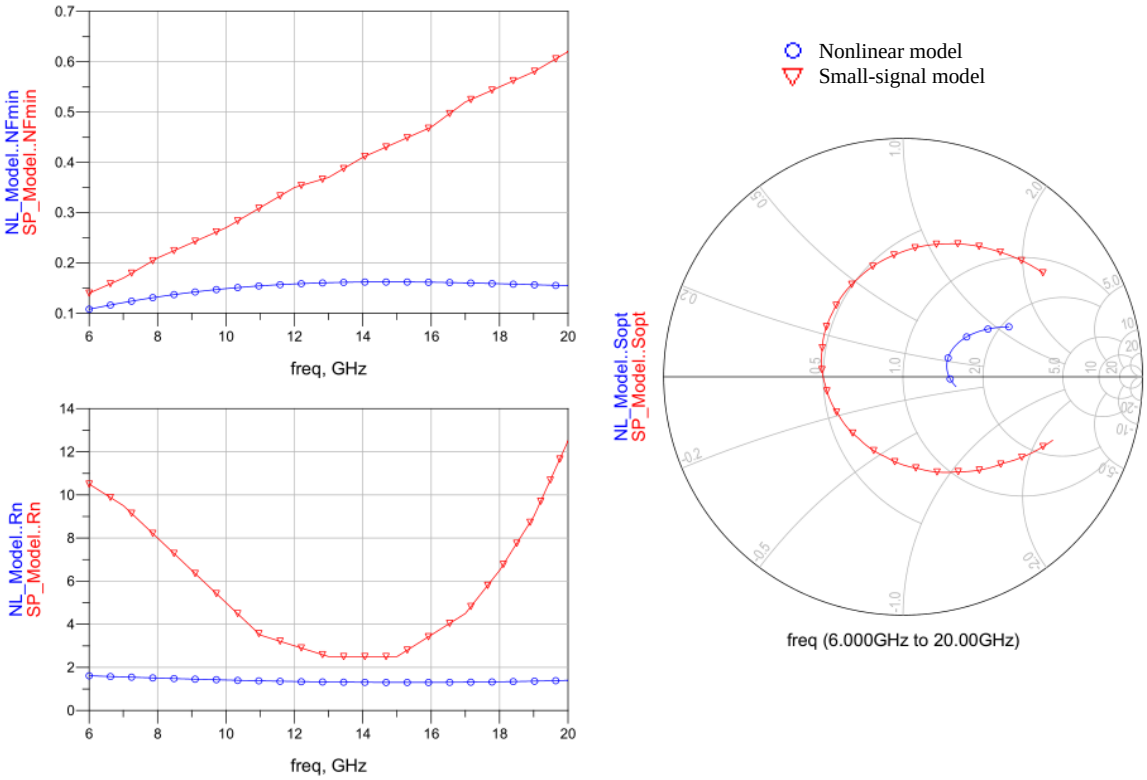

Figure 32: Noise data validation for the MGF4937AM.

On one hand, by analyzing Figure 31, the nonideal model of the MGF4937AM can minimally characterize the device according with the measured scattering parameters by the manufacturer. On the other hand, in terms of noise data we can notice the nonideal model is poor by observing Figure 32, and therefore its use for the design of matching networks is not recommended (especially for the input matching network). Similar conclusions were obtained with the validation of the nonideal model of the MGF4941AL.

Hereupon, the nonideal model would be exclusively used for the DC simulations while the measured scattering parameters and noise data would be used for the design of the matching networks. This procedure is constrained to the fixed bias conditions given by the manufacturer within the small-signal model. In general, for an accurate LNA design, this is the method adopted.

3.4.2 DC Bias Networks

A bias circuit is required by any transistor in order to set the correct operating point for a particular performance. A careful selection of a bias point allows finding

the best compromise between gain, noise figure and linearity for any given application [20]. However, due to what was mentioned in the previous section, the bias point is already fixed as the recommended operating point given by the manufacturer since a small-signal model approach was chosen.

A bias circuit requires a low DC resistance for biasing the transistor but a high RF resistance to ensure that the circuit is not loaded and signals do not flow onto the supply lines. A commonly used biasing scheme in microwave applications uses a radial stub immediately after a quarter-wave high impedance line (as seen in [1, 56]). The radial stub places a low impedance (ideally would be a short circuit) on one end of the quarter-wave high impedance line, which in turn transforms it into a high impedance (ideally would be an open circuit) on the other end, choking high frequency signals from the signal path while passing low frequency signals. The radial stub also shorts out to the ground any high frequency leakage that may enter through the quarter-wave high impedance line. This helps to achieve proper isolation of the DC supply from the in-band signals at the desired frequency, no matter what component is added after the quarter-wave bias line. Additionally, DC bypass capacitors are placed close to the DC supply in order to short any unwanted low frequency signals to the ground, especially signals from the voltage supply rail [9]. The biasing scheme used took the previous considerations into account and is presented in the figure below.

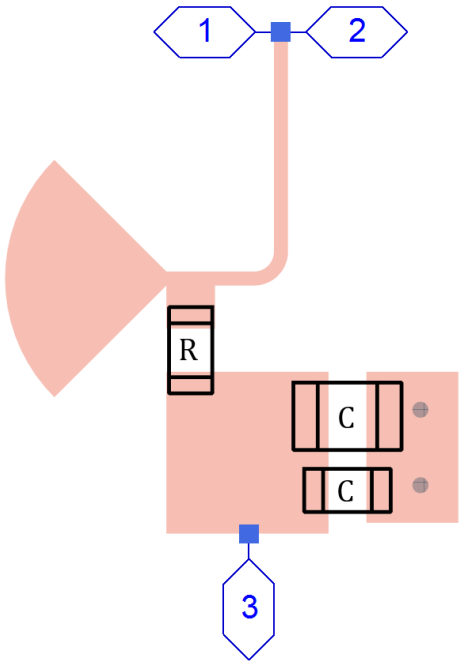

Figure 33: Biasing scheme.

At very low frequencies, microwave transistors have high gain and the quarter-wave transformer appears as a short circuit, so the DC bypass capacitors may apply a short circuit to the transistor causing instability [56]. In order to kill low frequency gain and improve stability, a small resistance was added as shown in Figure 33. This effect is more significant at the input of the transistor than at the output.

The performance of the bias network is shown below.

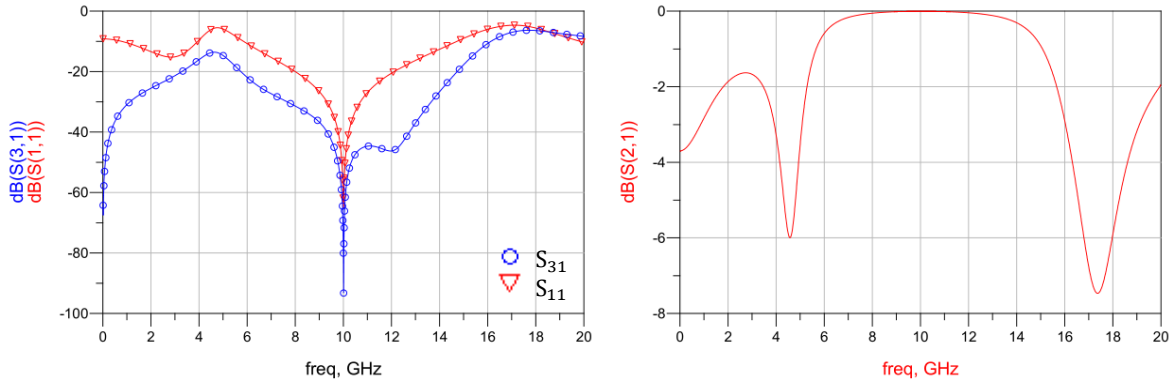

Figure 34: DC bias network performance.

3.4.3 Stability Check and Enhancement

The integration of a device in a design is verified in terms of stability. As already discussed, there are two approaches in terms of stability: unconditional or conditional. A two-stage LNA already imposes limits in the selection of the reflection coefficients due to the trade-offs mainly between gain and noise figure, and a potentially unstable approach would reduce even more our freedom in this selection since there would be unstable regions to avoid. Thus, unconditional stability of the LNA is required and this means that the circuit will not become unstable, i.e. will not oscillate, with any load presented either to the input or to the output of the device.

Both the candidates for the design were potentially unstable within the operating passband of the amplifier and unconditional stability was forced by stabilizing the transistor with a proper technique [39]. The selected method was an output filter matching for the frequency range of interest as shown in the following figure.

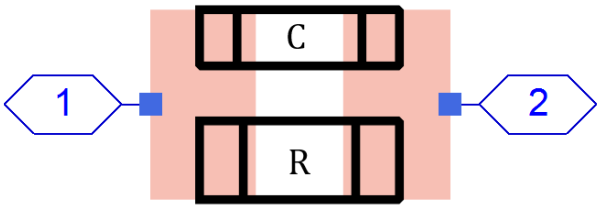

Figure 35: Stabilization network.

The bandpass of the stabilization network is within the amplifier's range of interest, as shown by its response in the figure below.

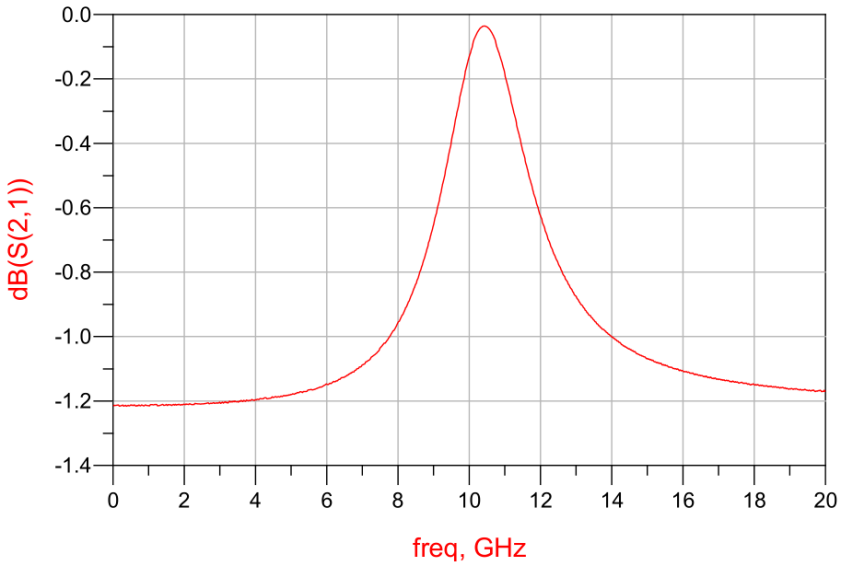

Figure 36: Stabilization network response.

This method implies resistive loading at the output to improve the stability in-band and out-of-band. At the frequency of interest, the gain and noise figure are not as degraded as they would be with a simple load resistor since the selected capacitor was the same as the one used for DC block, and therefore the loading will be the minimum necessary for stability near the operating passband. Additionally, the resistors of the bias networks also play their role in slightly improving the stability of the amplifier.

At this point, the DUT for design is composed by the transistor, the bias networks and the stabilization network, as it can be seen by the following figure.

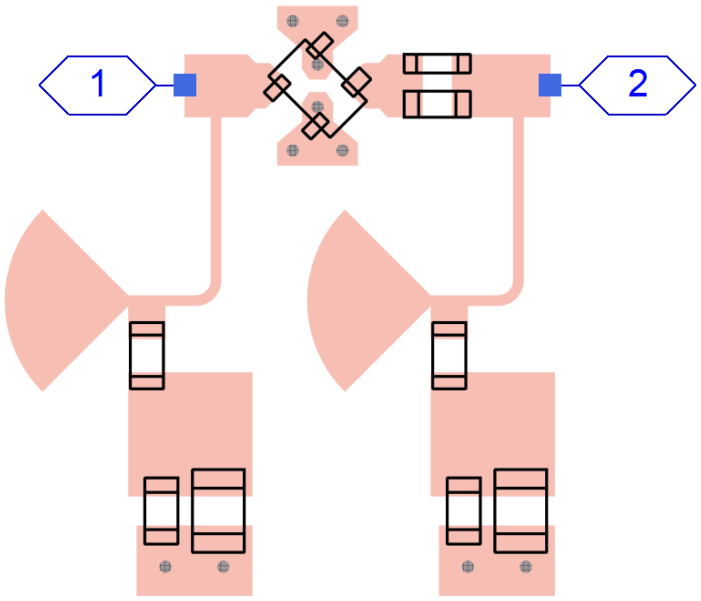

Figure 37: DUT for design (MGF4937AM).

The performance of the DUT for design is presented below.

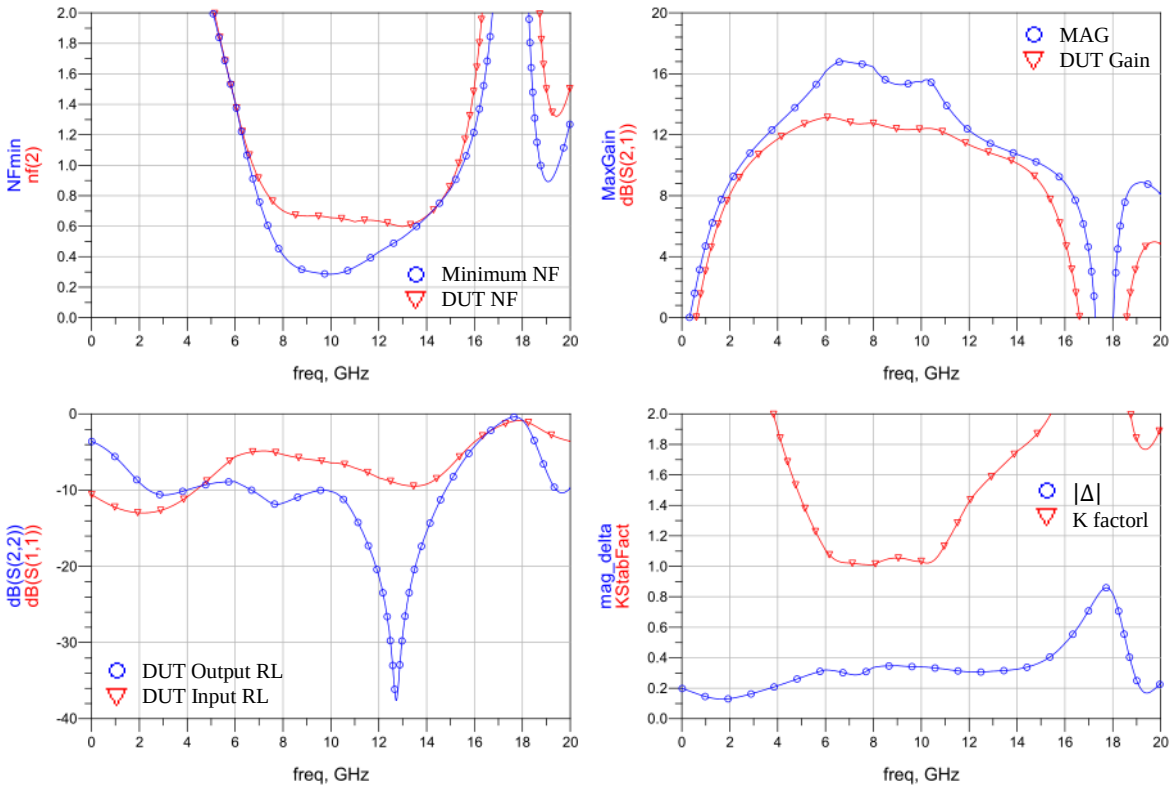

Figure 38: Characteristics of the DUT for design (MGF4937AM).

3.4.4 DC Simulation

At this point, the small-signal model is momentarily replaced by the large-signal model to allow a DC simulation to take place. The necessary supply voltages to feed the necessary current the transistor are defined. The necessary current consists in the one used at the moment of the small signal model characterization.

Table 2: Biasing values during simulation.

Transistor	Drain Current (mA)	Drain Voltage (V)	Supply Voltage	
			Gate (mV)	Drain (V)
MGF4937AM	9.86	2	-270	2.26
MGF4941AL	10.1	2	-330	2.22

3.5 Matching Networks Design

In terms of impedance matching, the simplest design that satisfies the required specifications is generally preferable, especially when a two-stage amplifier is already complex by nature. A simple matching technique is the single-stub tuning. Thus, two possible approaches were possible in realizing the stub: an open stub or a short stub. In terms of implementation, the former is easier to fabricate when it comes to printing a circuit layout, while the latter needs a via (or vias) to be drilled through the PCB all the way down to the ground layer. Moreover, due to its design, a short stub implies knowing its exact length beforehand, whereas an open stub can be manually adjusted later on. An open stub has an open-end capacitance that effectively makes it longer than desired while the short stub has a via hole whose inductance that effectively makes it shorter than desired. Due to the flexibility and ease in fabrication, only open stubs were chosen. Additionally, the transmission lines of the matching networks were constrained to a width corresponding to the characteristic impedance of the system in order to obtain a straightforward design.

As mentioned early on (recalling Figure 23), two different approaches were available for a two-stage LNA design due to the interstage matching network: a

cascade of individual stages and a single interstage matching network. A common step to both methods is the analysis of a DUT as candidate for each stage. The strategy adopted was a scattering parameter simulation and noise analysis of the device in order to allow the display of noise contours and available gain circles in the same Smith chart, i.e. in the Γ_S plane. The goal is to establish a trade-off between gain and noise figure by selecting an appropriate source reflection coefficient Γ_S. Thus, the resulting output reflection coefficient seen into the DUT is conjugately matched by considering $\Gamma_L = \Gamma_{OUT}^*$. Along with the available gain circles and noise contours, it is good practice to additionally plot the input stability circle even when evaluating an unconditional stable DUT. For the sake of completeness, the load reflection coefficient, which is calculated indirectly from the selection of Γ_S via $\Gamma_L = \Gamma_{OUT}^*$, should also be plotted on the same Smith chart along with the output stability circle for consistency. This technique allied to the automatic calculation of the associated transducer power gain provides a visual tool in establishing an input matching network for the best noise figure and gain trade-off and an output matching network for the best associated power gain. From this step, the following parameters for each DUT are obtained: desired noise figure, associated transducer power gain, source and load impedances and their equivalent reflection coefficients. Thereafter, the design methods diverge and are briefly explained in the following sections.

Cascade of individual stages method

1. The input matching network of the first stage was designed for the selected Γ_S and the input DC block was incorporated. Rightly after, the output matching network was also designed for the resulting $\Gamma_L = \Gamma_{OUT}^*$.
2. By using the cascaded overall noise factor formula, the specifications for the second stage were calculated. The losses of the interstage DC block were taken in account for this calculation.
3. The matching networks of the second stage were designed and the output DC block was also incorporated.
4. The first stage, the interstage DC block and the second stage were connected to each other.

Single interstage matching network method

1. The input matching network of the first stage was designed and the input DC block was incorporated.

2. By assuming a lossless interstage matching network (to simplify the task), the specifications for the second stage were obtained by the cascaded overall noise factor formula. The second stage was composed by the DUT and the interstage DC block directly connected at its input.

3. The output matching network of the second stage was designed including the output DC block.

4. The interstage matching network is designed by matching Γ_{L1}^{*} to Γ_{S2}^{*} and the first stage and the second stage are connected at its input and output, respectively.

3.6 Simulation Results

The low-noise match techniques employed usually provide a narrowband design, and therefore impedance mismatches were implemented intentionally, providing some bandwidth, improving gain flatness and establishing a trade-off between power gain, noise figure and return loss. These mismatches were implemented progressively along the design by tuning the transmission lines and optimizing the results in order to achieve an acceptable performance.

Thus, five amplifiers were designed differentiating themselves by method and DC block (capacitor or parallel coupled-line filter) employed. Following the optimization of the designs, the final simulated performance was obtained.

The simulated performance of only one of the amplifiers is presented in this section. The DC block of this amplifier makes use of the capacitor whose performance was shown in section 3.3.1 and the matching networks were designed using the cascade of individual stages method mentioned in section 3.5. The noise figure, gain and return loss results are presented in the following two figures.

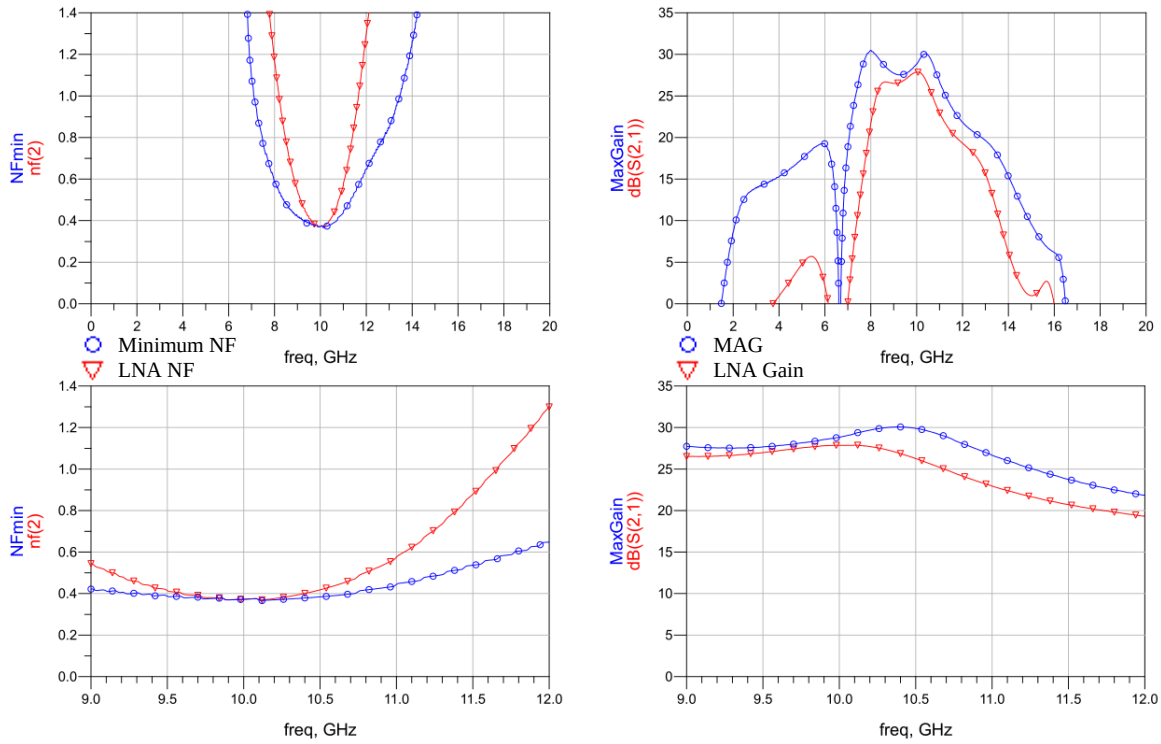

Figure 39: Noise figure and gain simulations.

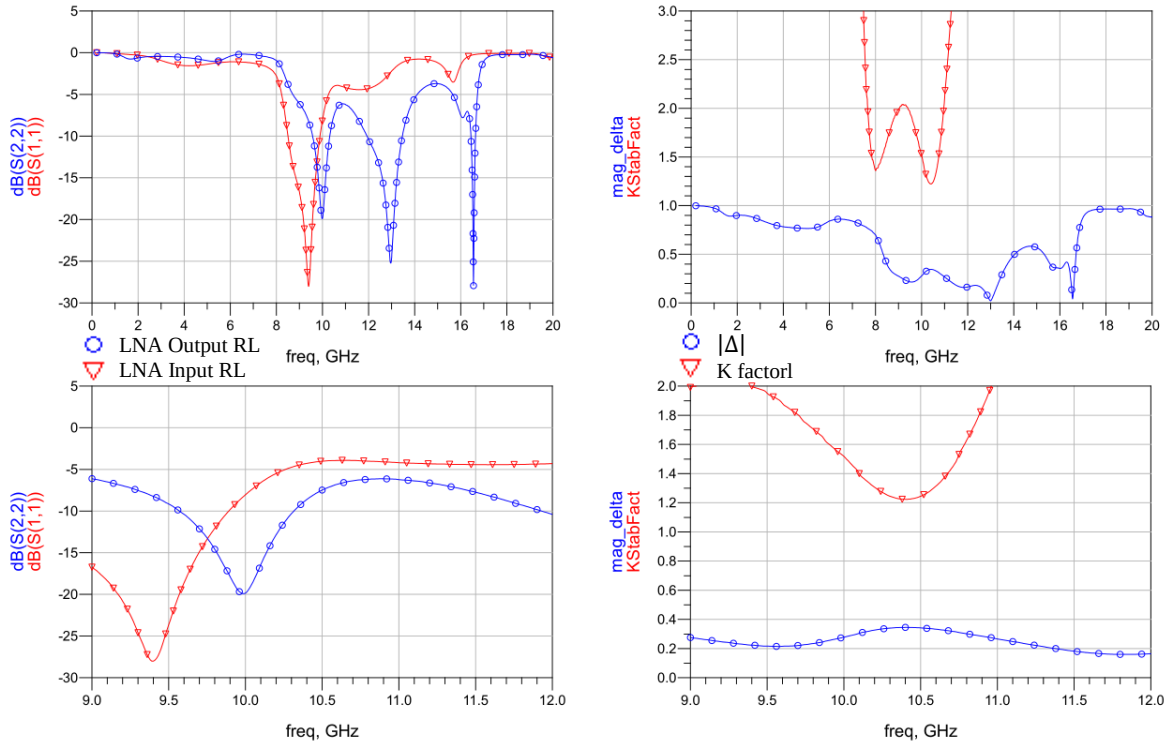

Figure 40: Return loss and overall stability simulations.

Table 3: LNA simulated performance.

Parameter	Performance	Unit
Center Frequency	10	GHz
Bandwidth	800	MHz
Gain	27.4 ± 0.5	dB
Noise Figure	0.39 ± 0.02	dB
Input Return Loss	-11.4 ± 7.2	dB
Output Return Loss	-14.3 ± 5.7	dB
Stability	Unconditional Stable	-

3.7 Layout and Implementation

The layouts of the circuit boards were designed using the optimized final schematic designs. As mentioned early on, the substrate RT/Duroid 5880 was used for the board application. Special attention was given to the land pattern of some components by designing several pads such as the input and output connector pads, the passive and active devices pads, the supply pads, and the vias holes grounding pads. The majority of these pads were already taken in account during the simulation.

The layout integration was also taken in account namely the shape of the quarter-wave transformer, the orientation of some devices and the total dimensions of the board. Since more than one amplifier was implemented, in order to simplify the implementation process, special attention was put into adjusting all layouts to the same total dimensions (20 x 64 mm). The layout of the amplifier whose performance was shown in the previous section is presented in the following figures along with the associated bill of materials. The layouts of the additional amplifiers can be seen in Appendix B.

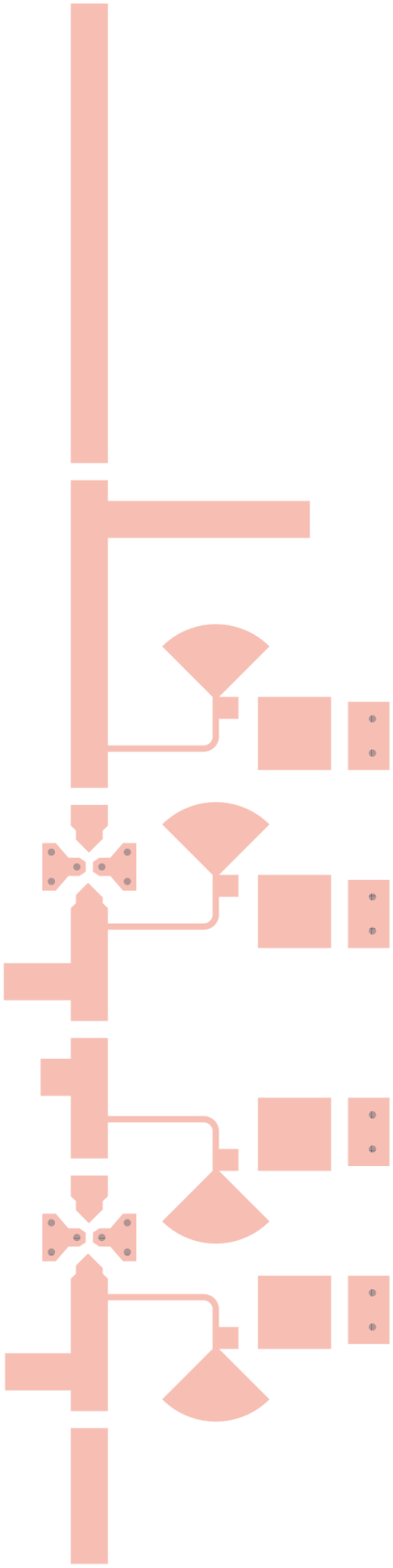

Figure 41: Layout of the implemented amplifier.

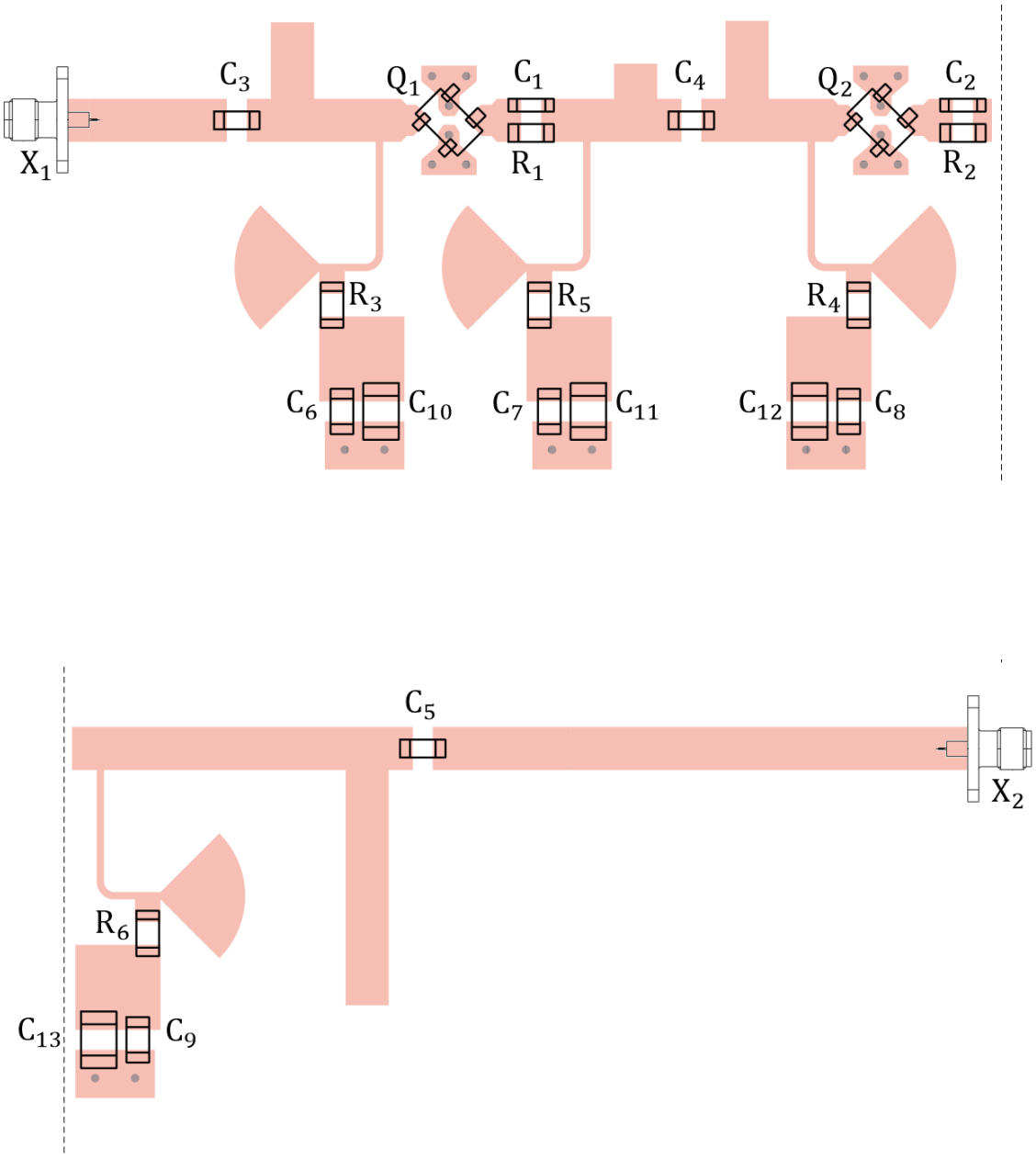

Figure 42: Assembly information for the implemented amplifier.

Table 4: Bill of materials of the implemented amplifier.

Reference Designator	Description	Value	Size	Part Number	Role
Q_1, Q_2	Transistor	-	2.05 x 2.10 mm	Mitsubishi MGF4937AM	DUT
C_1, C_2	Capacitor	0.3 pF	0603	AVX 06035J0R3PBSTR	Stability Signal Path
R_1, R_2	Resistor	15 Ω	0603	-*	Stability Signal Path
C_3, C_4, C_5	Capacitor	0.3 pF	0603	AVX 06035J0R3PBSTR	DC Block
R_3, R_4	Resistor	47 Ω	0603	-*	Stability Bias Path
R_5, R_6	Resistor	11 Ω	0603	-*	Stability Bias Path
C_6, C_7, C_8, C_9	Capacitor	0.1 µF	0603	-*	DC Bypass
$C_{10}, C_{11}, C_{12}, C_{13}$	Capacitor	1 µF	0805	-*	DC Bypass
X_1, X_2	RF Connector	-	-	TE Connectivity 1052902-1	RF Input/Output

* General purpose devices were used

At this point, the LNA was implemented, as it can be seen in the figure below.

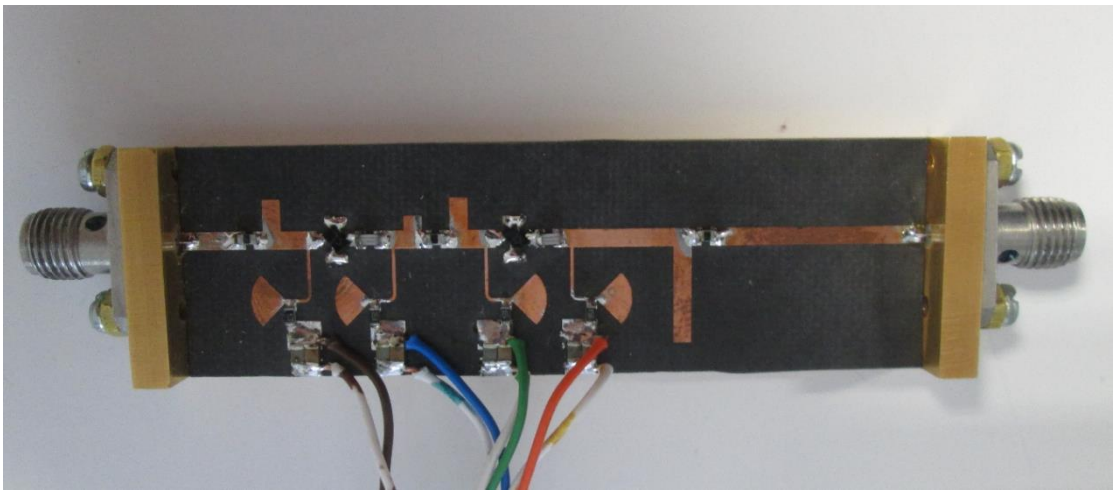

Figure 43: Complete assembled board with dimensions 20 x 64 mm.

The next step was the test of the device in a laboratory environment.

Chapter IV

4 Measurement and Results

The measurement was divided into two tests: characterization of the device's behavior through scattering parameters and evaluation of its noise performance. It is important to mention that only one amplifier was tested.

Before going any further, the definition of DUT is reviewed for measurement purposes. While in the design of the matching networks procedure the DUT was a transistor properly biased and stabilized, from this point forward the default DUT definition holds for the implemented amplifier until told otherwise.

4.1 Network Measurements

4.1.1 Equipment and Setup

The biasing of the amplifier was established by two power supplies, one for each stage: the HP E3631A and the Topward 6303DS. The biasing values from Table 2 were only a starting point for reaching an acceptable performance and an adjustment was made during the measurement, as it can be seen in Table 5 in the next page.

The measurement of the scattering parameters was carried out by the network analyzer Agilent PNA E8361C. The connection to the device was done by subminiature version A (SMA) cables from Mini-Circuits (CBL 1.5FT SMSM+). A short-open-load-through (SOLT) two-port calibration was made with the 85052D 3.5mm kit.

Table 5: Biasing values during measurement.

Stage	Transistor	Drain Current (mA)	Supply Voltage	
			Gate (mV)	Drain (V)
First	MGF4937AM	16	-100	2.26
Second		20	-30	2.26

The setup adopted to measure the scattering parameters of the implemented LNA is shown below.

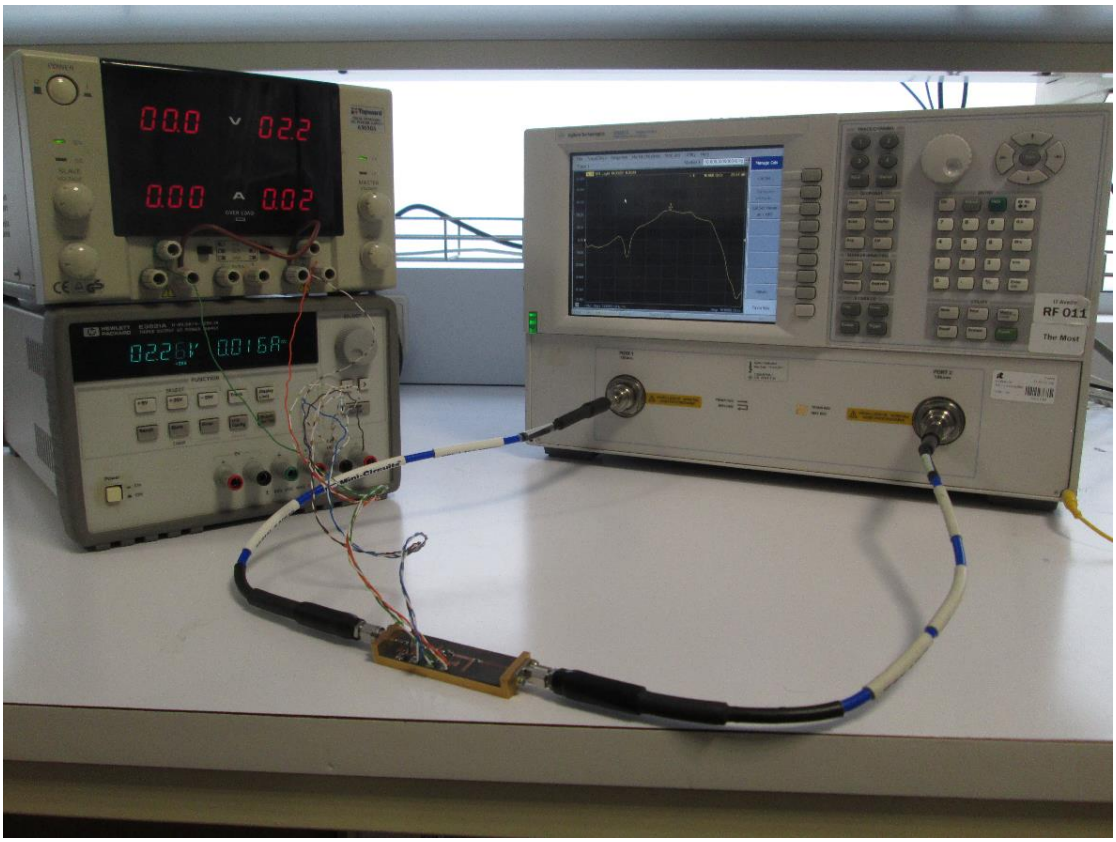

Figure 44: Scattering parameters measurement setup.

4.1.2 Results

The scattering parameters obtained by the setup presented in Figure 44 were imported into ADS. This section shows the results and compare them with the expected performance from simulation. The input and output reflection coefficients, the reverse and forward transmission coefficients and a stability analysis are shown in the following figures.

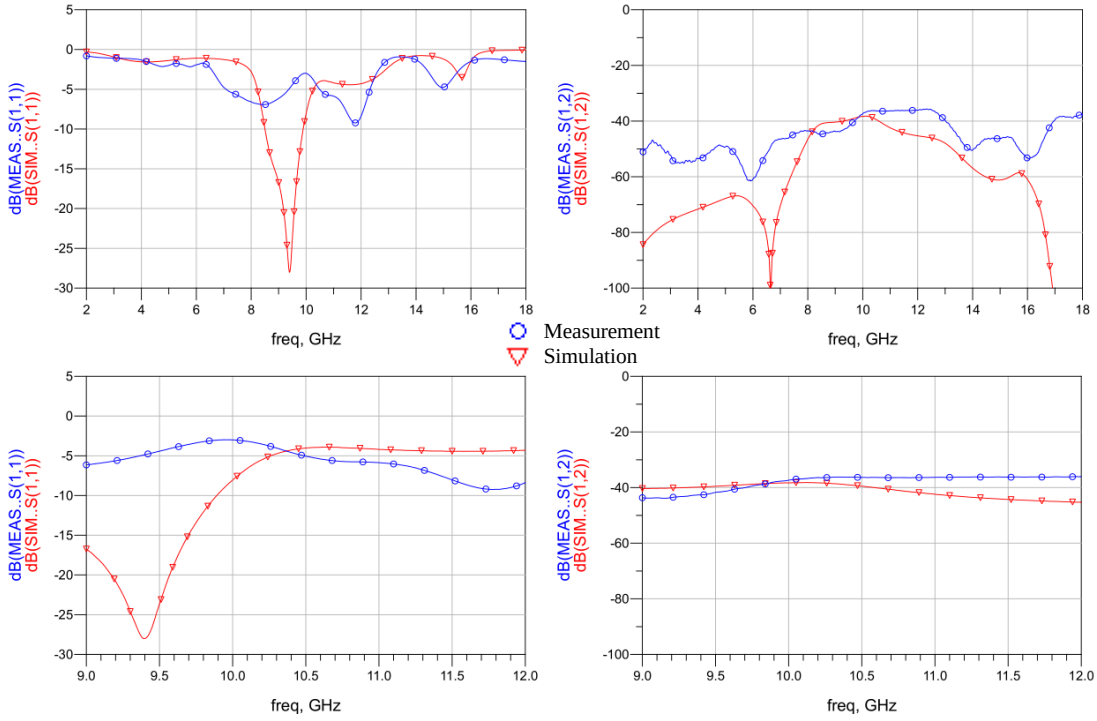

Figure 45: Input return loss (left) and isolation (right).

A compromise between noise figure and input return loss was performed in prejudice of the latter already back in the design and simulation. Thus, good results in the input return loss (Figure 45, left) were not expected. The output return loss (Figure 46, left), however, was satisfactory. In terms of gain (Figure 46, right), the results show a shift of the device's passband to a higher frequency with additional losses due to mismatches. Finally, Figure 47 shows that an unconditional stable amplifier was obtained.

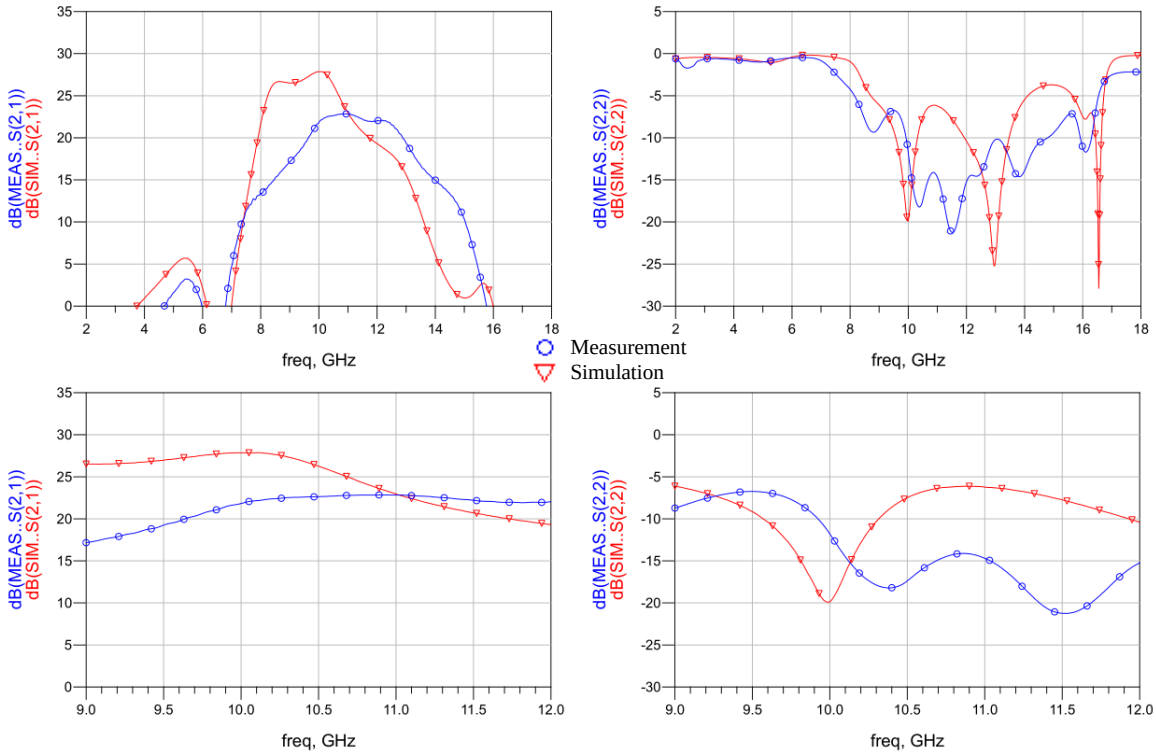

Figure 46: Output return loss (left) and gain (right).

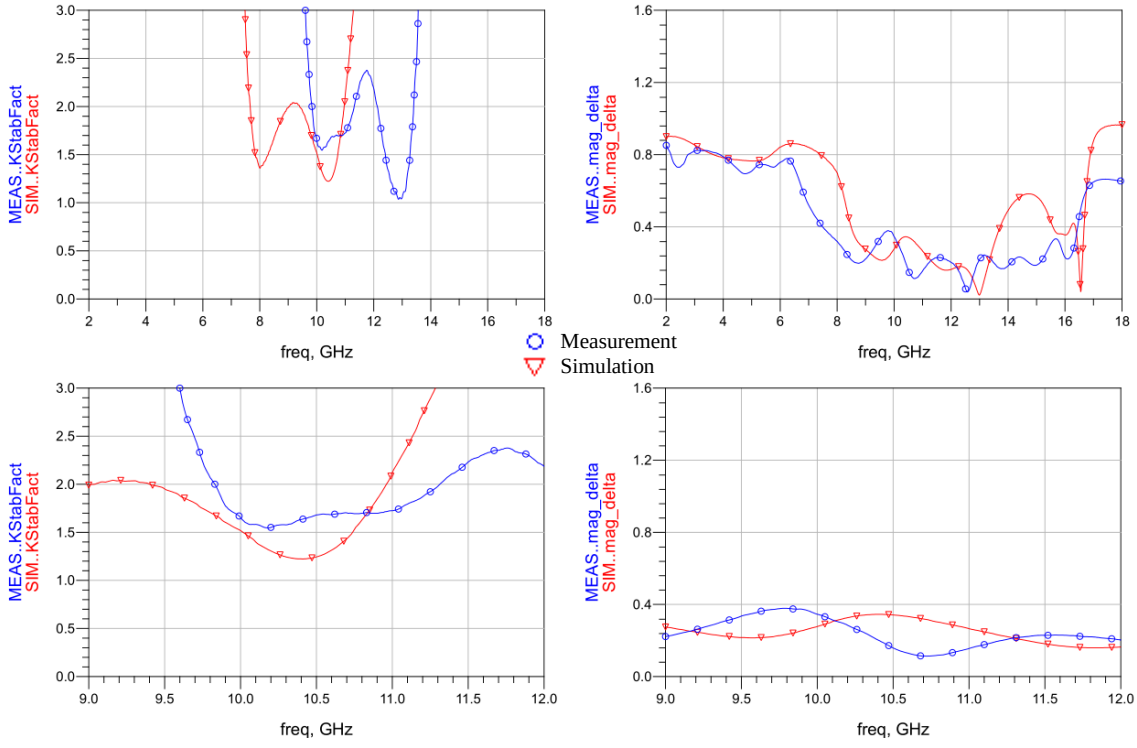

Figure 47: Stability analysis: K factor (left) and $|\Delta|$ (right).

4.2 Noise Measurements

4.2.1 Equipment and Setup

A HP 8970B Noise Figure Meter along with a HP 346C noise source were used to measure the performance of the prototype. The HP 8970B was only able to measure up to 1.6 GHz alone, and therefore external frequency conversion was necessary. A down conversion to an intermediate frequency (IF) that could be handled by the noise figure meter was carried out by a Marki M80412LZ mixer aided by a Wiltron 6769B generator acting as a local oscillator.

Noise figure measurement has limits of accuracy that can be improved by minimizing uncertainties wherever that is possible and quantifying the uncertainties that remain [2, 4, 31, 34]. Thus, a HP 8493C attenuator was used since a fixed attenuator helps minimizing impedance mismatch at the output of the DUT. Moreover, the IF was lowered to the minimum value that could be handled by the noise figure meter (10 MHz) to bring both the resulting lower and upper sidebands from the frequency conversion closer and minimize the effect of frequency difference. The random jitter was also reduced to a low level by averaging a sufficient number of readings (see Appendix A, in particular Equation 101). Additional equipment as SMA cables (CBL 3FT SMSM+) and SMA connectors were also employed. At this moment, recalling Figure 12, which describes the basis of noise figure measurement, allows placing and grouping the components as shown in Figure 48 in next page.

The noise figure meter was configured for a single frequency measurement. The calibration was accomplished by feeding the noise source directly into the RF port of the mixer and by enabling the output of the signal generator for the specified frequency. The meter then measured its own noise figure to be able to perform the second stage correction. Once calibration was complete, the corrected measurement could be carried out by inserting the DUT and additional components between the noise source and the second stage. Since the DUT did not include frequency conversion between the input and output, the measurement took place at the same frequency of the calibration step. Thereafter, this procedure was repeated for other values of frequency inserted manually into the signal generator.

A cryogenic low-noise amplifier (LNF LNC4 8A, see [38]) with a known performance was used as reference device to validate the adopted setup. It is

important to mention that due to the mixer used (see [41]) and the measurement method adopted, it was decided that the noise measurement would be constrained to the range from 9.5 GHz up to 11.9 GHz.

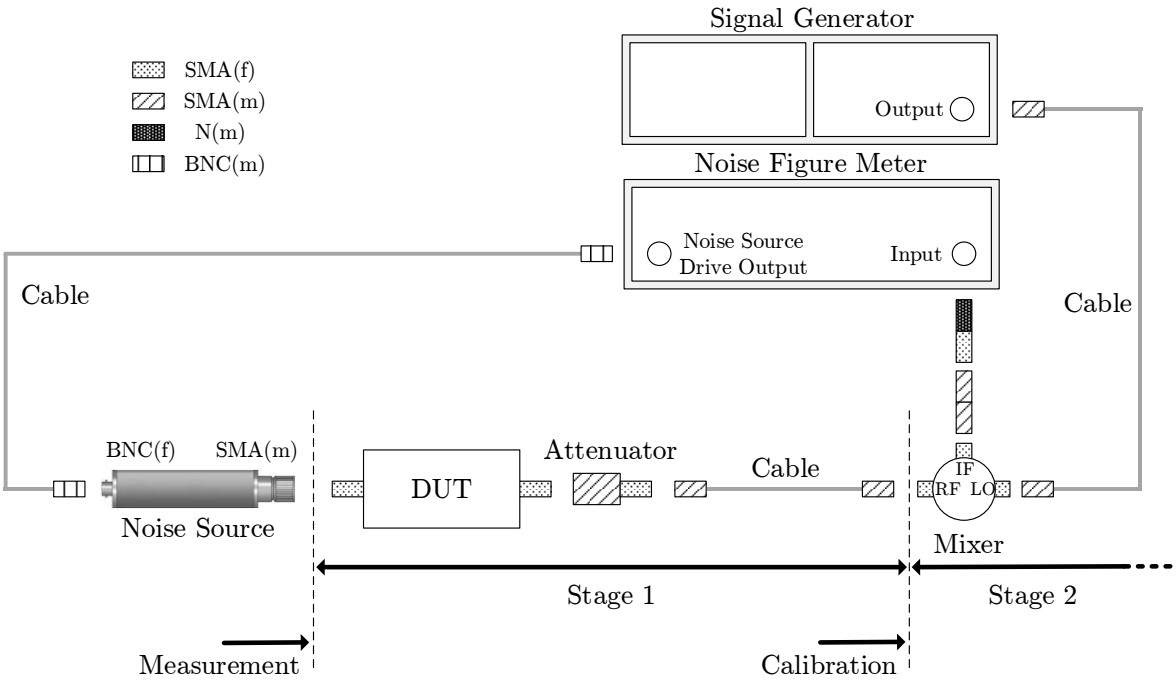

Figure 48: Component placement in the measurement of noise figure.

4.2.2 Measurement Corrections

When performing noise measurements, corrections are required for the residual errors due to losses and temperature. The measurement corrections in this section were applied to the physical temperature of the noise source and to its calibrated ENR values. Beyond that, the setup adopted (Figure 48) required noise temperature and gain corrections due to the lossy components employed. All corrections applied are outlined in [34].

Before going any further, it is important to acknowledge that the hot temperature of a noise source varies with changes in its physical temperature (cold temperature) since the thermal noise due to the latter is added both when the noise source is on and off. For the sake of accuracy, it is assumed that the noise change between the on and off states of the noise source remains constant with changes in the cold temperature. The temperature correction of a noise source includes two

steps: the temperature at the time of noise source calibration and the temperature at the time of noise figure measurement.

At the time of noise source calibration, the fixed noise temperatures of the noise source in its on and off states can be represented by T_H and T_C, respectively. However, the tabulated values of ENR are referenced to T_0 instead of T_C and are calculated by

$$ENR^{CAL} = \frac{T_H - T_0}{T_0} \tag{89}$$

where ENR^{CAL} is the original calibrated ENR value as read directly from the noise source. Thus, the following correction was applied

$$ENR^{CORR} = ENR^{CAL} + \frac{T_0 - T_C}{T_0} \tag{90}$$

where $ENR^{CORR} = (T_H - T_C)/T_0$ is the corrected ENR value and T_C is the physical temperature at the time of noise source calibration set by using the statistical average value, which for the noise source used (346C) corresponds to 304.8 K, since the value from the noise source calibration report is rarely available. Thus, the corrected ENR values were obtained via MATLAB and applied to the noise figure instrument before the calibration step. It is also important to acknowledge that the measurement frequency range adopted (9.5-11.9 GHz) required ENR values that were not available from the noise source ENR table. Although these ENR values are frequency dependent and are only defined at certain frequencies, values for intermediate frequencies could be obtained via linear interpolation with a negligible error.

The calculation of the Y-factor (Equation 44) at the time of noise figure measurement requires both T_S^{ON} and T_S^{OFF}. The physical temperature at the time of noise figure measurement (T_S^{OFF}) may be different from the physical temperature at the time of noise source calibration (T_C), and therefore the noise figure instrument needs correction for the actual value of T_S^{OFF}. Such a correction was applied by inserting the temperature value read by a thermometer at the time of each measurement into the noise figure instrument. Since the excess noise remains constant, T_S^{ON} was computed internally as follows

$$T_S^{ON} = T_0\, ENR^{CORR} + T_S^{OFF} \tag{91}$$

In the measurement setup of Figure 48, the first stage not only has the DUT but also further components that are lossy. Thus, additional insertion losses that were not present in the calibration step needed to be taken in account after the measurement as well as corrections for physical temperature of these lossy components. The setup adopted implied corrections for losses after the DUT to the components that had not been included in the calibration loop, and therefore for output losses the correction is to the noise temperature of the second stage (T_2) at the calibration step as follows

$$T_2^{CORR} = L_{OUT}\, T_2 + (L_{OUT} - 1)T_{OUT} \tag{92}$$

and also to the gain of the first stage (G_1)

$$G_1^{CORR} = G_1 L_{OUT} \tag{93}$$

where L_{OUT} is the output loss (attenuator along with the SMA cable) expressed as a ratio greater than unity and T_{OUT} the physical temperature of any dissipative losses.

The noise temperature value of the first stage corrected for output losses was calculated by inserting the corrected values T_2^{CORR} and G_1^{CORR} as obtained by Equations 92 and 93 into Equation 35 as

$$T_1^{CORR} = T_{12} - \frac{T_2^{CORR}}{G_1^{CORR}} \tag{94}$$

The correction of noise temperatures and gain of the DUT were computed once again via MATLAB.

4.2.3 Unavoidable uncertainties

After the minimization of all possible uncertainties it was necessary to quantify and calculate the ones that remained in order to obtain an accurate characterization of the performance of the device presented. The sources of

uncertainty in this measurement are: the noise figure of the second stage as measured in the calibration step (δNF_2); the noise figure of the system as measured in the measurement step (δNF_{12}); the impedance mismatch between noise source and instrument in the calibration step (δ_{NS-I}); the impedance mismatch between noise source and DUT in the measurement step (δ_{NS-DUT}); the impedance mismatch between DUT and instrument in the measurement step (δ_{DUT-I}) and instrument uncertainties, such as the ENR of the noise source (δENR), the instrument gain linearity (δG_i) and the instrument noise figure (δNF_i), as specified by the manufacturer. The following figure illustrates where these uncertainties arise in noise figure measurement.

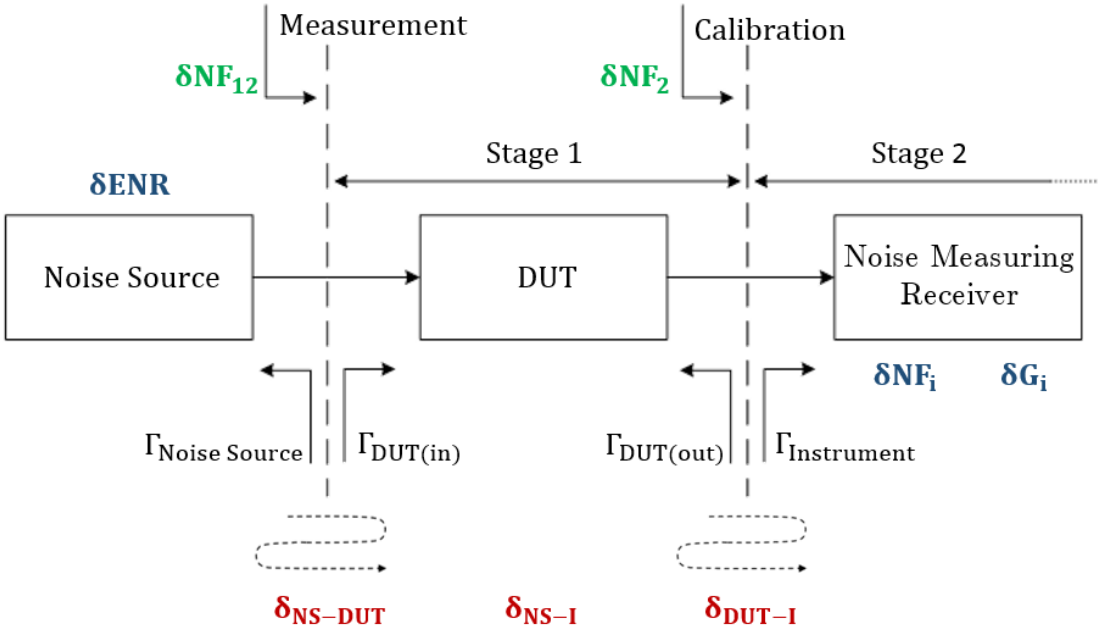

Figure 49: Uncertainty model.

While some uncertainties were obtained directly by inspection of the datasheets of both the noise source (see [32]) and noise figure instrument (see [25]), others were calculated by a useful noise figure uncertainty calculator that was available from Keysight Technologies in the form of a Microsoft Excel spreadsheet (see [35]). The same spreadsheet was also responsible for the calculation of the overall uncertainty of the measurement (δNF_1). Thereafter, the data obtained via the calculator was imported into MATLAB and handled.

4.2.4 Results

The results obtained by the setup of Figure 48 were collected manually and imported into MATLAB. In the following figures a comparison is made between uncorrected and corrected measurements (as mentioned in section 4.2.2).

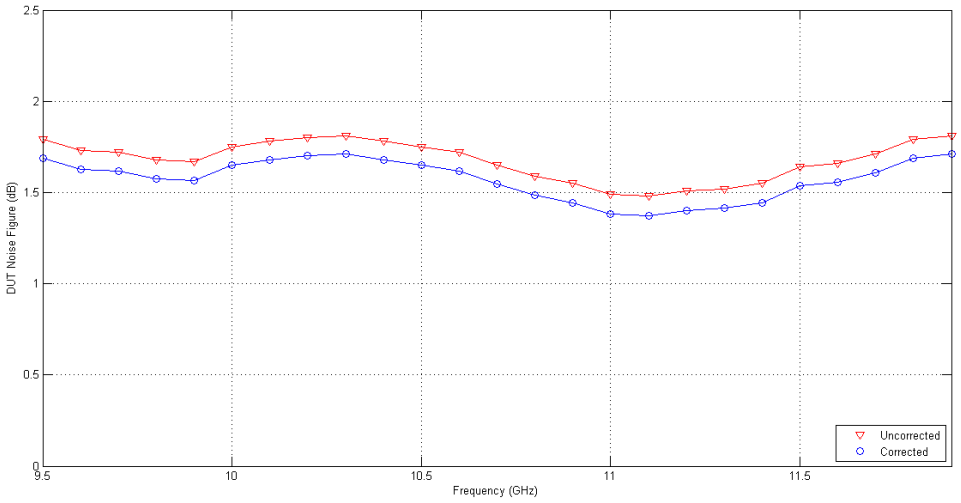

Figure 50: Uncorrected and corrected DUT noise performance.

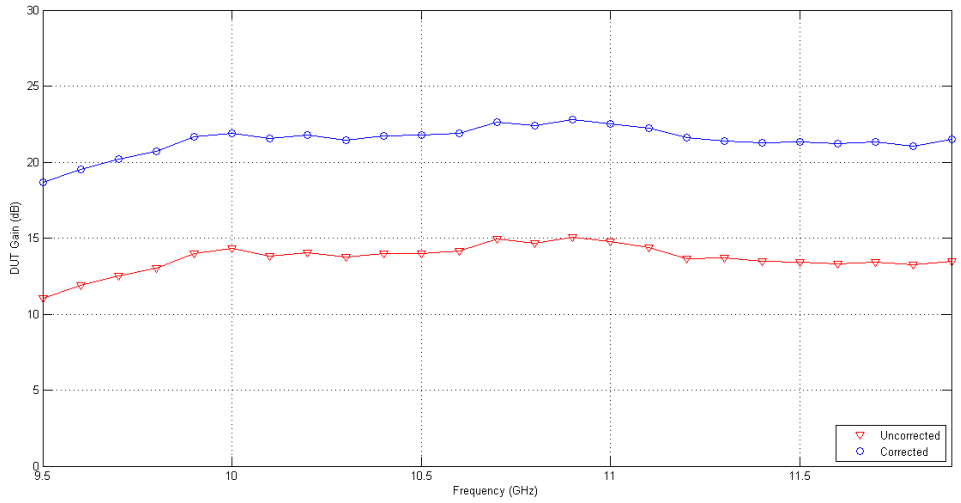

Figure 51: Uncorrected and corrected DUT gain.

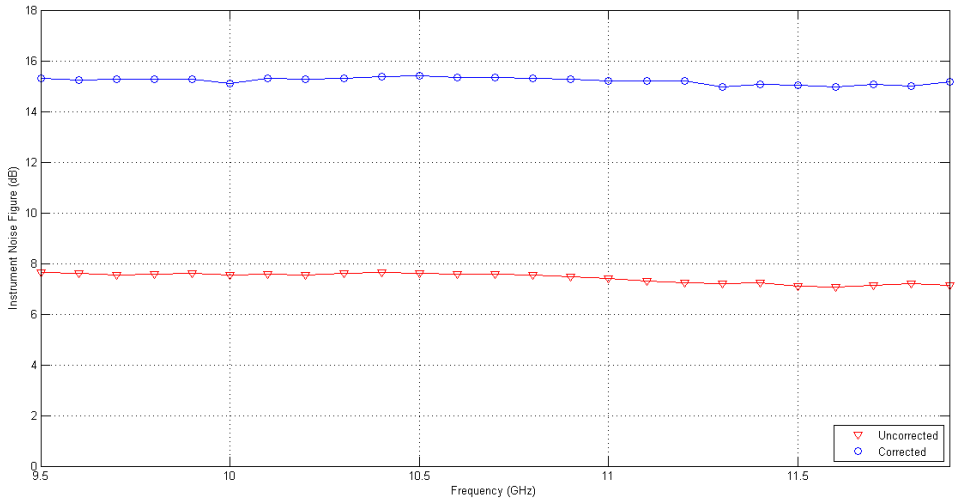

Figure 52: Uncorrected and corrected instrument noise figure.

In the following figures a comparison is made between the expected results from simulation (exported from ADS and imported into MATLAB) and the results obtained in the laboratory environment.

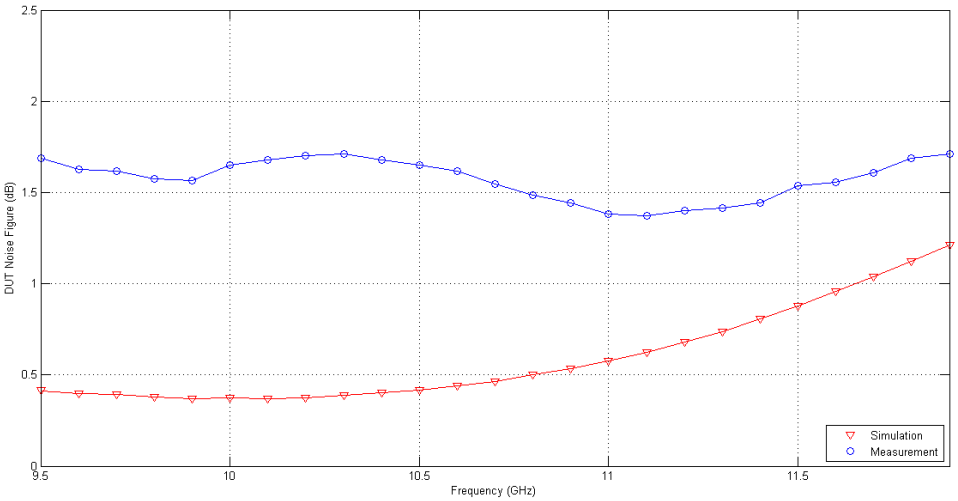

Figure 53: Comparison of simulated and measured DUT noise performance.

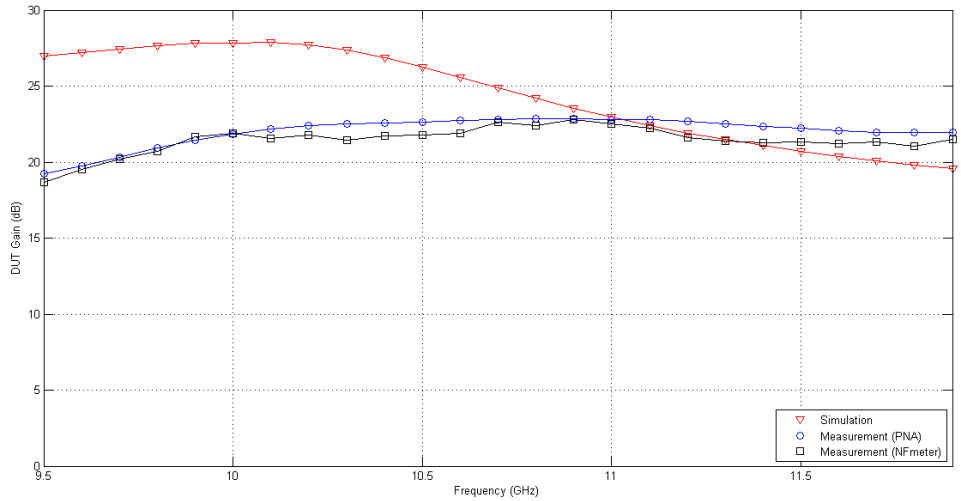

Figure 54: Comparison of simulated and measured DUT gain with measurement validation by two instruments.

In a design there is always a difference between the designed noise figure and the measured noise figure of the final amplifier but the measured value was the most frustrating result since it was about 1.3 dB above the simulated value (Figure 53).

Finally, the following figures show the variation of the uncertainty of noise figure measurement with different parameters.

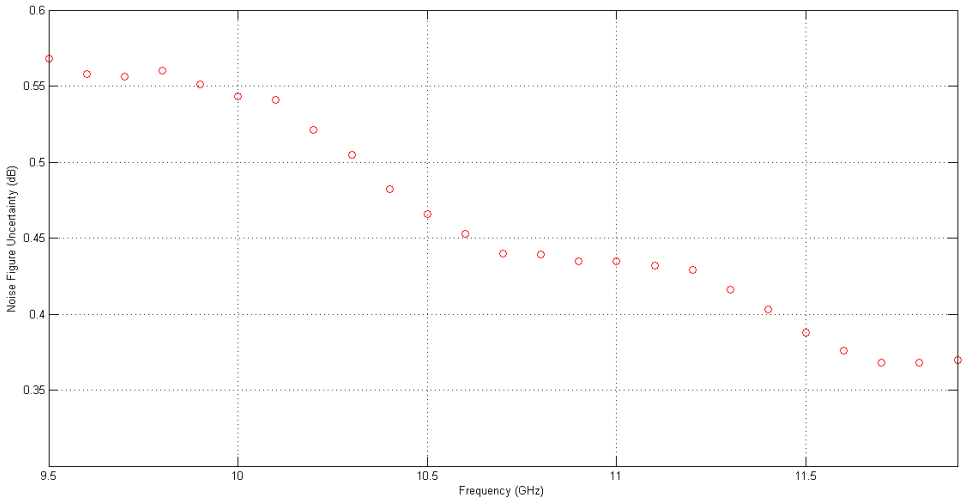

Figure 55: Measurement uncertainty as function of the frequency.

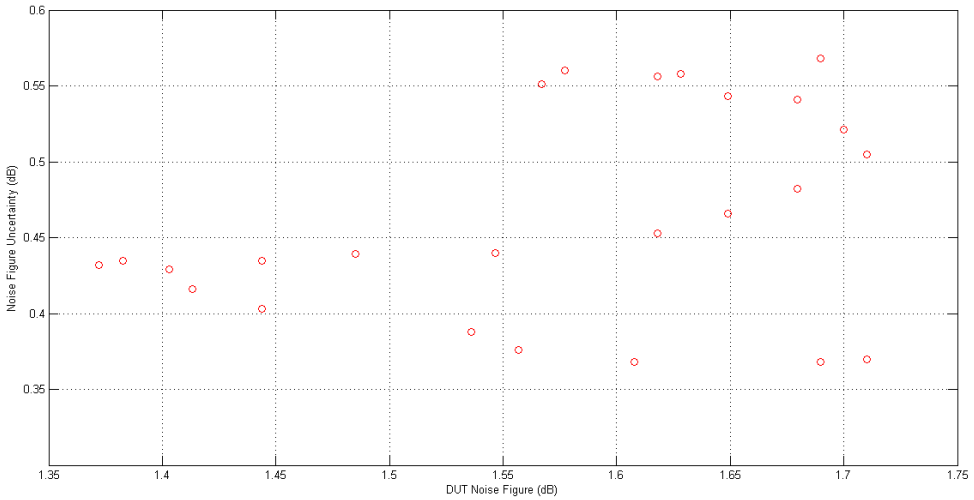

Figure 56: Measurement uncertainty as function of the DUT noise figure.

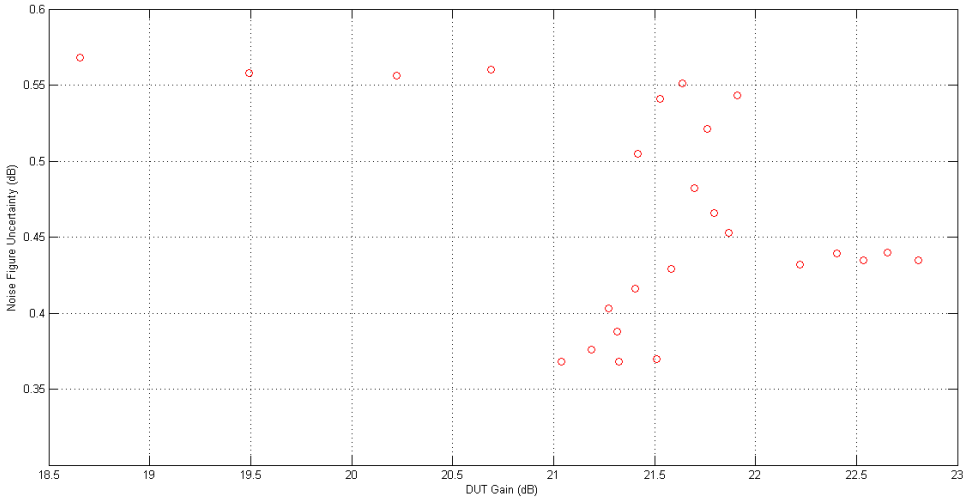

Figure 57: Measurement uncertainty as function of the DUT gain.

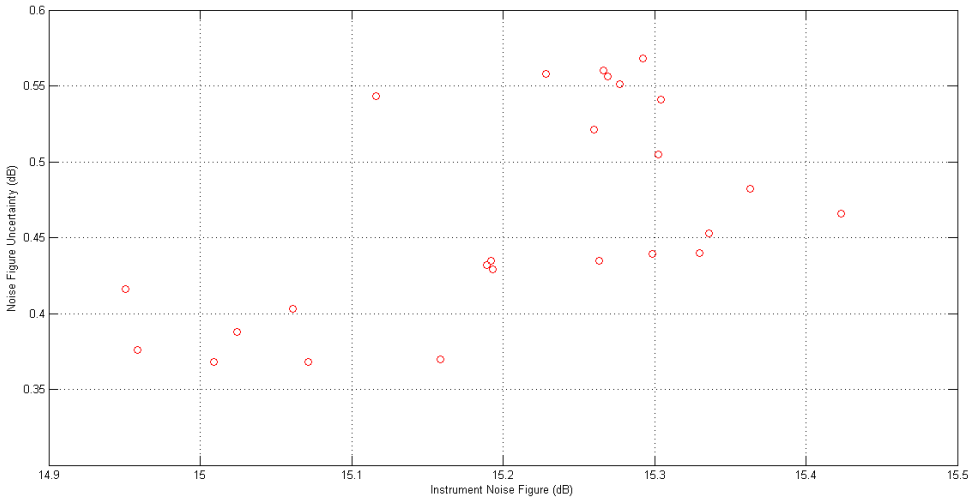

Figure 58: Measurement uncertainty as function of the instrument noise figure.

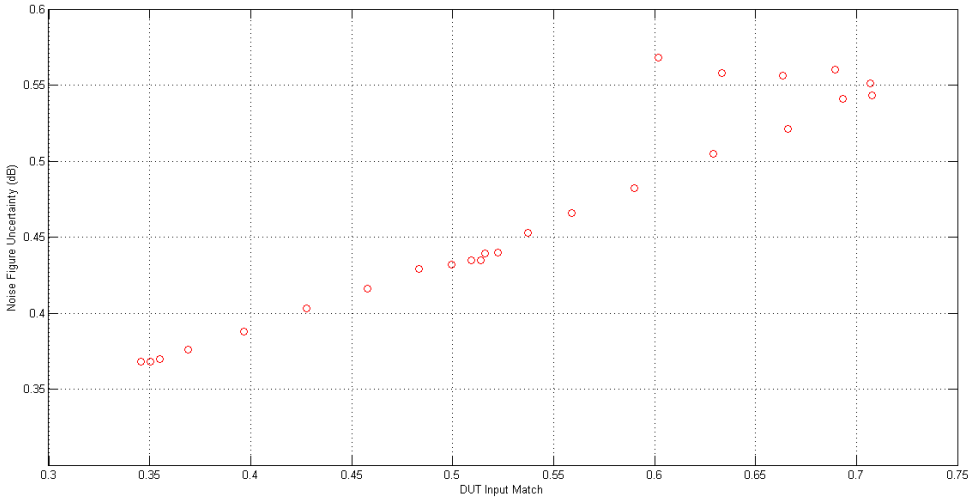

Figure 59: Measurement uncertainty as function of the DUT input match (reflection coefficient).

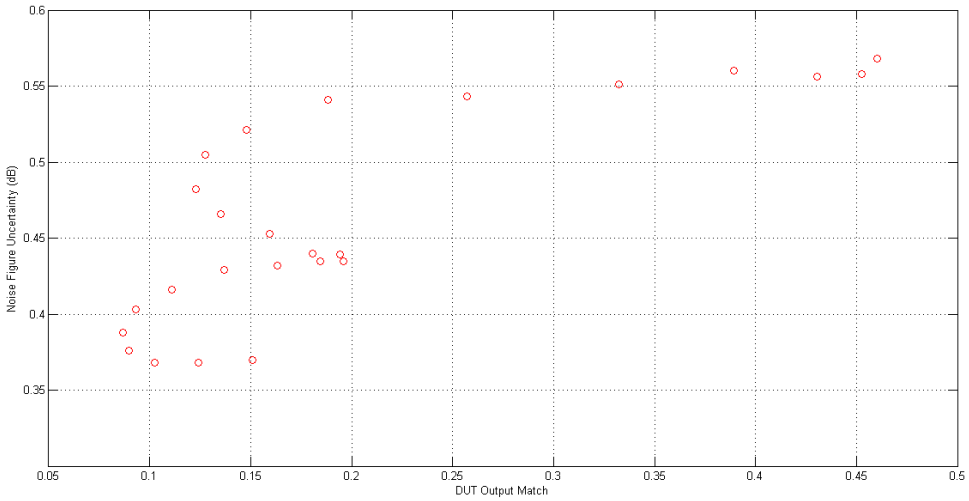

Figure 60: Measurement uncertainty as function of the DUT output match (reflection coefficient).

The uncertainty was higher at lower frequencies than at higher frequencies. The highest uncertainty was about ± 0.57 at 9.5 GHz and the lowest was about ± 0.37 on the other end of the measurement frequency region. Figure 59 and Figure 60 help to understand this situation since they show the strong dependence of the uncertainty with the mismatch at both input and output, respectively. In order to clarify the definition of measurement uncertainty, Table 6 (in the next page) shows the data points of the Figure 55 along with the respective measured noise performance. This set of data points allows the characterization of the DUT noise figure in terms of accuracy using an uncertainty window, as shown in the Figure 61.

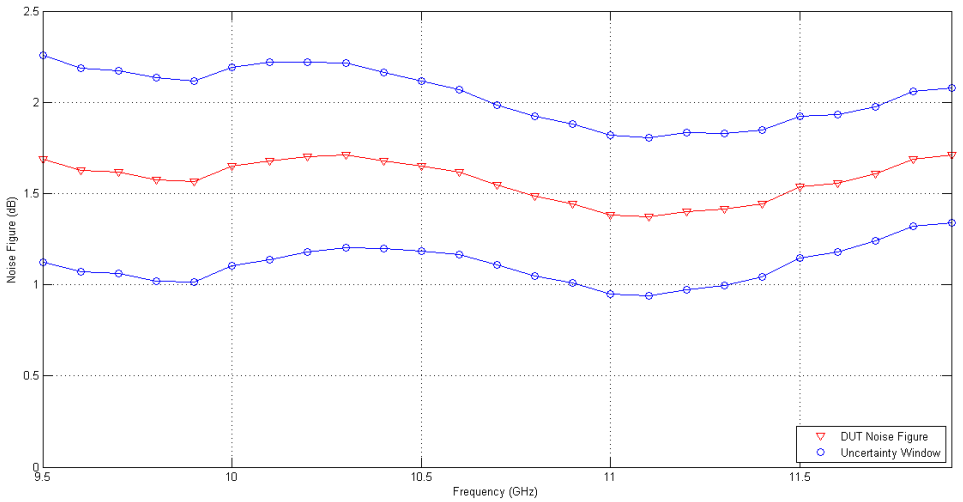

Figure 61: Noise figure uncertainty in the DUT.

Table 6: Noise figure measurement including associated uncertainty.

Frequency (GHz)	Noise Figure ± Uncertainty (dB)
9.5	1.69 ± 0.57
9.6	1.63 ± 0.56
9.7	1.62 ± 0.56
9.8	1.58 ± 0.56
9.9	1.57 ± 0.55
10	1.65 ± 0.54
10.1	1.68 ± 0.54
10.2	1.70 ± 0.52
10.3	1.71 ± 0.51
10.4	1.68 ± 0.48
10.5	1.65 ± 0.47
10.6	1.62 ± 0.45
10.7	1.55 ± 0.44
10.8	1.49 ± 0.44
10.9	1.44 ± 0.44
11	1.38 ± 0.44
11.1	1.37 ± 0.43
11.2	1.40 ± 0.43
11.3	1.41 ± 0.42
11.4	1.44 ± 0.40
11.5	1.54 ± 0.39
11.6	1.56 ± 0.38
11.7	1.61 ± 0.37
11.8	1.69 ± 0.37
11.9	1.71 ± 0.37

At this point, the work was accomplished. The results and the reasons behind some discrepancies as well as errors committed during this work will be discussed in the following chapter.

Chapter V

5 Conclusion and Future Work

This chapter summarizes the work accomplished in this thesis and also mentions additional work that could further improve this area of research. Thus, it is divided into two sections: conclusion and future work. In the former, a brief overview of this document is done and results are analyzed. In the later, there are presented possible improvements for the device developed and problems or limitations are identified and discussed. Different approaches or procedures are also suggested either to improve device's performance or accuracy in the measurement.

5.1 Conclusion

The main goal of this work was the design, implementation and characterization of a LNA operating in the X-band for applications in radio astronomy. This thesis also addressed common problems and limitations found while designing the proposed device and describing its performance.

The approach to solve the problem started by providing the necessary background theory for understanding the design of a LNA. Noise and its measurement were characterized, two-port networks were described in terms of their parameters and general considerations and methods in designing a LNA were explained. Afterwards, the adopted methodology in designing and implementing the amplifier was outlined and the simulated results were shown. Finally, the testing methods in characterizing the device were described in a how-to fashion and the behavior of the device in a laboratory environment was presented.

The following table summarizes the performance of the LNA implemented according with the results from section 4.

Table 7: LNA measurement results.

Parameter	Performance			Unit
	Test 1	Test 2	Test 3	
Center Frequency	10	11.2	11.1	GHz
Bandwidth	800	1400	600	MHz
Gain	21.2 ± 1.4	22.4 ± 0.5	22.6 ± 0.2	dB
Noise Figure	1.64 ± 0.07	1.54 ± 0.17	1.43 ± 0.06	dB
Input Return Loss	-3.8 ± 0.8	-7.1 ± 2.1	-6.6 ± 0.8	dB
Output Return Loss	-12.6 ± 5.6	-17.7 ± 3.6	-17.4 ± 3.3	dB
Stability	Unconditional Stable			-

Test 1 shows the performance of the device in the same region covered by the simulated performance (as shown in Table 3), which in turn also agrees with the required performance (as shown in Table 1). Thus, test 1 allows to establish a comparison between the measured, simulated and required performances for the LNA in the same frequency region. Test 1 shows that the results were not the best at the design frequency. Test 2 represents a wide region where the LNA proved to have the best performance during the laboratory tests. Test 3 simply consists in a less wide region within the one from test 2 where the device presents a performance with reduced tolerances.

Regarding the results, the network performance was close to what was expected with admissible and common errors in this type of work (taking into account the operating frequency and the equipment available). Unfortunately, the measured noise performance falls short of what was predicted by simulation, and although the noise performance did not meet the expectations, the overall performance of the design was satisfactory for a first attempt in a LNA design by the author.

Another thing to take into account, which is often overlooked, is the uncertainty in the noise figure measurement. Analysis of measurement uncertainties can motivate setup changes for improved measurement repeatability and allow to establish the correct values of the specifications of the device.

At this point, it is necessary to understand and point out what went wrong. The value obtained of noise figure uncertainty was between ± 0.37 dB and ± 0.57 dB,

which is kind of bizarre since the target specification of noise figure was below 0.4 dB. In this situation, a new measurement should take place with a different setup in order to reduce this uncertainty value to an admissible value. Some mistakes were committed in the noise figure measurement setup such as the use of a noise source with a nominal value of 15 dB instead of a noise source with 6 dB that was not available, the absence of a highpass filter in the calibration loop in order to eliminate the 10 MHz component of the noise source and the use of the attenuator outside the calibration loop (Figure 48). After the measurements, an unnecessary correction of the physical temperature was also performed. However, the major mistake was committed when establishing the operating point of the transistor in the first stage since a higher supply current than the one recommended by the manufacturer was selected improving the overall gain response but degrading the overall noise figure, which can explain the discrepancy between the value of the measured noise figure and the expected value. Additionally, due to the field of research of this work, typical radio astronomy experiments should have been performed in order to validate the LNA for applications in this area.

In summary, this work represents a contribution for the implementation of low-noise amplifiers for the X-band.

5.2 Future Work

Although the results were satisfactory for a first attempt in this field, there is still room to improve. This work essentially consisted in a preliminary approach to the problems that may be encountered by a circuit designer while designing a LNA with similar requirements to the ones proposed here. Thus, the author leaves additional recommendations for next works in this field that may reduce the difference between the simulated and measured performance.

Evidently, the most important step in any LNA design is the choice of the transistor, and since the performance of commercially available devices is evolving, the market should be careful analyzed every time a device is needed in order to obtain the best device available and avoiding obsolete products. The same also applies to the choice of a capacitor when playing the role of a DC block. While having a transistor whose manufacturer provides an accurate large-signal model and a small-signal model for different bias conditions is a huge advantage for any design, it is also important that we have the possibility of characterizing the device by

obtaining our own small-signal model in a laboratory test by making use of appropriate bias tees and imposing test conditions. A similar laboratory test could also be applied to the DC block chosen (either a capacitor or any other mentioned in this work) but without the need of DC bias. By using this procedure, our devices could be better characterized and the performance of each independent device in a laboratory environment could be obtained beforehand. Still concerning the transistor, it is of interest the parasitic inductance inserted in the source of the device by increasing the length of the source pad. This effect shifts the reflection coefficients presented by the device and for some devices their performance can be increased by this technique since it could be possible to shift the optimum noise reflection coefficient closer to the reflection coefficient that provides maximum gain.

A situation overlooked in this work was the effect of the chosen SMA connectors. The one at the input has a critical effect in the noise performance of the device and therefore should be also characterized in order to predict accurately the results. A noise source with a nominal value of 6 dB should always be used over a noise source with 15 dB whenever the target noise figure value to measure is low. One more recommendation is connected to the matching networks. In this work, single-stub tuning was used with open stubs. After fabricating the prototype, we should have in mind that for increasing the performance of our circuit the open stubs can be manually adjusted when measuring the performance of the amplifier. A temperature simulation in a laboratory environment is also desirable since the LNA for the proposed applications may need to operate at low temperatures. Lastly, as any practical amplifier, it is also important to decrease its size while maintaining an acceptable performance or even in the best case improving it.

This document and the acquired knowledge can also be a starting point for different works such as the modeling of the transistors used, in order to obtain an accurate nonideal model for each one of them, and the design of additional components like filters, a mixer or an IF amplifier to obtain a whole receiver system for the required application.

Appendices

A. The Radiometer

Since this work falls within the radio astronomy scientific field, a case of interest in terms of noise measuring receivers is the radiometer, which was briefly mentioned in the opening chapter. The operation of a radiometer requires additional knowledge about radiometry theory and concepts that will be explained shortly.

A.1 Black-body Radiation

Any object whose temperature is above the absolute zero, i.e. 0 K, is said to be warm, and therefore radiates EM energy [55]. The EMR emitted by a body held at constant temperature is radiated isotropically according to Planck's radiation law, meaning that it has a specific spectrum and intensity that depends on the temperature of the body alone [51].

A black body, also called a perfect emitter, is defined as an idealized material that absorbs all incident EMR, regardless of frequency or angle of incidence, and reflects none [60]. The black body, which is heated up by the radiation absorbed, radiates EM energy, called black-body radiation, at the same rate as it absorbs it, thus maintaining thermal equilibrium [51]. On the other hand, a nonideal body in thermodynamic equilibrium with its environment will partially reflect incident energy, and so it does not radiate as much power as a black body would at the same temperature. A relative measure of the power radiated by a body is the emissivity, ε, defined as

$$\varepsilon = \frac{P_{nonideal}}{P_{ideal}} \tag{95}$$

Emissivity is simply defined as the ratio between the power radiated by a nonideal body and the power that would be emitted by a perfect black body at the same temperature. Thus, $0 \leq \varepsilon \leq 1$ and $\varepsilon = 1$ stands for a perfect black body. Emissivity may be thought of as the efficiency of black-body radiation [60].

A.2 Brightness Source Temperature

Every object with a physical temperature T above absolute zero possesses heat energy whose power is expressed using Equation 4. However, the noise power radiated by an object depends not only on its physical temperature but also on the ability of its surface to let the heat out [55], and so we redefine emissivity as

$$\varepsilon = 1 - |\Gamma|^2 \tag{96}$$

where Γ is the reflection coefficient of the body. Hence, the radiated noise power is associated with an equivalent noise temperature via the power-temperature relation rather than the physical temperature of the object directly established by Equation 4. This equivalent noise temperature is called the source brightness temperature, T_b. This is a property of a one-port, such as a noise source, and corresponds to the temperature that yields the power emerging from the output port of the noise source when it is connected to a matched load. The brightness temperature has a dependence of the physical temperature of the body, T, as follows

$$T_b = \varepsilon\, T \tag{97}$$

where ε stands for the emissivity of the body as defined previously. This shows that a body never looks hotter than its actual physical temperature, since $0 \leq \varepsilon \leq 1$. Equation 97 gives an equality between the source brightness and the physical temperatures for a black body, since $\varepsilon = 1$, and therefore Equation 4 gives its noise power as it happens with a resistor. A resistor, which plays an important role in radio astronomy, is any electrical device that absorbs all of the electrical power applied to it, and so it can be considered the "black body" of electric circuits [51]. Thus, we can loosely say that Equation 4 strictly applies only to a "black body".

In the case of a nonideal body, $0 < \varepsilon < 1$ stands and the radiated noise power is given by

$$P_b = kT_bB \tag{98}$$

Also called brightness power, this is the same noise power as that of an equivalent resistor at temperature T_b. An arbitrary, thermal or nonthermal, white noise source can be modelled as an equivalent thermal noise source, and characterized with a source brightness temperature.

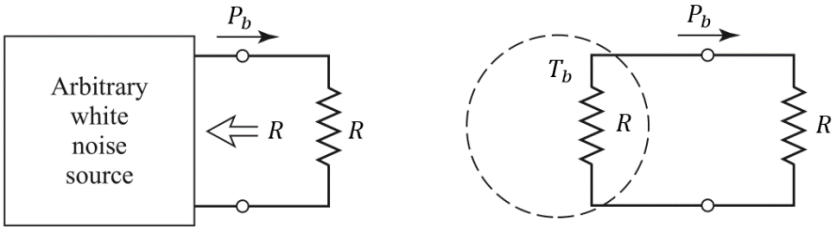

Figure 62: Source brightness temperature of an arbitrary white noise source [60].

A.3 Antenna Noise Temperature

Another important concept is connected to the external noise coupled into a receiver through an antenna, which in turn is surrounded by noise sources. The power radiated by a body, when intercepted by an antenna, generates power at its terminals given by

$$P_a = kT_aB \tag{99}$$

The equivalent noise temperature associated with the received power at the antenna terminals is called the antenna noise temperature of the object, T_a. The measured power at the antenna terminals, also called the antenna noise power, depends of the bright bodies [55]. Thus, the antenna noise temperature is function of the scene under observation and therefore function of the source brightness temperature. The relation between both quantities is already outside of the scope of this work and in case of interest the reader is advised to see [19] and [55].

The concept of antenna noise temperature is critical in understanding the relation between an object's temperature and the power it can generate at the antenna terminals, which is used in radiometry. In low-noise radio astronomy systems, as far as noise and only noise is concerned, an antenna can be modelled by a warm resistor, at the temperature T_a, that will appear at the input of the receiver.

A.4 The Total Power Radiometer

At this point, the definition of radiometer is resumed. A radiometer is a sensitive, calibrated microwave receiver that can distinguish between the usually weak desired external radiometric noise and the inherent noise of the receiver [60, 65].

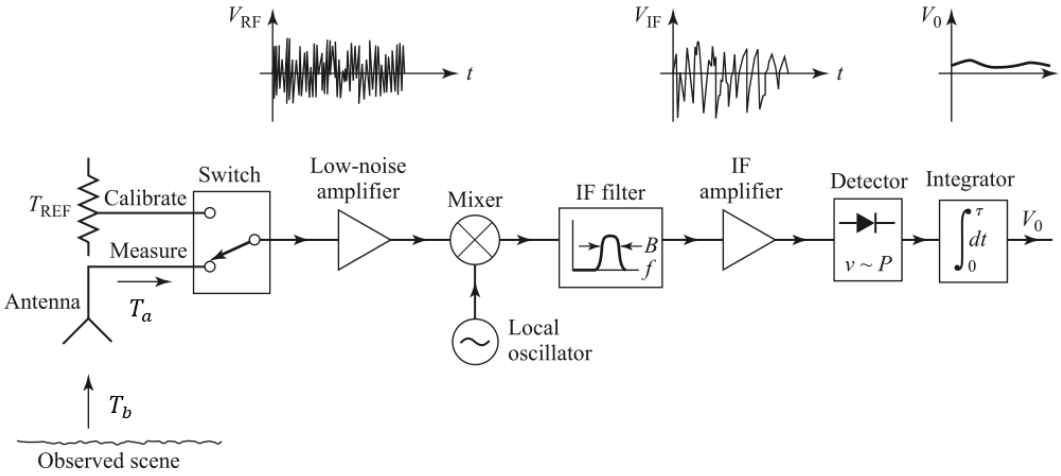

Figure 63: Total power radiometer block diagram [60].

The total power radiometer uses the superheterodyne principle and like any receiver, employs front-end circuitry, which has two prime tasks: input frequency band selection and amplifying the incoming signal to a proper level for the detector and subsequent low-frequency circuitry [65]. The system bandwidth is defined by the intermediate frequency filter. The detector is generally a square-law device, so that its output voltage is proportional to the input power. The signal from the detector is smoothed by the integrator to reduce fluctuations in the output.

If the antenna is pointed towards to a background scene with a brightness temperature T_b, the signal at the input of the radiometer will be the power generated

at the terminals of the antenna, which is characterized by an antenna noise temperature T_a. Additionally, the system generates noise within itself with an overall effective input noise temperature T_e. Thus, the output voltage of the radiometer is

$$U_{out} = G(T_a + T_e)kB \tag{100}$$

where G is the overall gain constant of the radiometer. The calibration procedure implies replacing the antenna input with two calibrated noise sources (similarly to the Y-factor method described in section 2.2.3) in order to obtain the system constants GkB and GT_ekB. Then, the antenna noise temperature can be obtained. The goal of the measurement is usually to relate the antenna temperature to the brightness temperature of the scene under observation with sufficient resolution and accuracy that this connection can be made [65].

Two types of errors occur with this radiometer due to instabilities. The first is due to the random nature of the noise and consists in noise fluctuations of the measured temperature. The basic radiometer sensitivity formula [60, 65] gives the standard deviation of the output signal as

$$\Delta T_N = \frac{T_a + T_e}{\sqrt{B\tau}} \tag{101}$$

In the ideal case the fluctuations can be reduced by averaging (integration), and so a longer measurement time τ can reduce this error to a negligible value.

The second error occurs due to gain variations between calibration and measurement procedures [60] as

$$\Delta T_G = (T_a + T_e)\frac{\Delta G}{G} \tag{102}$$

where ΔG is the change in the system gain, G.

B. Additional Low-Noise Amplifiers Designed

In this section the layouts of the additional amplifiers designed are presented. All the following amplifiers make use of the parallel coupled-line filter shown in section 3.3.2 as DC block.

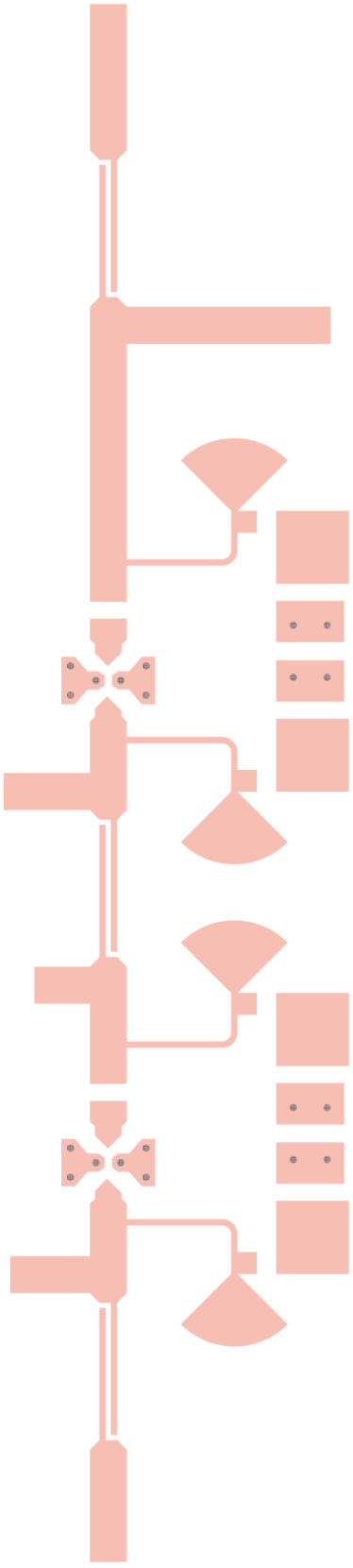

Figure 64: LNA designed with the cascade of single stages method (MGF4937AM).

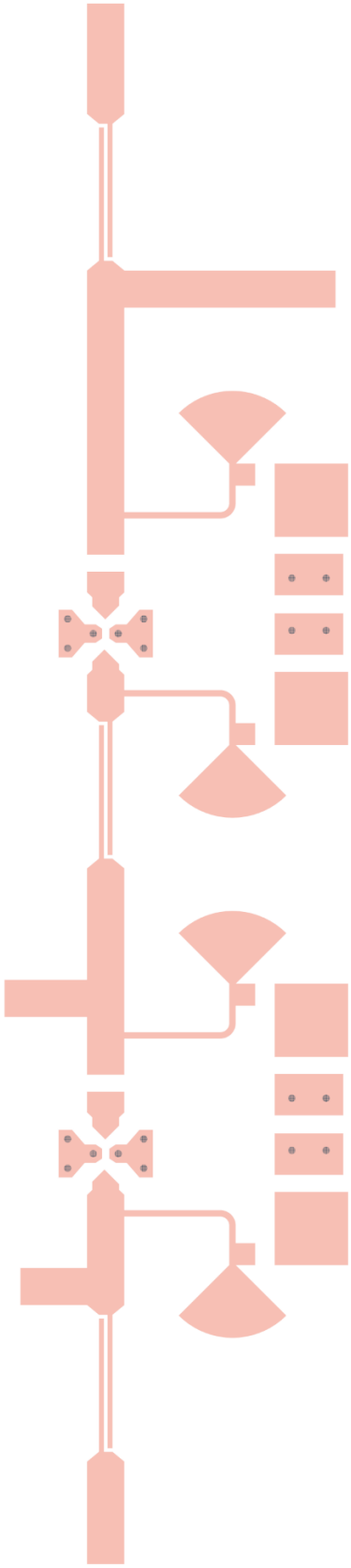

Figure 65: LNA designed with the single interstage matching network method (MGF4937AM).

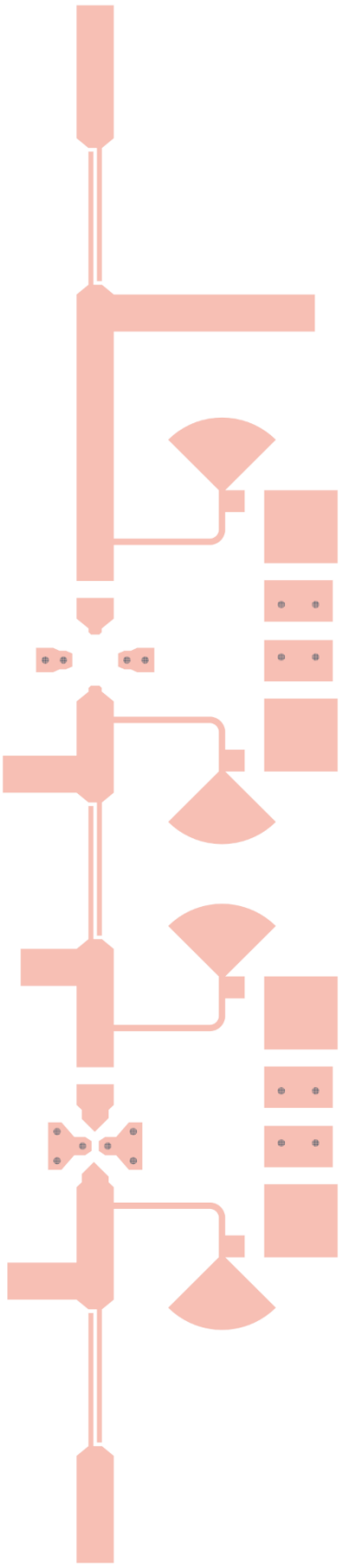

Figure 66: LNA designed with the cascade of single stages method (MGF4937AM and MGF4941AL).

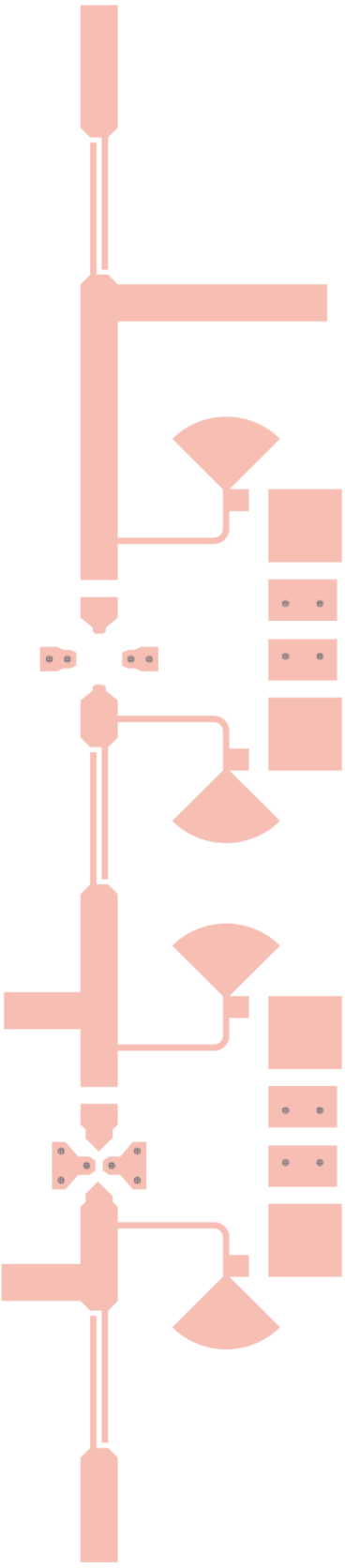

Figure 67: LNA designed with the single interstage matching network method (MGF4937AM and MGF4941AL).

References

[1] Agilent Technologies, "1 and 2 Stage 10.7 to 12.7 GHz Amplifiers Using the ATF-36163 Low Noise PHEMT," Appl. Note 1091, 1999.

[2] Agilent Technologies, “10 Hints for Making Successful Noise Figure Measurements,” Appl. Note 5980-0288E.

[3] Agilent Technologies, “High-Accuracy Noise Figure Measurements Using the PNA-X Series Network Analyzer,” Appl. Note 5990-5800EN.

[4] Agilent Technologies, “Practical Noise-Figure Measurement and Analysis for Low-Noise Amplifier Designs,” Appl. Note 5980-1916E.

[5] S. Akamatsu, S. Muir and L. Dunleavy, "Simulation Procedures for Successful Low Noise Amplifier (LNA) Design Using Discrete Components (Modelithics Appl. Note 045)," *High Frequency Electronics Design Magazine*, pp. 22-30, 10 January 2012.

[6] American Technical Ceramics, "Selecting RF Chip Capacitors for Wireless Applications," Appl. Note 001-821, 1996 [Revised October 2005].

[7] Australia Telescope National Facility, "Square Kilometre Array," [Online]. Available: http://www.atnf.csiro.au/projects/ska/index.html. [Accessed 19 June 2015].

[8] Australia Telescope National Facility, "What is Radio Astronomy?," [Online]. Available: http://www.atnf.csiro.au/outreach/education/everyone/radio-astronomy/index.html. [Accessed 19 June 2015].

[9] Avago Technologies, "70 to 500 MHz Amplifier for IF Applications using the Avago Technologies MGA-31189 Amplifier," Appl. Note 5482.

[10] AVX, "Introduction to Microwave Capacitors," Appl. Note.

[11] AVX, "Thin-Film RF/Microwave Capacitor Technology Accu-P," Accu-P Series Datasheet.

[12] T. Baker, "Successful LNA design involves performance trade-offs," *RF Design*, p. 68, November 2006.

[13] M. Bergano, L. Cupido, A. Rocha and D. Barbosa, "A 5 GHz LNA for a Radio-Astronomy Experiment".

[14] A. Bevilacqua and A. Niknejad, "An Ultrawideband CMOS Low-Noise Amplifier for 3.1-10.6-GHz Wireless Receivers," *IEEE Journal of Solid-State Circuits*, vol. 39, no. 12, pp. 2259 - 2268, 2004.

[15] Q. Bu, N. Li, K. Okada and A. Matsuzawa, "A Wideband LNA with an Excellent Gain Flatness for 60 GHz 16QAM Modulation in 65 nm CMOS," in *Proceedings of the Asia-Pacific Microwave Conference*, 2011.

[16] California Eastern Laboratories, "Designing Low Noise Amplifiers for PCS Application," Appl. Note 1022.

[17] Circuitotal, "Tecnologia," [Online]. Available: http://www.circuitotal.com/website/index.php/pt/tecnologia. [Accessed 19 June 2015].

[18] J. Coonrod, "Microwave Materials Lay Foundation For PAs," Microwaves and RF, 17 December 2009. [Online]. Available: http://mwrf.com/materials/microwave-materials-lay-foundation-pas. [Accessed 19 June 2015].

[19] L. Cupido, "EME and Radio Astronomy," in *8th 432 MHz and above EME Conference*, Paris, 1998.

[20] T. Das, "Practical Considerations for Low Noise Amplifier Design," Freescale Semiconductor, White Paper, 2013.

[21] L. P. Dunleavy, "Understanding Noise Parameter Measurements," *Microwave Journal (Modelithics, Appl. Note 033)*, February 2009.

[22] R. Fiore, "Capacitors in Broadband Applications," American Technical Ceramics, Appl. Note 001-951, 2001 [Revised January 2005].

[23] G. Gonzalez, Microwave Transistor Amplifiers: Analysis and Design, Upper Saddle River, New Jersey: Prentice-Hall, 1997.

[24] Hewlett-Packard, "Applications and Operation of the 8970A Noise Figure Meter," Product Note 8970A-1.

[25] Hewlett-Packard, "HP 8970B Noise Figure Meter Operation Manual," 1998.

[26] Hittite Microwave Corporation, "Broadband Biasing of Amplifiers," Appl. Note, 2010.

[27] Infineon Technologies, "Low Noise Amplifier for 5 to 6 GHz WLAN Application using BFP840ESD," Appl. Note 316, 2013.

[28] S. Joardar, S. Bhattacharyya, A. B. Bhattacharya and C. R. Datta, "Radio Astronomy and Super-Synthesis: A Survey," *Progress In Electromagnetics Research B,* vol. 22, pp. 73-102, 2010.

[29] Johanson Technology, "SRF & PRF and Their Relation to RF Capacitor Applications," Appl. Note, 1999.

[30] J. B. Johnson, "Thermal Agitation of Electricity in Conductors," *Physical Review,* vol. 32, pp. 97-109, 1928.

[31] Keysight Technologies, "Fundamentals of RF and Microwave Noise Figure Measurements," Appl. Note 5952-8255E.

[32] Keysight Technologies, "Keysight 346A/B/C Noise Source (Including Options 001, 002, and 004)," Operation and Service Manual, 2014.

[33] Keysight Technologies, "Keysight 8491A/B, 8493A/B/C, 11581A, 11582A and 11583C Coaxial Attenuators," Technical Overview, 2014.

[34] Keysight Technologies, "Noise Figure Measurement Accuracy - The Y-Factor Method," Appl. Note 5952-3706E.

[35] Keysight Technologies, "Noise Figure Uncertainty Calculator," [Online]. Available: http://www.keysight.com/find/nfu. [Accessed 19 June 2015].

[36] T. H. Lee, The Design of CMOS Radio-Frequency Integrated Circuits, Cambridge: Cambridge University Press, 2004.

[37] M. Leffel and R. Daniel, "The Y-Factor Technique for Noise Figure Measurements," Rohde & Schwarz, Appl. Note 1MA178_0E, 2012.

[38] Low Noise Factory, "4-8 GHz Cryogenic Low Noise Amplifier," LNF-LNC4_8A Datasheet, 2 June 2008.

[39] J. Lucek and R. Damen, "Designing an LNA for a CDMA front end," *RF Design,* pp. 20-30, 1999.

[40] G. Magerl and W. Ehrlich-Schupita, "RF Techniques," Lecture Notes on RF Techniques (354.058 VU), Vienna University of Technology.

[41] Marki Microwave, "Double-Balanced Mixers," M8-0412 Datasheet.

[42] Maxim Integrated, "Three Methods of Noise Figure Measurement," Appl. Note 2875, 21 November 2003. [Online]. Available: http://www.maximintegrated.com/en/app-notes/index.mvp/id/2875. [Accessed 19 June 2015].

[43] Mini-Circuits, "Amplifier Terms Defined," Appl. Note 60-038, 2010.

[44] Mini-Circuits, "Test Cable," CBL-1.5FT-SMSM+ Datasheet.

[45] Mini-Circuits, "Test Cable," CBL-3FT-SMSM+ Datasheet.

[46] Mitsubishi Electric Corporation, "MGF4937AM," Datasheet, 2014.

[47] Mitsubishi Electric Corporation, "MGF4941AL," Datasheet, 2011.

[48] Mitsubishi Electric Corporation, "Nonlinear packaged device model for MGF4937AM," Amplifier design for ADS user Ver. 1.10, 2014.

[49] Mitsubishi Electric Corporation, "Nonlinear packaged device model for MGF4941AL," Amplifier design for ADS user Ver. 2.30, 2013.

[50] R. K. Mongia, I. J. Bahl, P. Bhartia and J. Hong, RF and Microwave Coupled-Line Circuits, Norwood, Massachusetts: Artech House, 2007.

[51] National Radio Astronomy Observatory, "Blackbody Radiation," [Online]. Available: http://www.cv.nrao.edu/course/astr534/BlackBodyRad.html. [Accessed 19 June 2015].

[52] National Radio Astronomy Observatory, "Introduction to Radio Astronomy," [Online]. Available: http://www.cv.nrao.edu/course/astr534/Introradastro.html. [Accessed 19 June 2015].

[53] National Radio Astronomy Observatory, "Radio Telescopes," [Online]. Available: http://www.cv.nrao.edu/course/astr534/RadioTelescopes.html. [Accessed 19 June 2015].

[54] National Radio Astronomy Observatory, "Radiometers," [Online]. Available: http://www.cv.nrao.edu/course/astr534/Radiometers.html. [Accessed 19 June 2015].

[55] N. K. Nikolova, "Lecture 7: Antenna Noise Temperature and System Signal-to-Noise Ratio," Lecture Notes on Modern Antennas in Wireless Telecommunications (ECE753), McMaster University, 2014.

[56] NXP Semiconductors, "Single stage Ku band LNA using BFU730F," Appl. Note 11010, 2011.

[57] H. Nyquist, "Thermal Agitation of Electric Charge in Conductors," *Physical Review*, vol. 32, pp. 110-113, 1928.

[58] M. Panahi, "LNA Considerations for Square Kilometre Array," Ph.D. dissertation, University of Manchester, Manchester, 2012.

[59] K. Payne, "Practical RF Amplifier Design Using the Available Gain Procedure and the Advanced Design System EM/Circuit Co-Simulation Capability," Keysight Technologies, White Paper, 2014.

[60] D. M. Pozar, Microwave Engineering, John Wiley & Sons, 2012.

[61] B. Razavi, RF Microelectronics, Prentice-Hall, 2012.

[62] Rogers Corporation, "RT/duroid 5870 /5880 High Frequency Laminates," Datasheet, 2013.

[63] T. Schmitz and M. Wong, "Choosing and Using Bypass Capacitors," Intersil, Appl. Note 1325, 2011.

[64] D. Shaeffer and T. Lee, "A 1.5-V, 1.5-GHz CMOS low noise amplifier," *IEEE Journal of Solid-State Circuits*, vol. 32, no. 5, pp. 745-759, 1997.

[65] N. Skou and D. Le Vine, Microwave Radiometer Systems Design and Analysis, Norwood, Massachusetts: Artech House, 2006.

[66] J. R. Smith, Modern Communication Circuits, McGraw-Hill, 1998.

[67] Square Kilometre Array Africa, "Everything you wanted to know about the SKA," March 2014. [Online]. Available: http://www.ska.ac.za/qa/. [Accessed 19 June 2015].

[68] Square Kilometre Array Australia, "The SKA Telescopes," [Online]. Available: http://www.ska.gov.au/About/Pages/Telescope.aspx. [Accessed 19 June 2015].

[69] Square Kilometre Array Telescope, "SKA Technology," 2015. [Online]. Available: https://www.skatelescope.org/technology/. [Accessed 19 June 2015].

[70] Square Kilometre Array Telescope, "What Is Radio Astronomy?," 2015. [Online]. Available: https://www.skatelescope.org/radio-astronomy/. [Accessed 19 June 2015].

[71] M. Steer, Microwave and RF Design: A Systems Approach, Raleigh, North Carolina: SciTech Publishing, 2010.

[72] J. Stiles, "Noise in Microwave Systems," Lecture Notes on Microwave and Radio Transmission Systems, University of Kansas, 2007.

[73] TopLine, "Surface Mount Nomenclature and Packaging," Appl. Note.

[74] Tyco Electronics, "RF Coax Products," Catalog 1307191, p. 119, 2007.

[75] G. Wevers, "A low-cost, two-stage, low noise amplifier for 5 GHz to 6 GHz applications using the silicon-germanium BFP640 transistor," *RF Design*, November 2003.